Universidade do Minho
Escola de Ciências

Hugo André Capela Alvarães

Characterization of metallized polymeric films for high thermal performance applications

Maio de 2022

Characterization of metallized polymeric films for high thermal performance applications

Hugo André Capela Alvarães

UMinho | 2022

Universidade do Minho
Escola de Ciências

Hugo André Capela Alvarães

Characterization of metallized polymeric films for high thermal performance applications

Dissertação de Mestrado
Técnicas de Caracterização e Análise Química

Trabalho efetuado sob a orientação do(a)
Professora Doutora Maria Gabriela Botelho
Mestre Sílvia Patrícia Santos

Maio de 2022

DIREITOS DE AUTOR E CONDIÇÕES DE UTILIZAÇÃO DO TRABALHO POR TERCEIROS

Acknowledgments

The present section of the dissertation is dedicated to all the people without whom the completion of this research would not be possible.

First, I would like to say thanks to Vishay Electrónica Portugal Lda. for accepting me into this research and giving the resources needed for all the purposed analysis that made this research possible.

A special thanks to Master Silvia Santos, product development engineer, and Engineer José Campos Aurélio, R&D manager, for all the guidance and trust given to me during the elaboration of this project.

To Professor Doctor Maria Gabriela Coutinho Soares Lema Botelho, from Escola de Ciências da Universidade do Minho, my sincere gratitude for all the dedication and knowledge that was transmitted and for being always available to help and motivate me.

Many thanks to my parents, Carlos Alvarães and Eva Capela, and sister, Bruna Alvarães, for all the support and emotional guidance that led me to surpass all barriers and fulfil my objectives.

I am also thankful to my partner, Sara Fernandes, for encouraging me to keep going and hearing me on all my doubts and problems.

I would like to extend my sincere thanks to all the professors of Departamento de Química da Escola de Ciências da Universidade do Minho that guided me during the master's course of "Técnicas de Caracterização e Análise Química" which gave me many tools and knowledge needed for this research.

STATEMENT OF INTEGRITY

I hereby declare having conducted this academic work with integrity. I confirm that I have not used plagiarism or any form of undue use of information or falsification of results along the process leading to its elaboration.

I further declare that I have fully acknowledged the Code of Ethical Conduct of the University of Minho.

Characterization of metallized polymeric films for high thermal performance applications

Abstract

A capacitor is an electrical component capable of storing electrical current, conduct alternate current (AC) and block different voltage levels of a direct current (DC) power source. It's basically composed by electrodes which are separated by a non-conductive material, namely, the dielectric, involved in an epoxy resin while inserted in a plastic case. Ceramic, electrolytic or plastic materials can be used as dielectrics in capacitors. These different materials possess different electric properties such as dielectric constant, dissipation factor and dielectric strength, which influence the capacitor performance and long-term reliability. Due to the good stability towards a large range of frequencies and temperatures, low dissipation factors, high lifetime, high dielectric strength and crystallinity, polymeric films are greatly used as dielectrics. Polypropylene base films are commonly used as a dielectric in metallized film capacitors. The need of subjecting capacitors to higher voltage applications and operating temperatures above 105°C led to the investigation of new base materials to be used as dielectrics in capacitors. Compound X is an amorphous material with good thermal resistance and high dimensional stability and is being increasingly added to polypropylene films to maximize its thermal performance in electrical applications. On the present dissertation, five metallized biaxially oriented films were analysed through various characterization techniques such as Differential Scanning Calorimetry, Fourier Transform Infrared Spectroscopy – Attenuated Total Reflectance, Atomic Force Microscopy and Scanning electron Microscopy. Additionally, mechanical tests were performed in machine direction as well as temperature shrinkage evaluations in machine and transverse directions. Three of the five films consist in polypropylene modified with compound X while the two remaining films contain polypropylene only. Beyond the base film effect, other factors such as film thickness and metallizer (A and B) are investigated. Compound X presence leads to an overall lower crystallinity and young modulus, a fibre structure morphology, higher roughness and better dimensional stability when exposed to high temperatures, with emphasis in the higher thickness film. Thickness had a negative effect on crystallinity and overall mechanical parameters except for the strain at break. Metallizer B promoted the appearance of a metallization pattern in segmented areas of the film and higher film roughness.

Keywords: Compound X, metallized film capacitors, polypropylene.

Characterization of metallized polymeric films for high thermal performance applications

Resumo

Um condensador é um componente elétrico capaz de armazenar corrente elétrica, conduzir corrente alternada (AC) e bloquear diferente níveis voltaicos em fontes de corrente direta (DC). Possui elétrodos que se encontram separados por um material não condutor, o dielétrico, inseridos num copo plástico com resina époxi. Materiais cerâmicos, eletrolíticos ou plásticos podem ser utilizados como dielétricos em condensadores. Estes materiais possuem propriedades diferentes como constante dielétrica, fator de dissipação e força dielétrica que influenciam o desempenho do condensador e a sua estabilidade a longo prazo. Devido à boa estabilidade perante uma larga gama de frequências e temperaturas, reduzido fator de dissipação, elevado tempo de vida, grande força dielétrica e cristalinidade, os filmes poliméricos são frequentemente utilizados como dielétricos. Filmes de polipropileno são bastante utilizados como dielétricos em condensadores de filme metalizado. A necessidade de sujeitar condensadores a aplicações de elevada tensão e, consequentemente, a elevadas temperaturas (acima de 105°C), levou à investigação de novos dielétricos. O composto X é um material amorfo com boa resistência térmica e estabilidade dimensional e é cada vez mais utilizado juntamente com o polipropileno, em filmes, de forma a melhorar o seu desempenho térmico. Na presente dissertação, cinco filmes metalizados e biaxialmente esticados foram analisados por várias técnicas de caracterização tais como Calorimetria Diferencial de Varrimento, Espetroscopia de Infravermelho por Transformada de Fourier – Refletância Total Atenuada, Microscopia de Força Atómica e Microscopia Eletrónica de Varrimento. Adicionalmente, foram realizados testes mecânicos na direção longitudinal e foi avaliada a taxa de encolhimento das amostras na direção longitudinal e transversal quando expostas a temperaturas elevadas. Três dos cinco filmes estudados são compostos por polipropileno modificado com composto X enquanto os restantes apenas contêm polipropileno. Para além do tipo de base de filme, outros fatores como espessura do filme e metalizador (A e B) também foram estudados. O composto X diminuiu a cristalinidade e o módulo de *young* do filme, promoveu o aparecimento de uma morfologia fibrosa, aumentou a rugosidade do filme e melhorou a estabilidade dimensional destes, com ênfase no filme de maior espessura. Maior espessura do filme diminui a cristalinidade e o módulo de *young* mas melhora a capacidade de esticamento. O Metalizador B produz um padrão de metalização nos segmentos e maior rugosidade do filme.

Palavras-chave: Composto X, condensadores de filme metalizado, polipropileno.

Index

List of figures

List of tables

Abbreviations

A	
AC	Alternate current
α_c	Capacitance thermal coefficient
AFM	Atomic Force Microscopy
ALD	Atomic Layer Deposition
aPP	Atactic polypropylene
ATR	Attenuated total reflectance
B	
β_c	Humidity coefficient
BOPP	Biaxially oriented Polypropylene
C	
C%	Crystallinity
COC	Cycloolefin copolymer
Cp	Heat capacity
D	
DC	Direct current
DF	Dissipation factor
DSC	Differential Scanning Calorimetry
E	
EDX	Energy Dispersive X-Ray spectroscopy
EM	Electron microscopy
ESR	Equivalent Series Resistance
F	
FAF	Film with aluminum foil
FIR	Far infrared
FTIR-ATR	Fourier Transform Infrared Spectroscopy – Attenuated Total Reflectance
H	
HPP	Homopolymer polypropylene
I	
IATF	International Automotive Task Force
ICP	Impact copolymer
iPP	Isotactic polypropylene
IR	Infrared radiation
ISO	International Organization for Standardization
M	
MD	Machine direction
MeF	Metallized film
MFP	Metallized polypropylene foil
MFT	Metallized polyethylene terephthalate foil
MIR	Middle infrared
MK	Metallized plastic film
MKP	Metallized polypropylene film
MKT	Metallized polyethylene terephthalate film
MKN	Metallized polyethylene naphthalate film
MLF	Multilayered film

MP	Metallized plastic foil
N	
NIR	Near infrared
O	
OM	Optical microscopy
P	
PA	Polyamide
PC	Polycarbonate
PE	Polyethylene
PEN	Polyethylene naphthalate
PET	Polyethylene terephthalate
pF	Pico-farad
PP	Polypropylene
PPS	Polyphenylene sulfide
PS	Polystyrene
PTFE	Polytetrafluoroethylene
PVC	Polyvinyl chloride
PVDF	Polyvinylidene fluoride
R	
R	Roughness
R_a	Average roughness
RCP	Random copolymer
R_T	Maximum height of the profile
ROMP	Ring-opening metathesis polymerization
R_p	Maximum profile peak height
R_{pm}	Average maximum profile peak heights
R_q	Root mean square roughness
R_t	Total roughness
R_{tm}	Average total roughness
R_v	Maximum profile valley depth
R_{vm}	Average maximum profile valley depths
R_z	Ten-point average roughness
R_{3Zi}	Third highest peak to third lowest valley height
S	
SE	Secondary electron
SEM	Scanning Electron Microscopy
sPP	Syntactic polypropylene
T	
TD	Transverse direction
Tg	Glass transition temperature
U	
UV	Ultra-violet
W	
Wt%	Weight total percentage

Chapter 1 - Introduction

1.1 Vishay Intertechnology

Vishay Intertechnology is a multinational company that was founded in 1962 by Dr. Felix Zandman[1]. It's one of the world's most trusted manufacturers of electronic components, producing a great variety of semiconductors and passive components. Vishay is present in various market segments like the automotive industry, military, medical and space, for example[1,2]. Vishay has extensive testing laboratories at its facilities to ensure the final product quality of every product line. With that, the company was able to obtain and maintain qualifications to a wide range of specifications that are vital to the different market segments[3].

Dr. Felix Zandman leadership was responsible for the growth of Vishay into a worldwide manufacturer, having over 22.000 employees and various facilities across the Americas, Asia, Europe, and Israel[4]. In 1992, Vishay Electrónica Portugal Lda was founded through the acquisition of the Roederstein Group by Vishay Intertechnology. Located in Calendário, Vila Nova de Famalicão, Vishay Electrónica Portugal mainly focus on the production of metallized film capacitors[5].

Vishay is committed in having a worldwide operation that includes social responsibility, environment protection and a safe and healthy workplace for all its employees. So, in order to achieve such objectives, Vishay obtained ISO 45001[6] (occupational health and safety) and ISO 14001[7] (environmental management system) certifications[3]. It's also certified by ISO 9001[8] and IATF 16949[9] which are essential norms for the automotive industry.

1.2 Objectives

The present dissertation aims to study and investigate, through several characterization techniques, some new films with high thermal resistance, capable of withstand working temperatures higher than 105°C. Two different base films are used, namely, biaxially oriented polypropylene (BOPP) and biaxially oriented polypropylene with compound X.

Various techniques will be applied to the different samples such as Differential Scanning Calorimetry (DSC) to observe the thermal behavior of the samples, Fourier Transform Infrared Spectroscopy – Attenuated Total Reflectance (FTIR-ATR) for molecular structure analysis of the samples, Scanning Electron Microscopy (SEM) and Atomic Force Microscopy (AFM) to evaluate the samples morphology, Energy Dispersive X-Ray spectroscopy (EDX) for a qualitative and quantitative evaluation of the chemical elements present on the different samples, shrinkage tests to observe the shrinkage rates

in machine direction (MD) and transverse direction (TD) and mechanical tests where the young modulus, tensile strength, elongation at break (%) and strain at break (%) are determined for each sample.

1.3 Dissertation organization

This dissertation is organized into five chapters. The first chapter, “Introduction” aims to give a subtle context of the company history and activity and also the objectives of the present study. Chapter two, “State of art”, is dedicated to the theoretical fundamentals of capacitors and the dielectrics involved. Several topics are briefly addressed such as the functioning of capacitors, the different types of capacitors, test parameters of capacitors, dielectric materials that can be used in capacitors, plastic materials with focus in polypropylene and film capacitors where their base construction, dielectric, rupture, and operating conditions are addressed. In chapter three, “Materials and methods”, the equipment and methods used to characterize and investigate the different samples are presented. In Chapter four, “Results and discussion”, the obtained results of the different samples are presented, compared, and discussed. Finally, in chapter five, “Conclusion”, the conclusions regarding the different studied factors are presented.

Chapter 2 - State of art

2.1 Capacitors

A capacitor is a passive electrical component which means that it can't add or amplify electrical current in an electric circuit[10]. It's able to accumulate electric energy when it's connected to a power source, conduct alternate current (AC) and block different voltage levels of a direct current power source[11]. In this way, we can consider that capacitors work like rechargeable batteries. Capacitors also have the capability to attenuate energy source electric current[5]. One way to distinguish capacitors is through the materials used in its construction. The different properties of a capacitor depend on the type of materials applied in the capacitor. Understanding the construction of the capacitors, the materials involved and how these materials influence the capacitors properties, it's possible to select a type of capacitor to a specific purpose[11].

All capacitors have the same base structure shown in **figure 1**. They have two metallic plates that work like electrodes properly separated by a non-conductive material, the dielectric[5,11]. When an electric current is applied to the capacitor, a potential difference is generated in the metallic plates, creating an electric field[11]. The capacitor can retain that charge in the dielectric until it reaches the voltage level of the power source and the electric current in the capacitor is null.

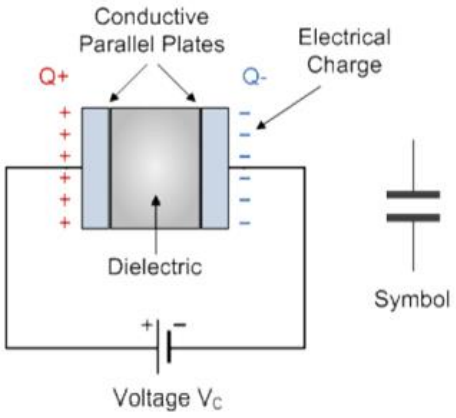

Figure 1 - Capacitor basic structure (adapted from[11]).

After disconnecting the capacitor from the power source, the electric energy previously received is stored and can be used/discharged when needed. In an ideal situation, the user should be able to use all the stored electrical energy but this is not possible do to the current leakage that occurs over time[5].

At the end of the productive process of capacitors, they are subjected to electrical tests to check its correct operability. These tests measure some specific characteristics like capacitance (C), dissipation factor (tan δ) and insulator resistance (R_{IS})[12].

2.1.1 Capacitance (*C*)

The capacitance of capacitors corresponds to its capability of storing electric charge (Q)[11–13]. This property can be expressed through an equation (1) that involves the charge (Q) that can be stored and the voltage (V) applied to the capacitor[13].

$$C = \frac{Q}{V} \quad \textbf{Equation 1}$$

Capacitance is measured in Farad (F), that is, coulomb per volt. 1 coulomb equals to $6.24*10^{18}$ electrons[11,12]. Since one unit of Farad is very high, the capacitance value often comes in micro-farads (μF) or pico-farads (pF)[13]. Capacitors are produced with the objective of presenting a specific capacitance, designated as "rated capacitance". This value must be achieved, and some deviation tolerance is allowed. The capacitance value is measured in specific reference temperature and humidity conditions, which are 23±1°C and 50±2%, respectively[14].

The capacitance of a capacitor has a near linear relation with the metallic plates area and their distance[13]. Increasing the metallic plates area (A) will lead to a capacitance increase but, longer distances (d) between the metallic plates will reduce the capacitance[11–13]. This relation can be expressed through the following equation (2) which also includes the permittivity of vacuum (ε_0) that has a value of $8.85*10^{-12}$F/m[11,12].

$$C = \varepsilon_0 * \frac{A}{d} \quad \textbf{Equation 2}$$

Usually, to increase the capacitor capacitance, a dielectric material is introduced between the metallic plates. This dielectric is an electric insulator and can be of various types such as plastic material (polymer), ceramic material, air or electrolytic gels in case of super-capacitors[13]. Different material composition will have different dielectric constants (k) which will influence the capacitor capacitance[11]. Some of these materials and respective dielectric constant (k) are represented in **table 1**.

Table 1. Some dielectric materials and their respective dielectric constants (k) (adapted from[11]).

Dielectric material	Dielectric Constant (k)
Vacuum	1.0
Air	1.0006
Polypropylene (PP)	2.2
Polyphenylene Sulfide (PPS)	3.0
Polyester (PET)	3.3
Polyester (PEN)	3.0
Impregnated paper	2.0-6.0
Mica	6.8
Tantalum Oxide	27.7
Aluminium Oxide	8.5

When a dielectric material is introduced in the capacitor, the equation 2 suffers some changes in order to include the dielectric constant (k) and the capacitance value without the dielectric material (C_0)[13]. These changes are present in the following equation 3.

$$C = k * \varepsilon^0 * \frac{A}{d} = k * C_0 \quad \textbf{Equation 3}$$

The electric energy (U) stored in the capacitor depends on the capacitor capacitance (C), voltage between the two metallic plates (V) and the stored charge (Q)[13]. This relation is present in the following equation 4.

$$U = \frac{1}{2} * \frac{Q}{C} * Q = \frac{1}{2} * C * V^2 \quad \textbf{Equation 4}$$

The different variables involved in the capacitor can be viewed in the following **figure 2**.

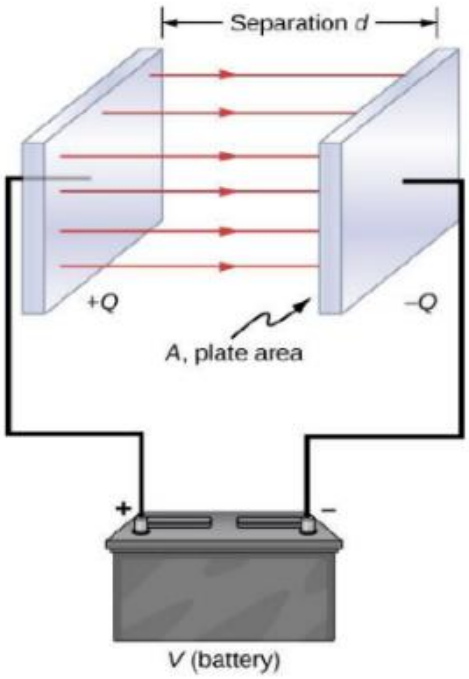

Figure 2 - Different variables involved in the capacitor, namely the separation between the metallic plates (d), the metallic plates area (A), the associated positive and negative charge (+Q and -Q, respectively) and the applied voltage (V) through a power source (battery) (adapted from[15]).

Equation 1 shows that the capacitance depends on the charge (Q) and the voltage (V) but, if we change one of these variables, the other will also change. So, the capacitance value will only be influenced by the capacitor geometry. This means that with a certain applied voltage to the capacitor, increasing the metallic plates area (A) will increase the capacitance (C) but, if the area remains constant and the applied voltage changes, the capacitance values doesn't change[13].

The applied voltage will induce the movement and storage of charge in the capacitor. After some time, the flow of charge stops due to stabilization of the potential difference between the metallic plates, leading to a stop in the electric current flow and the electric field between the metallic plates stays constant. Through this, it can be observed that the bigger the area of the capacitors metallic plates, higher capacitance can be obtained, leading to an improvement in the capacitor[11].

2.1.2 Dissipation factor (tan δ)

When a certain tension is applied to the capacitor, an electric current flow in all conductive parts of the component. The dielectric material and the conductive parts have an associated resistance that interfere with the electric current course. This resistance is also known as equivalent series resistance (ESR) and will lead to the dissipation of part of the electric current which will cause an increase in the capacitor temperature. The resistance of the dielectric material is determined by its dissipation factor[11].

The amount of energy that was lost through a dielectric material can be determined with its dissipation factor. Comparing the dissipated energy with a reference value of the dielectric material will allow the determination of the amount of energy lost. The dissipation factor (DF) is then considered as a ration between the electric current used to charge the capacitor (Ic) and the electric current intensity lost (Ir)[16], as it can be seen in equation (5).

$$DF = \frac{Ir}{Ic} = \sqrt{\frac{I^2 - Ic^2}{Ic}}$$ **Equation 5**

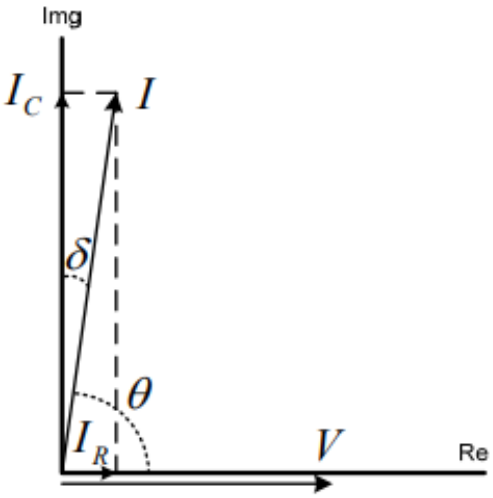

Figure 3 - Formation of angle δ (adapted from[16]).

Figure 3 shows the angle δ formed due to the difference between the initial electrical current intensity (Ic) and the electrical current intensity lost (Ir). Each dielectric material possesses a specific dissipation factor that is sensible to the frequency and temperature[11,17]. An ideal capacitor doesn't lose electric energy through dissipation. In the following **figure 4**, different materials and their respective dissipation factor intervals are presented.

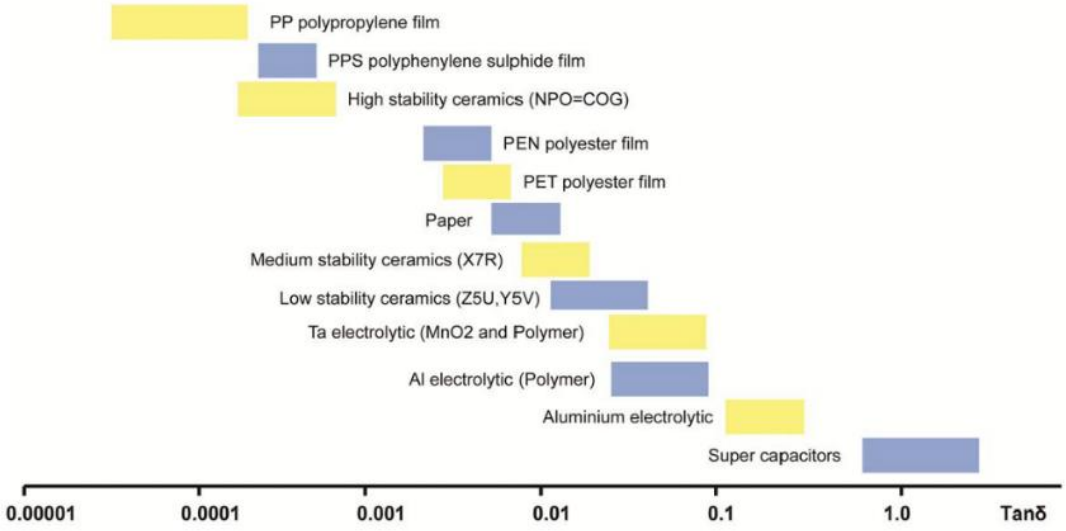

Figure 4 - Different types of dielectric materials that can applied into film capacitors and their dissipation factor values (adapted from[11]).

Through **figure 4**, the dielectric material with the lowest dissipation factor is the plastic polypropylene, which makes it a good choice for capacitor that require good energy efficiency.

2.1.3 Insulation resistance (R_{is})

The dielectric materials aren't perfect insulators, and, because of this, some electric energy is lost/leaked during operating time, leading to the capacitor discharge. As the capacitor loses electric energy previously stored, the potential difference in its electrodes will also decrease[11]. In a general way, higher capacitance of a capacitor will lead to reduced insulation resistance[11]. The insulation resistance depends on the applied voltage (V) and the leak current (I)[17], according to the following equation (6).

$$Ris = \frac{V}{I}$$ **Equation 6**

Changes in temperature or relative humidity will cause variations in the insulation resistance. R_{is} tends do decrease with an increase in the temperature and relative humidity[17]. Lower values of R_{is} will lead to a temperature increase in the capacitor, increasing the probability of damaging the component[10]. Different dielectric materials have certain properties and qualities that influence the R_{is}[17]. The insulation resistance is expressed in Mega-ohms for lower capacitances and Ohm-Farads for higher capacitances[11,12].

2.2 Plastic materials

Plastic materials are increasingly being used in substitution of other materials like wood, metal and ceramics. This was possible due to the ease in processing plastics in various shapes and sizes rapidly, with low cost, in relatively easy processes like extrusion, injection molding and compression molding. The fact that plastics have low densities and large range of specific properties makes them suitable for various applications[18].

In the year 2000, about 50 million tons of synthetic polymers were produced in Western Europe[18]. Plastic materials can be categorized into four groups, namely, thermoplastics, elastomers, thermosets and the polymer compounds[19].

2.2.1 Plastic groups

The physical properties and macromolecular structures are different depending on the group in which the plastic belongs. Elastomers present higher elastic flexibility while thermosets have greater rigidity. Plastics belonging to the thermoplastics may present a certain degree of crystallinity that can range from amorphous (non-crystalline) to semi-crystalline. One particularity of this thermoplastics is that they can change their conformation towards a temperature variation where, at higher temperatures, these materials acquire higher flexibility and, at lower temperatures they become more rigid[19]. Some examples of amorphous materials are polycarbonate (PC), polystyrene (PS) and polyvinyl chloride (PVC). Polypropylene (PP) and polyamide (PA) are semi-crystalline materials, for example[19].

Of all the synthetic polymers that are produced, the larger fraction is constituted by the following thermoplastics: PP, polyethylene (PE), PVC, PS and polyethylene terephthalate (PET). The usage of these materials has been increasing with emphasis on the isotactic propylene (iPP) where predictions points that it will be the most used polymer in the construction sector[18].

2.2.2 Polypropylene

PP was discovered in 1954[19] and belongs to the polyolefin group, meaning that it possesses a monomer with the CH_2CHR molecular structure[18]. This monomer is presented in **figure 5**. Some positive aspects of this material are that it has high commercial value due to his low cost, versatility, recyclability and good mechanic performance in various applications[20] but, on the other hand, it has some limitations like a glass transition temperature (Tg) lower than the environmental temperature and a high thermal expansion coefficient which causes dimensional instability and limits its application at high temperatures[21].

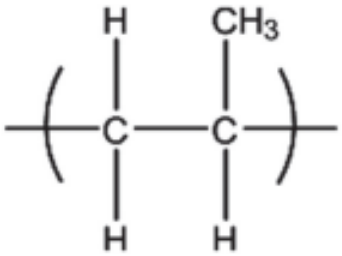

Figure 5 - Repeating unit of polypropylene (adapted from[23]).

Commercial PP can be produced through a catalytic polymerization process where propylene molecules are polymerized in long polymeric chains. The catalytic system can be based on Ziegler-Natta catalyst like an organometallic compound (triethyl aluminum, for example) and a transition metal compound (titanium chloride, for example) which will react producing a radical responsible for the polymerization[23]. There are some methods that can improve the polymerization like the suspension polymerization, gaseous phase polymerization, solution polymerization or mass polymerization[19].

The production of new types of polyolefins have also been done through the usage of metallocene catalysts. Plastics derived from metallocene are more controllable because the catalysis through metallocene is more homogeneous in comparison with the Ziegler-Natta polymerization[24]. Due to this, the products from metallocene catalysis are more homogeneous in terms of mass distribution and stereo chemical regularity, allowing a better control of the molecular characteristics of the polymer. In this way, PP produced through metallocene catalysts have lower mass distribution compared with traditional PP[24,25].

2.2.2.1 Polypropylene properties

The properties of PP depend on the conditions involved in its production like temperature and pressure[24], molecular weight and molecular weight distribution, etc.[19]. This material has a very low density (≈0.90g/cm^3) compared with others commodity polymers and can be easily processed through injection molding or extrusion. Other good characteristics of this material is that it has good mechanical properties, electric resistance, thermal resistance and good chemical resistance[19,26]. This chemical resistance varies according with the chemical compounds present in the environment where PP has an excellent resistance against concentrated or diluted acids, good resistance against aldehydes, esters, aliphatic hydrocarbons, ketones and limited resistance against halogenated hydrocarbons, oxidizing agents and aromatic compounds[19]. This polymer also presents a rigid crystalline structure due to the methyl (CH_3) groups presents in the molecular structure, a high melting point comparatively with other polymers from the thermoplastic class and a good resistance against physical impacts[19]. However, changes in the polymer crystallinity will affect its mechanical properties[24].

All these characteristics previously mentioned, the possibility of obtaining various structural designs which influence the mechanical properties and the diverse morphological structures that can be created through the incorporation of additives like fiber glass, elastomers, flame retarding agents, etc., which optimize the material, makes the PP one of the most important polyolefin within the polyolefins[19,26].

It's possible to introduce ramifications into linear chain polypropylene, promoting an increase in the product molecular weight and improving the materials characteristics such as thermal resistance and mechanic resistance, requiring greater force to deform the material[19]. The chain characteristics depends on the polymerization reactions so, the type of catalysts used will influence the primary chain architecture[27]. The mean number of ramifications per molecule (β) and the number of ramification points per 10^3 carbons (λ) are two ramification parameters that can be calculated to identify the polymers structures and properties. It's important to stablish a relation between the polymers molecular weight and these ramification parameters in order to develop polymers with unique properties. The ramification efficiency is usually related to the temperature and the chemical composition of the reaction[19]. Continuously branching a linear chain will lead to the development of a molecular architecture where all chains are all connected, forming a large "network" polymer[22] as it can be observed in **figure 6**.

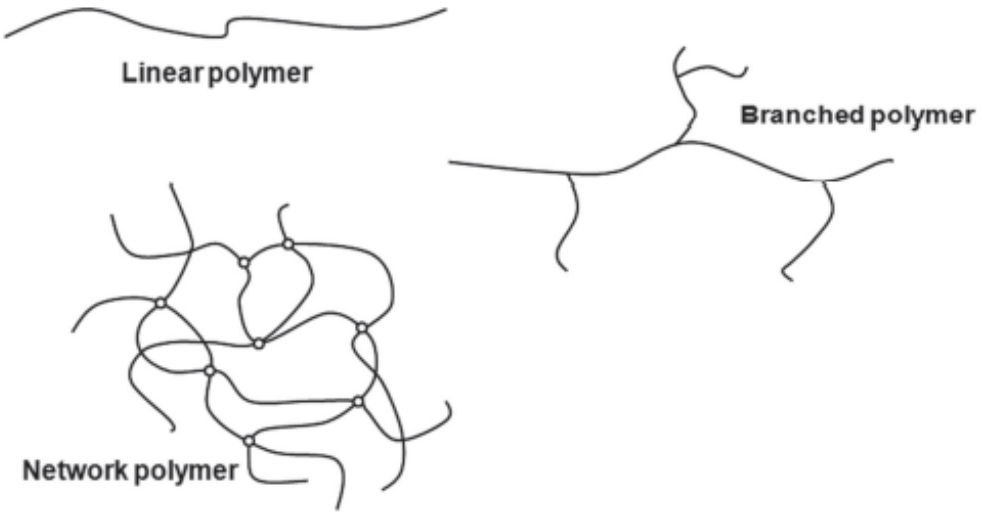

Figure 6 - Different types of polymer structure architectures (adapted from[22]).

As previously mentioned, PP can be reinforced through the addition of fiber glass or carbon, creating a PP composite reinforced with fibers. These composites are mechanically more resistant (deformation resistance), have longer durability and better humidity resistance properties[19]. Synthetic fibers have better mechanical properties than the natural fibers[19]. An important parameter is the fiber diameter present in the composite where higher diameters can cause a decrease in the composite resistance[19,28]. Fibers (carbon, glass, PET, etc.) and nanoparticles present in PP will influence the material morphology, affecting its crystallization and fusion behavior[24].

2.2.2.2 Polypropylene structural configurations

PP can present three structural configurations depending on the stereochemistry of the repeating units, namely, isotactic polypropylene (iPP), syntactic polypropylene (sPP) and atactic polypropylene (aPP)[18–20,22]. In the iPP configuration, the methyl groups are equally distributed, being present only on one side of the polymeric chain. In the sPP configuration, the methyl groups are alternately distributed on both sides of the polymer chain. Lastly, when the polymer chain structural configuration is atactic (or random), there is no preferential ordering of the methyl groups[18,19,22]. These methyl groups, in addition to setting the structural configuration of the chain, will influence the molecular structure conformation, inducing a significate impact in the materials crystallization and crystals shape[20,22]. Of all these three configurations, the iPP is the one that has more commercial relevance[18]. It has greater crystallization tendency due to the regular molecular structure, good dielectric properties, is chemically resistant and have lower specific weight[20]. The lack of structural order of methyl groups in aPP configuration has a negative effect on its crystallization degree[18]. Of all the iPP applications, about 17% correspond to the production of flexible films[18]. The three PP structural configurations are presented in the following **figure 7**.

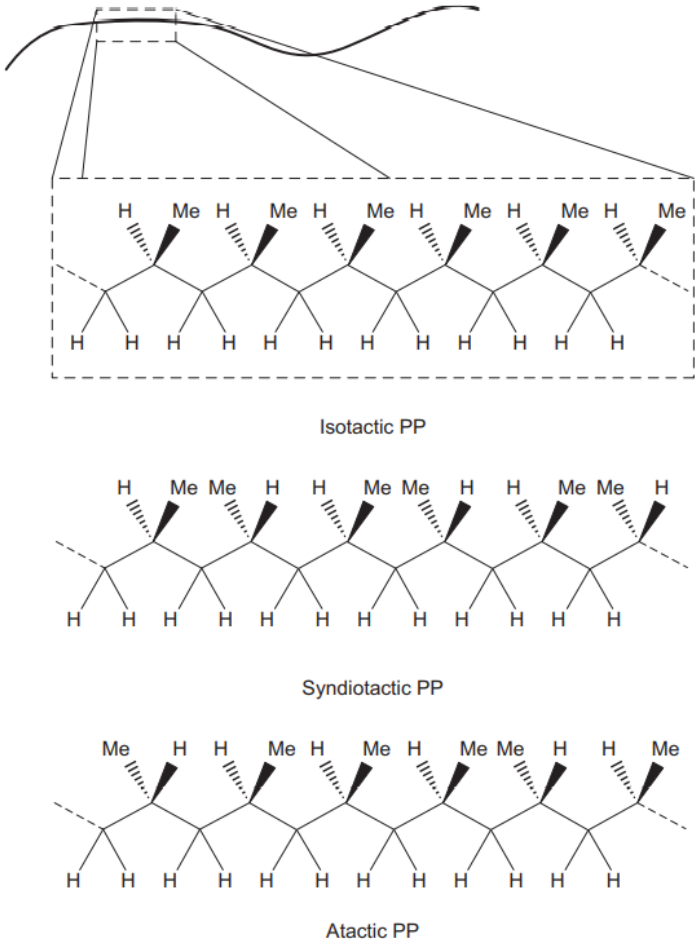

Figure 7 - Isotactic, syndiotactic and atactic structural configurations of polypropylene. "Me" stands for methyl group (adapted from[27]).

The three structure configurations previously mentioned will affect the materials melting temperature. A completely isotactic PP will present a melting temperature of, approximately, 171°C, while a sPP with 30% crystallinity will have a fusion temperature of 130°C, lower than iPP[19,28]. Commercial iPP usually has a fusion temperature comprised between 160°C - 166°C[28].

2.2.2.3 Types of polypropylene

There are three types of polypropylene, namely, the homopolymer polypropylene (HPP), the random copolymer (RCP) and the impact copolymer (ICP). The HPP is a type of PP that only contains the propylene monomer in a semi-crystalline form. The crystallinity present in the HPP is due to the presence of iPP which promotes several characteristics like high fusion temperature and high structural stiffness at environmental temperature. Adding other monomers types to the molecular structure will change the classification of the PP, depending on the amount of monomers added. The RCP is a PP that, in addition of having the propylene monomer, it also has the ethylene monomer in a quantity of 1-8% of the material.

Increasing the ethylene monomer content in the RCP to 45-65% will classify the PP as ICP, assuming that the remaining chain is constituted by several units of propylene monomer[19].

Various PP variations with different characteristics like average molecular weight, molecular weight distribution, type of co-monomers present, crystallinity and type of additive added are commercialized[19,25]. Improving the PP properties through additives will make it suitable to be used in strict applications like polymeric film[19]. The following **table 2** presents some mechanical, thermal and physical properties of different PP variations.

Table 2. PP variations and some of their respective properties (adapted from[25]).

Property	Unit	HPP	Random PP	Block copolymers	PP-T20 (Talcum)
Density	g/cm^3	≈0.90	≈0.90	≈0.90	1.04 - 1.06
Tensile Modulus of elasticity	MPa	1300-1800	600-1200	800-1300	2200-2800
Yield stress	%	25-40	18-30	20-30	32-38
Elongation at yield	%	8-18	10-18	10-20	5-7
Elongation at break	%	>50	>50	>50	>20
Melting temperature	°C	162-168	135-155	160-168	162-168
Thermal coefficient of linear expansion, parallel (22-55°C)	10^{-5}/K	12-15	12-15	12-15	10-11
Dielectric constant (100 Hz)	-	2.3	2.3	2.3	2.4-2.8
Dielectric loss factor (100 Hz)	10^{-4}	2.5	2.5	2.5	7-10
Dielectric strength	kV/mm	35-40	35-40	35-40	45
Moisture absorption (23°C/50% rel. saturation)	%	<0.1	<0.1	<0.1	<0.1

2.2.2.4 Polypropylene crystalline polymorphism

An interesting and unique characteristic of iPP is that it can have three different crystalline polymorphs, namely α monoclinic, β-pseudo hexagonal, γ-pseudo orthorhombic[18,20,29] and can also present a mesomorph phase[18,20]. All these forms present a chain conformation consisting in a 3/1 helix

conformations, where the methyl groups position can be in a "up" or "down" (**figure 8**), and a repeating distance of 6.4Å[18,27].

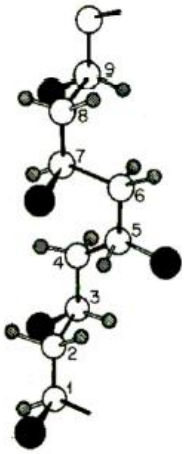

Figure 8 - Helix conformation of the iPP chain with the methyl groups (black circles) in a "down" position (adapted from[27]).

In addition to what was previously mentioned, iPP can manifest an intrinsic morphological phenomenon named homoepitaxial crystallization that promotes the development of a secondary lamellae with a well-defined geometric relation comparatively with the original lamellae[18].

Due to the different geometries involved in the helix packing, the resulting crystalline structures will vary. These packing geometries of the helix will differ due to the crystallization conditions and the molecular characteristics of the material. The crystallization behavior of the PP semi-crystalline phase will influence its mechanical properties[20].

The α-form is the most common crystalline state present in iPP and, due to the different positioning of the methyl groups, it has two isomorphic helices[20]. β-phase is thermodynamically less stable than α-form and high β-phase content in iPP will significantly change its mechanical properties, acquiring a better impact strength, toughness and lower stiffness[20,24,30].

The previously mentioned crystals will promote the appearance of lamellar like crystallites. These lamellae structures generally have a thickness of tens of nanometres and are usually separated by amorphous layers with similar thickness. When two or more lamellae are separated by the amorphous layer, they can form a fibril structure. The growing of various lamellae structures in a radial way from a central nucleus will lead to a formation of an aggregate of primary crystallites with spherical shape, which is also known as spherulite. The formation of this spherulitic structures depend on various factors such as the crystallization conditions (isothermal or non-isothermal), flow conditions, pressure, presence of nucleating agents and molecular constitution[27].

2.3 Film Capacitors

Capacitors can be divided into two groups: electrostatic capacitors and electrolytic capacitors[11]. The electrolytic capacitors have an asymmetric and polarized construction. The fact that they are polarized leads to the need of higher precautions in the moment of inserting it in an electric circuit. These capacitors have an electrolyte capable of maintaining the dielectric material and create a negative connection (cathode). In order to generate the anode, multiple metallic foils are used. The formation of an oxide in the metallic anode promotes the development of the dielectric layer[11]. The electrostatic capacitors possess a symmetric and non-polarized construction. The dielectric can be composed of a plastic or ceramic material while the electrode is based on a metal layer. These parts aren't, initially, polarized so, they can be inserted in an electric circuit without the need to correctly orient the terminals[11]. The following **figure 9** shows the categorization of different capacitor technologies.

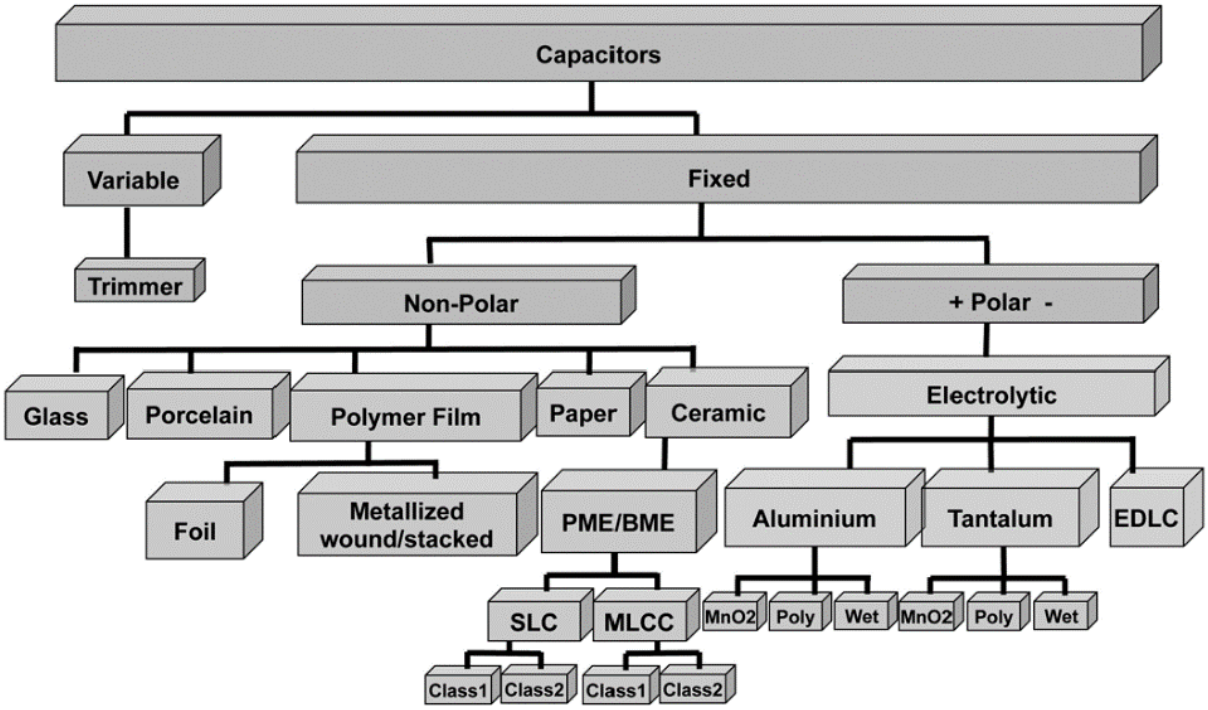

Figure 9 - Different capacitors technologies (adapted from[11]).

The metallized film capacitors can have innumerous applications such as energy storage, electromagnetic interference filtration, direct current (DC) filtration in the automotive industry, etc.[31]. The most commonly used dielectric materials are PP and PET[32]. Other polymers such as polyethylene naphthalate (PEN) and polyphenylene sulfide (PPS) can also be used[33].

2.3.1 Base construction of film capacitors

Metallized film capacitors can display two types of base construction, as shown in **figure 10**, namely, FAF (film with aluminum foil) and MeF (Metallized film).

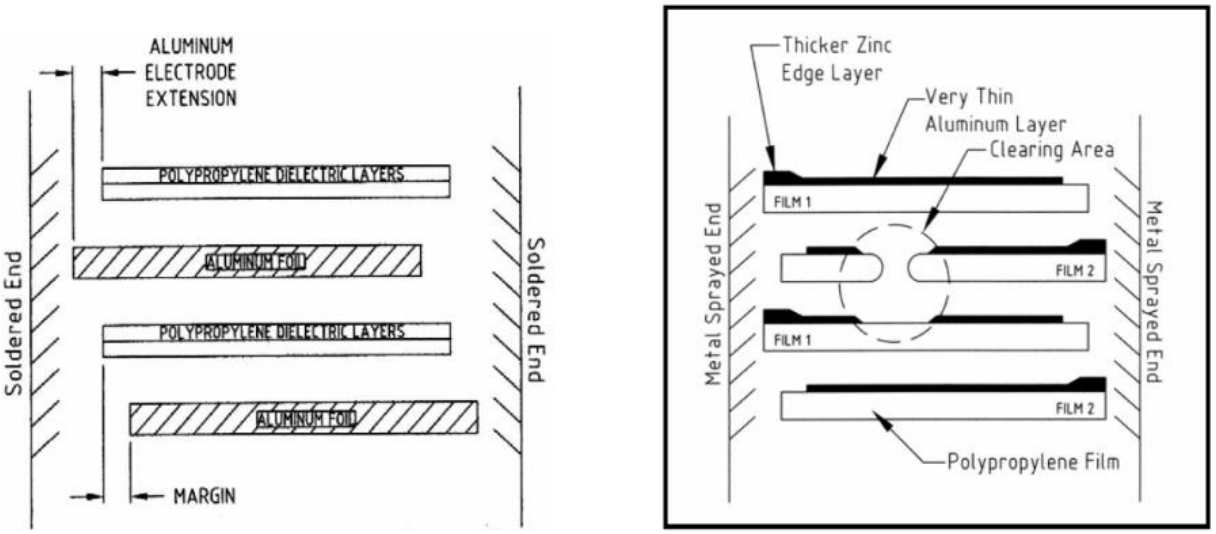

Figure 10 - Different types of film capacitor base construction (adapted from[34]).

FAF type capacitors (left schematic from **figure 10**) possess a metallic cup filled with oil. Most of these capacitors are limited to an operation temperature of 85°C. MeF capacitors (right schematic from **figure 10**) use a dielectric material with high structural crystallinity in order to obtain advantages in thermal and electric resistance, making it possible to sustain high tension inputs[34]. The MeF type capacitors are constituted by two polymeric films (FILM 1 and FILM 2 present in the right image of figure 8) that are metallized in only a few nanometers thick. These two films are then rolled through winding. At the end, a lateral metallic layer is applied through a process named "schoopage" in order to secure the correct connection of the electrodes to the external circuit[32]. They are then inserted in a metallic or plastic case that will be filled with a resin or oil (both insulators). Depending on the type of insulator and cup used, these capacitors are capable of reaching operating temperatures of 115°C[34]. The following **figure 11** shows the basic structure of an MeF type capacitor without being inserted in a case.

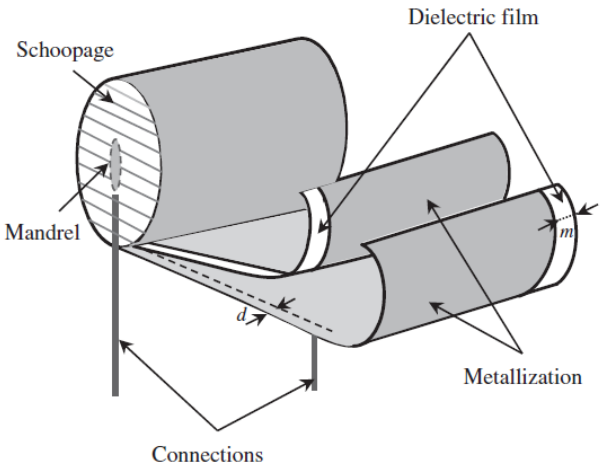

Figure 11 - Basic structure of an MeF type capacitor (adapted from[32]).

2.3.2 Polypropylene as a dielectric in film capacitors

PET or PP films are the most common materials used as dielectric materials[35]. In the last 65 years, PP films have been largely used in film capacitors due to their high dielectric strength, low dielectric loss, moisture resistance and crystallinity[36]. The great use of polymeric films as dielectric bases on the fact they present a good stability towards a large range of frequencies and temperatures, have a low thermal dissipation factor[32], high lifetime comparatively with other dielectric materials[34], high dielectric strength, crystallinity, reduced humidity absorption and a high investment has been done to produce polymeric films[36]. Because of the low and stable dissipation factor and a constant dielectric loss factor to frequencies up 1MHz of PP, this material is the most used in film capacitors[34] but, due to its low melting point temperature, it cannot be used in applications that require operating temperatures of 125°C. In these cases, PET is the most used dielectric material[33,35].

2.3.3 Dielectric rupture zones

The presence of defects in the polymeric film, the aging of the capacitor or the application of voltage above the capacitor limit are some examples of aspects that may damage the dielectric material where it cannot withstand the electric field present between the electrodes, promoting the appearance of ruptures zones in the dielectric[11,31,32,37]. These zones gain electric conductivity due to the chemical compounds present, such as carbon compounds[11]. This rupture zone (breakdown) creates a discharge channel where part of the stored energy is discharged, increasing the site temperature[38]. When this happens, the capacitor is no longer functional and starts short-circuiting[11]. Depending on the dielectric material and the way the electrodes were developed, the capacitor can prevent its continuous degradation through a process named “self-healing”[11,31]. Film capacitors with low thickness electrodes (about 1/1000

human hair diameter) can carry out this process[11]. It occurs when the electric current, that passes through the rupture zones, increases the temperature of the adjacent metallic layer (electrode), leading to its evaporation and oxidation, isolating the short-circuit zone from the rest of the capacitor[11,31] at the expense of a small capacitance loss[38]. This process can be observed in the following **figure 12**.

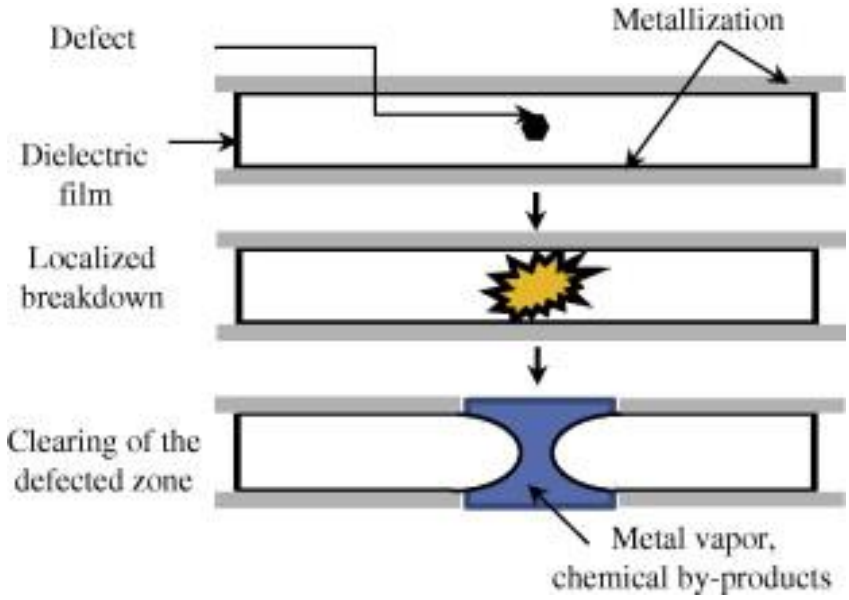

Figure 12 - Self-healing process (adapted from[32]).

If the self-healing process fails, the continuous discharge will lead to the capacitor failure where the generated heat will carbonize the multiple PP layers[38]. Continuous self-healing events will accumulate vaporized metal inside the capacitor which will increase the capacitors pressure. This higher pressure can also lead to the capacitor failure by bursting the capacitor casing or causing a flashover event due to the accumulation of metallic vapour gases[35,39].

It's essential to determine and identify critical thermal zones of the capacitor. The electric breakdown strength of polymers also depends on the room temperature. Continuously increasing the room temperature will lead to a loss of breakdown strength[38,40]. With high temperatures, the molecular structure of the dielectric will rearrange leading to the appearance of free volume between molecules. Free electrons can travel through these volumes and can be accelerated by the applied electric field, increasing the probability of ionization through collision and thus leading to polymer breakdown[41]. Another theory bases on the thermal imbalance present in the film. Since there are field-conductivity and thermal-conductivity relations, continuously increasing the applied voltage will lead to a heat accumulation, meaning that heat is being stored in the dielectric at a higher rate than its removal, leading to thermal breakdown[42]. Heat can be generated by the time-varying external voltage applied to the capacitor and film breakdowns events which will raise the capacitor temperature and lead to its degradation[43]. The

appearance of these “hot-spots” are related to the external electric field applied to the capacitors that can cause loss of dielectric capacity and resistance[34]. So, the operating temperature of capacitors depends on internal factors and external factors, such as the adjacent electric components[34].

The development of MeF type capacitors, such as PP film, but with a segmented metallic zone decreases the probability of appearing high-pressure zones inside the cup[34]. Various types of segments are available in the market such as “T segments”, “mosaic pattern” and “special segments”[44]. An example of a metallic segment type is presented in **figure 13**.

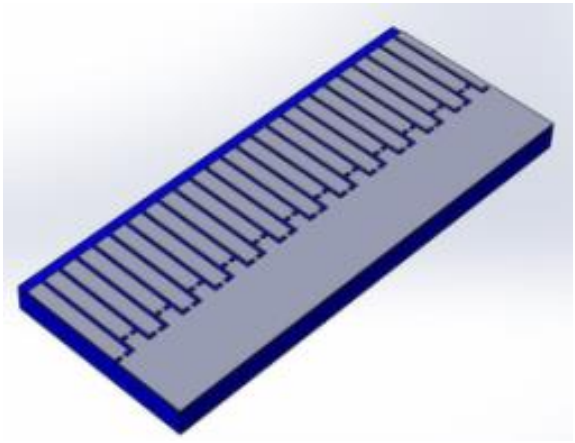

Figure 13 - "Special segment" that can be applied in films for capacitors (adapted from[44]).

The dissipation factor of PP is very low (>5*10^{-4}) and, because of that, the dielectric loss factor doesn’t change towards a given external electrical range applied to the capacitor. The non-dielectric losses can be manipulated during the development/assembling of the capacitor. It’s important to reduce the ESR through changes in the material used as terminals and conductors and by optimizing the capacitor geometry[34].

The heat generated by the electric current is conducted through the metallization present in the PP film but, due to the PP low thermal conductivity (k=0.16), it will not radiate through the dielectric. Another important factor to consider is the traveled distance by the heat where the shorter the distance, the lower the temperature increment. So, a capacitor with short-distance electrodes will have less temperature increase compared with longer distance electrodes[34].

2.3.4 Influence of the operation conditions in the film capacitor

As previously mentioned, the temperature and voltage can influence the capacitor operation over time. The most sensible component of a metalized film capacitor working at high temperatures is the dielectric, being considered as the limiting agent of the capacitor operation temperature. It’s crucial to

keep the operating temperature within the acceptable thermal range of the dielectric material because, when exposed to inadequate temperatures, its physical and dielectric properties may change[32].

High temperatures can trigger chemical reactions that changes the polymer chemical structure and, consequently, causes its degradation. Usually, the chemical reactions involved in the material degradation follow the free radical process. A free radical is produced when a molecule loses one or more electrons from the outer electronic layer. The appearance of free radicals results of the materials exposure to high temperatures, ionic radiation, ultra-violet (UV) radiation and even the presence of impurities[32]. These radicals provide instability to the polymer molecular structure, inducing the chemical reactions such as oxidation, hydrolysis and even reactions between different polymers, such as depolymerization[32,45].

2.3.4.1 Temperature effect on capacitance

The capacitance value of a film capacitor will suffer reversible changes when the electric component is exposed to temperatures out of the acceptable thermal range. The capacitance gradient as a function of temperature is given by the capacitance thermal coefficient (α_c). It corresponds to the mean capacitance variation, compared with the capacitance measured at 20±2°C, when the capacitor is submitted to a temperature variation of "T1" to "T2"[14]. This thermal coefficient of capacitance depends on the dielectric material properties, capacitor construction and production parameters[14].

The PP film capacitors have negative thermal coefficients while PEN and PET film capacitors have positive thermal coefficients. This can be observed in **figure 14** where PP (MKP and MFP), PET (MKT and MFT) and PEN (MKN) capacitance variations are compared in a specific temperature range. MK and MF designations correspond to "metalized plastic film" and "metalized foil film", respectively.

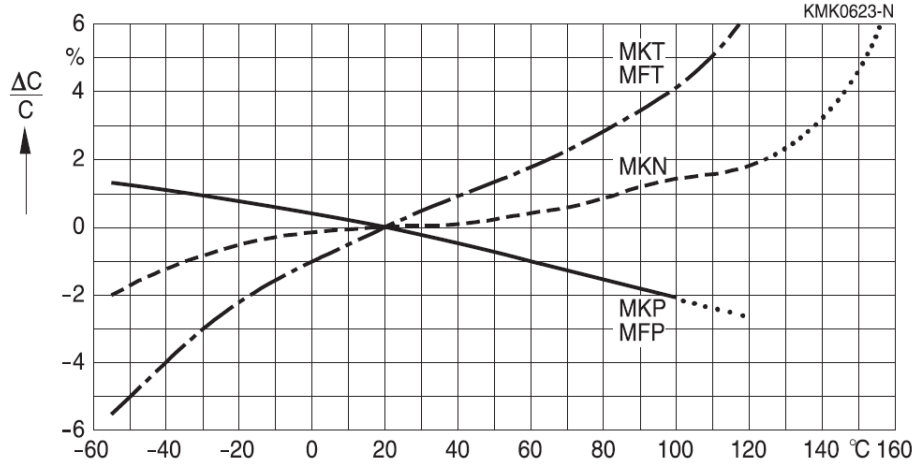

Figure 14 - Capacitance variations of different dielectric materials as a function of temperature (adapted from[14]).

2.3.4.2 Humidity effect on capacitance

The metallized layer of film capacitors is susceptible to corrosion due to the atmospheric moisture. This corrosion progresses from the outer layers of the capacitor cylinder to the middle ones, causing an uneven distribution of current that can lead to localized heat spots at the film capable of causing capacitor failure[35,46].

The humidity present in the metallized film capacitor also influences, in a reversible way, its capacitance through a reaction between the dielectric and small air volumes present in the polymeric film with environment humidity. The humidity coefficient (β_c) corresponds to the relative capacitance variation in response to a humidity variation of 1%, assuming that the remaining conditions such as temperature remain constant[14].

The following **table 3** shows that the dielectric material PP have lower values of β_c, compared with the PET and PEN, while increasing the relative humidity present.

Table 3. Evolution of the humidity coefficient (βc) of PP, PET and PEN with the increase in the relative humidity (adapted from[14]).

Dielectric		PP	PET	PEN
C Humidity coefficient β_c (50 ... 95%)	10^{-6}/% r.h.	40 ... 100	500 ... 700	700 ... 900

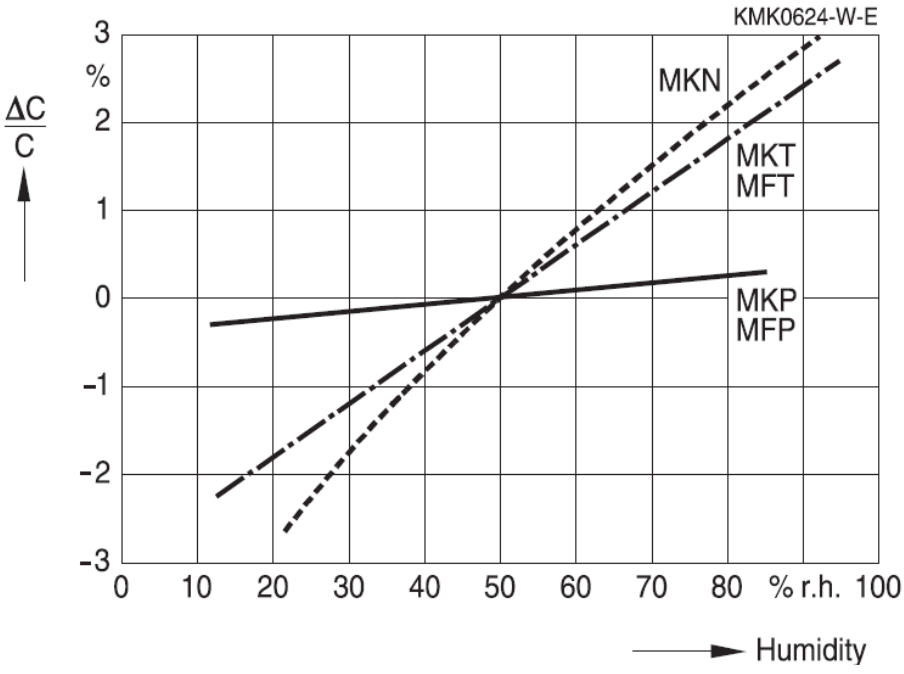

Figure 15 - Relative capacitance variation, of different dielectric materials, subjected to an relative humidity increase (adapted from[14]).

Observing **figure 15**, it's possible to verify that the PP film suffers the smallest relative capacitance variation compared with the PET and PEN film when exposed to the same relative humidity variation.

So, the useful life of a metalized film capacitor depends on various factors such as temperature, voltage, and humidity. Capacitors will be exposed to these factors during their operating time leading to a continuous decrease of its capacitance and increase of ESR[32]. Li et al.[38] observed that higher working temperatures, environment temperatures and working voltages negatively influence the metalized PP film capacitors lifetime, increasing the probability of catastrophic failure. Also, with higher temperature conditions, the discharge energy occurred during self-healing events becomes larger under the same breakdown voltage[35]. A correct monitoring of the capacitance loss and ESR gains can help with the identification and determination of the capacitor operational phase[32].

In addition to what was previously mentioned, the productive process of metalized film capacitors can also influence its service-time. Characteristics like the metal layer thickness, the film thickness and the applied metallic surface quality that are planned in the productive process have a significant impact in the capacitor service-time[32].

2.4 Polymeric films for high temperature applications

There's an increasing need to subject the films to higher temperatures. Therefore, the possibility of replacing the dielectric material has been investigated[36]. One of the substitutes investigated is polytetrafluoroethylene (PTFE) which seems to be having promising results related to the thermal resistance but its incorporation in capacitors is difficult due to the high cost, difficulties in large-scale production and low performance[47]. It has also been investigated some PP structural modifications, by changing the functional groups present in the molecular structure so it can improve its dielectric constant and/or energy density but this approach was unsuccessful due to the increased dielectric loss, cost, and film process difficulties[36]. Wu, X et al.[36] tried to improve the dielectric strength and high temperature stability of a previously biaxially oriented PP (BOPP) film by adding an ultrathin coat of inorganic compound such as aluminum oxide (Al_2O_3), aluminum nitride (AlN) and zinc oxide (ZnO) through atomic layer deposition technique (ALD). The addition of inorganic coatings to the BOPP significantly improved its mechanical strength and breakdown strength at higher temperatures, having thermal resistance to temperatures as high as 150°C[36].

Some other approaches have been made to develop a film capable of operating at high temperatures. The blend of PP with cycloolefin copolymers (COC) or the development of multilayered films (MLF) are some interesting options.

2.4.1 COC

Two or more polymers can be blended for their beneficial properties. The characteristics of the blended material depends on several aspects such as molecular weight, crystallization behavior, compatibility, etc.[48,49]. Since different polymers have different compatibilities, their selection is crucial to obtain a material with improved properties. Thermal, mechanical, and chemical properties of the blended material will define its applicability[48].

The incorporation of a new class of polymers, such as COC which contain cyclo-olefin monomers and ethene has been studied by various authors[50]. These materials are a new type of thermoplastics derived from ethylene and norbornene with a ring shape[21] (**figure 16**).

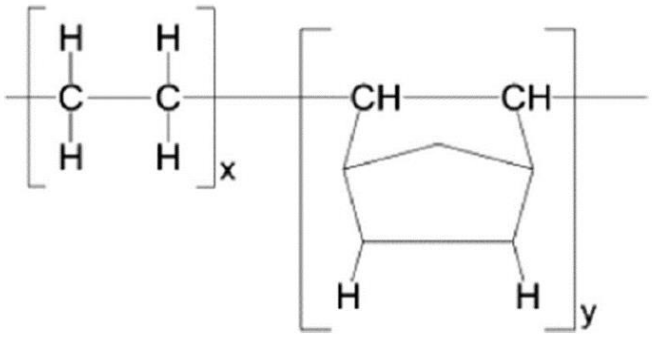

Figure 16 – Cycloolefin copolymer molecular structure composed of ethene (left structure) and norbornene (right structure) (adapted from[48]).

COC has an amorphous structure and good mechanical properties, high transparency, reduced dielectric loss, low humidity absorption, good chemical resistance, good thermal resistance and high dimensional stability[21,48,49,51,52]. Can also show a high glass transition temperatures that can reach temperatures up to 180°C depending on the norbornene content in the molecular structure[21] and low shrinkage[50]. All these characteristics are useful to satisfy the industrial requirements of society and makes it an appropriate material to be blended with PP to improve its properties, namely, thermal resistance, dimensional stability and lifetime[21]. It can be produced from different cyclic monomers and polymerization methods. One of the methods is the copolymerization of cyclic monomers such as norbornene, or tetracyclododecene, with ethene through a metallocene catalyst[48,50] (**figure 17**). It can also be produced through a ring-opening metathesis polymerization (ROMP) followed by hydrogenation[50]. The COC Tg depends on the material backbone microstructure where alternating ethylene and norbornene units will induce lower Tg while long norbornene sequences in its microstructure will enhance the chain stiffness, leading to an increase in the Tg[51].

2.4.1.1 Different COC grades

Different COC variations are available in the market, such as APEL and TOPAS[53]. In the next sub-chapters, a brief description of these grades, molecular structure, main applications and properties is presented.

2.4.1.1.1 TOPAS

The norbornene-type COC is frequently commercialized by the name TOPAS which is the name of the manufacturer, Topas Advanced Polymers Gmbh[53]. The different TOPAS grades have various properties (high purity, high clarity, thermal, moisture, chemical and shrinkage resistance and dielectric performance) that make it suitable for multiple applications in various sectors such as healthcare, packaging and electronics[54].

The different available basic grades from TOPAS differ in their heat deflection temperature which is determined by the comonomers ratio. High cyclo-olefin content will lead to a higher thermal resistance. Some of the basic grades are the TOPAS 8007 (suitable for packaging of moisture sensitive products), TOPAS 5013 (good for optical applications such as lenses, for example), TOPAS 6013 (useful for labware products), TOPAS 6015 and TOPAS 6017[55]. Some properties of these different grades are presented in the following **table 4**.

Table 4. Comparison of different basic TOPAS grades properties (adapted from[53,55]).

Property	Test method	TOPAS 8007	TOPAS 6013	TOPAS 6015	TOPAS 5013	TOPAS 6017
Tg (°C)	-	80-180				
Density (g/cm³)	ISO 1183	1.02				
Tensile strength (MPa)	ISO 527	63	63	60	46	58
Elongation at break (%)	ISO 527	10	2.7	2.5	1.7	2.4
Tensile modulus (MPa)	ISO 527	2600	2900	3000	3200	3000
Impact strength (kJ/m²)	ISO 179/1eU	20	15	15	13	15
Dielectric constant (k)	-	2.35				
Dissipation factor (tan δ)	-	0.0002				
Water absorption (%)	ISO 62	<0.01	<0.01	<0.01	<0.01	<0.01

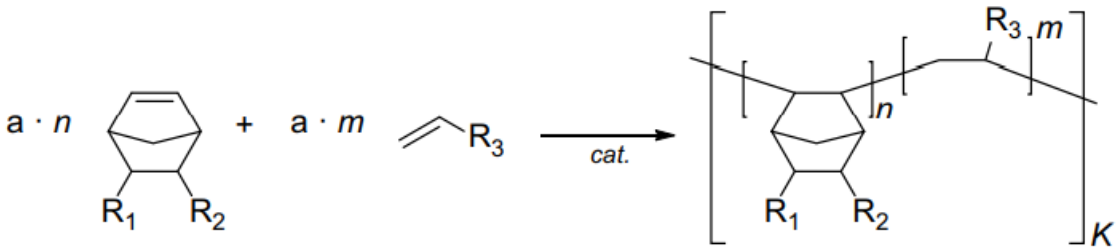

Figure 17 – TOPAS COC synthesis (adapted from[53]).

2.4.1.1.2 APEL

APEL COC, developed by Mitsui Chemicals, is similar to TOPAS type in a structural perspective with the particularity of being produced through Ziegler polymerization[53,56]. This material has excellent electrical insulation properties, good moisture barrier, significant clarity and transparency, high Tg, good gas barrier and excellent chemical and heat resistance. It can be used for optical applications, packaging applications and in high performance films[56]. In the following **figure 18**, different APEL COC grades with different Tg and content (mol%) are presented. APL6509T, APL6011T, APL6013T and APL6015T grades are used for general purposes while APL5014DP and APL5014CL grades are used for optical applications[56].

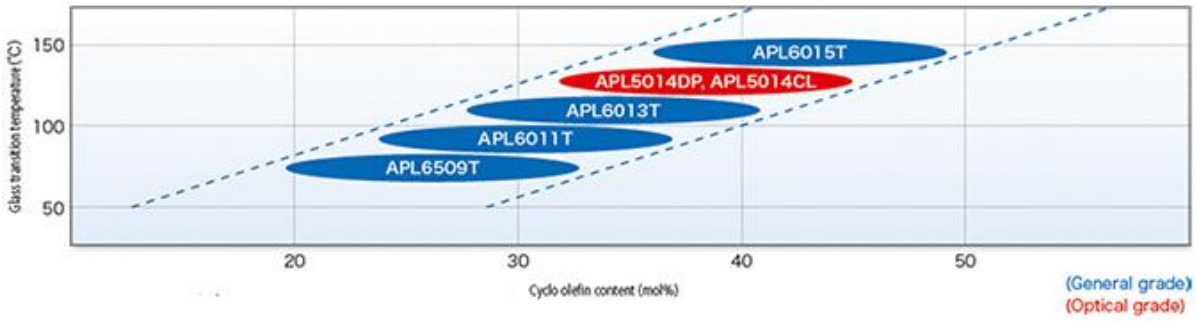

Figure 18 - Different APEL COC grades (adapted from[56]).

In the following **table 5**, some properties of the different general APEL grades are compared.

Table 5. Comparison between different general APEL grades properties (adapted from[56]).

Property	APL6509T	APL6011T	APL6013T	APL6015T
Tg (°C)	80	105	125	145
Specific gravity	1.02	1.03	1.04	1.04
Tensile strength at yield (MPa)	60	60	60	60
Tensile strength at break (%)	60	3	3	3
Flexural Modulus (MPa)	2500	2700	3000	3200
Flexural strength (MPa)	100	110	110	110
Moisture permeability ($g.mm/m^2.d$)	0.09	0.09	0.09	0.09
Mold shrinkage (MD/TD)	0.6/0.5	0.6/0.5	0.6/0.5	0.6/0.5
Water absorption (%)	<0.01	<0.01	<0.01	<0.01
Application sample	Film sheet	Industrial parts	Industrial parts	Medical packages

2.4.1.2 Mechanical, thermal and electrical effects of PP/COC

Blending PP with COC will produce a material with enhanced mechanical and thermal properties[48]. PP/COC blends tend to form fibril structures oriented according with the injection process along the polymeric matrix. If the PP/COC blend has a higher portion of PP, then COC fibers are present in the PP matrix. If COC is present in higher quantities, then PP fibers will be present in a COC matrix. In equal portions of PP and COC in PP/COC blends, a co-continuous phase of both materials is present[21,51,57]. Šlouf, M. et al.[51] observed that increasing the COC content in PP/COC will lead to an increase in the COC fiber diameter.

The amount of COC present in the blend and its distribution will also affect the impact resistance of the blend[48]. Gopanna A. et al.[21] observed that PP/COC blend have weaker impact resistance compared with pure PP and that one of the reasons of this behavior is due to the immiscibility between the semicrystalline phase of PP and amorphous COC. Fambri, L. et al.[52] equally observed that there was no miscibility between PP and COC because the Tg of the blend didn't change significantly with the different weight fractions of PP/COC.

The presence of oriented COC fibril structures in the blended material will influence its mechanical strength[21,48]. According to Gopanna, A. et al.[21], increasing the COC portion in the PP/COC

blend will lead to an increase in the blend tensile strength, young modulus, flexural modulus and flexural strength. The existence of fibers in PP/COC blends can offer greater mechanical improvements in terms of modulus, yield strength and resistance to creep, for example, than co-continuous phases[51,57]. The amorphous COC structure will impact the crystallization process of PP[48,52]. Fambri, L. et al.[52] observed that PP/COC blends with higher amount of COC (25/75) lead to a decrease in the melting temperature, crystallization temperature and crystallinity of the blend, meaning that the amorphous phase affects the structural organization of PP.

Since the blending of COC and PP can improve the final film mechanical and thermal properties, its introduction as a dielectric film in capacitors for high temperature applications is a promising possibility. Alba, C et al.[58] subjected BOPP/COC film capacitors and BOPP film capacitors with the same metallization and similar film thickness to three electric tests, namely, the ESR test at room temperature with frequency range of 20 Hz to 7 MHz, the DC leakage current test through an applied electric field of 200 V/μm at different temperatures and the DC voltage endurance test where an electric field higher than 200 V/μm was applied in a room temperature above 120°C during 1000-2000 hours. They observed that the BOPP/COC metallized film capacitor had better performance in the DC leakage current test and the DC voltage endurance test. At higher temperatures, the BOPP/COC film capacitor had a lower leakage current compared with the BOPP film capacitor. In fact, at a temperature of 125°C, the BOPP/COC film had a leakage current value similar to the PP film capacitor at 95°C. In the DC voltage endurance test, the BOPP based capacitors collapsed in the first 1000 hours of testing with a 260 V/μm electric field, evidencing self-healing failures, while BOPP/COC film capacitors where capable to endure longer testing times (2000 hours) and higher electric fields (280 V/μm). The lower conductivity of BOPP/COC film, which causes lower leakage currents[38], had a major role in the endurance tests since it avoided the collapsing of the film due to thermal and electric stresses. Also, the self-healing energy was different for the studied films where the blended film had lower self-healing energy than the BOPP film.

2.4.2 Bi-axially oriented PP (BOPP)

Another way to improve the PP characteristics involve the method used in stretching during its production. Usually, the PP film subjected to biaxial stretching is highly isotactic where its regular molecular structure will enable a more compact packing crystallization, enabling the production of higher crystalline films with lower losses and conductivity[59,60]. The purity of the dielectric is also important where higher purity will lead to lower dielectric losses, lower conductivity and higher performance at high temperatures[59].

A typical BOPP film manufacturing line consists in the casting sheet extrusion, biaxial stretching, after treatment, winding and cutting[61]. The tenter-frame process or the tubular process can be used to manufacture these type of films[62,63]. Both these processes can produce single layer films or co-extruded films[63]. In the tenter-frame process, the granular PP is extruded through a flat die, forming a sheet. This sheet is then cooled on a casting unit under controlled conditions. The sheet is then reheated above the softening temperature but below the melting point and passed through a system or rolls with different speeds. While passing through these rolls, the sheets gain orientation in the machine direction. After the rolls systems, the edges of the film are gripped by multiple clips and gets stretched in the transverse direction. In the last zone of TD stretching, heat setting is performed, providing the required annealing to the film and the adjustment of the film thickness. Lastly, after the annealing, the unoriented zones of the film are removed followed by the film winding and cut to the roll size specified by the client[63,64]. In the tubular process, a thick tube is produced after the extrusion instead of a sheet. Another difference between these processes is based in the stretching mode where, in the tubular process, warm air is blown to the thick tube while the film is in the rolls, leading to expansion of the tube diameter[64].

The film can be stretched in two different modes, the sequential mode or the simultaneous mode[59,61]. These two different stretching modes are presented in **figure 19**. In the sequential stretching mode, the film is first stretched in the MD direction, leading to the orientation and crystallization of the film along the rolling direction, followed by TD stretching, which will cause the disorientation of the initial crystal orientation. In the simultaneous stretching mode, the extruded film is stretched by clips in both directions simultaneously, leading to a more isotropic distributed film physical properties in both directions[61].

The manufacturing process and conditions such as temperature of crystallization, stretching mode applied and MD and TD stretching ratio, for example, will affect the final film physical (morphology, roughness, film thickness), mechanical and electrical properties[61,63,64].

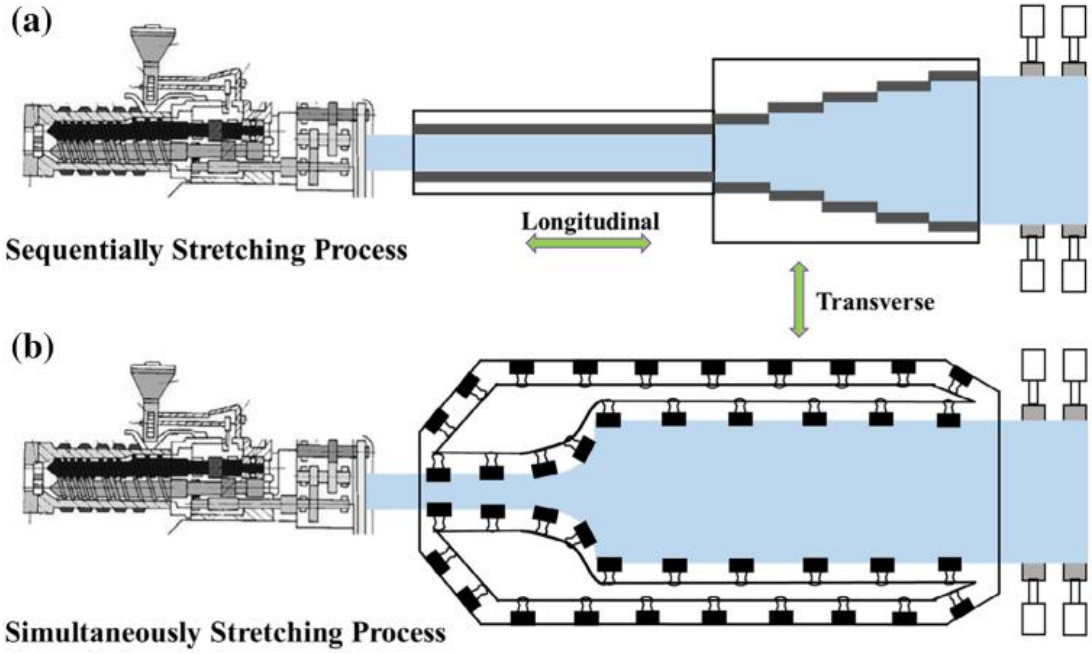

Figure 19 - Different stretching modes (sequential and simultaneous) that can be applied to the extruded PP in order to obtain a BOPP (adapted from[61]).

The biaxial stretching of the film (machine direction and transverse direction) will improve its dielectric properties[36]. According to Xiong, J. et al.[61] study, the simultaneously BOPP and the sequentially BOPP had differences in terms of physical (crystallinity and crystal orientation), mechanical and electrical properties where the simultaneously BOPP had higher crystallinity and a isotropic degree of crystal orientation in both TD and MD directions while the sequential BOPP has a different degree of orientation between the two directions. The higher crystallinity and isotropic orientation of crystals of simultaneous BOPP led to improved electrical properties such as greater breakdown strength, lower dielectric loss (tan δ), lower charge injection and transportation speeds[61].

It is estimated that the biaxial stretching improves the film crystallinity by 60% to 70%[36] and its mechanical strength due to the development of an extended lamellar morphology[65]. BOPP films have energy densities of 5-6 J/cm^3 but, with the development of society, higher energy densities up to 15-20 J/cm^3 and low loss factors are required[66]. Additionally, above 105°C, BOPP films start suffering severe limitations that compromise the capacitor operation[58].

2.4.3 Multilayered film (MLF)

The energy density needs can be satisfied with the development of multilayered film (MLF) capacitors which presents several benefits such as superior energy density, low dissipation factor and cost-efficiency solvent free[66].

The MLF are produced through microlayer coextrusion which is a conventional stacking technique that enables the production of layered films (**figure 20**). Polymers are combined to obtain a film with improved properties. MLF can have several layers ranging from 2 to 4096 layers and a layer thickness of 0.5μm to 1μm. Also, it can have two (A and B) or three polymers (A, B and C) with different layer arrangements such as ABABABA (most common) or ABCBABCBA[66].

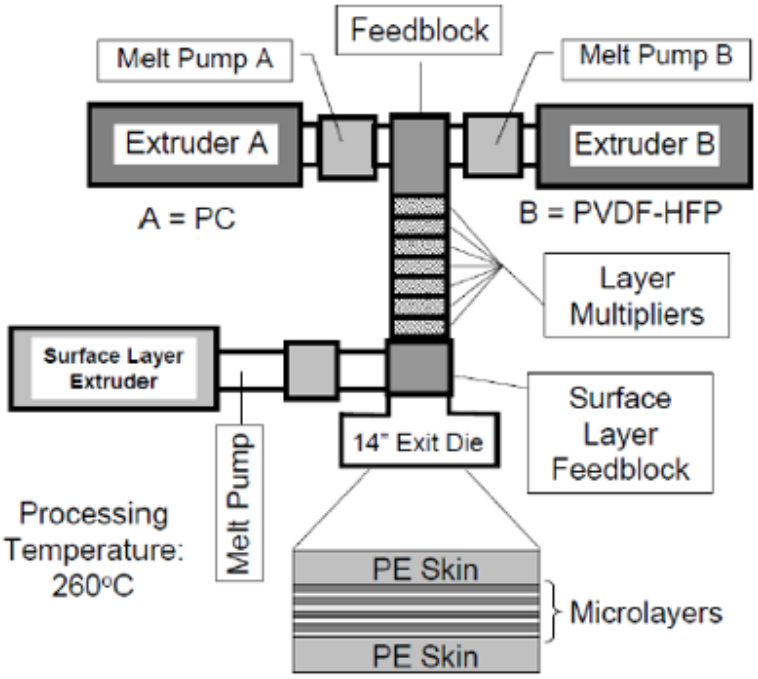

Figure 20 - Microlayer coextrusion process (adapted from[66]).

Considering that the energy density of a capacitor improves with higher dielectric constant and breakdown strength, a combination of two polymers with these characteristics can produce an improved polymer film to be applied in capacitors. An MLF consisting in Polyvinylidene fluoride type polymers (PVDF) and polycarbonate (PC) can be used since they have high dielectric constant and breakdown strength, respectively[67]. Different polymers with different characteristics can be used to form a multilayered film with different properties. So, an optimization in terms of higher energy densities and lower dielectric losses can be done with selection of appropriate polymers[66]. Also, varying the number, composition and thickness of the layers enables the film optimization to the required properties[66].

It's important to develop film capacitors capable of reaching an operating temperature of 125°C without losses in its performance.

Chapter 3 – Materials and methods

3.1 Materials

In the present dissertation, five different metallized films/samples were analyzed. The base film present on these metallized films is different where sample 1, sample 2 and sample 3 are composed by a modified BOPP designated as "BOPP/X", in which compound X was added, while sample 4 and sample 5 are made of BOPP. These five samples also have different thicknesses and metallizers. The different samples characteristics are described on the following **table 6**.

Table 6. Identification of the different films/samples in study.

Sample	Thickness (µm)	Base film	Metallizer*
1	≈3.0	BOPP/X	A
2	≈3.0	BOPP/X	B
3	≈4.0	BOPP/X	B
4	≈2.0	BOPP	A
5	≈2.0	BOPP	B

*due to confidentiality purposes, the metallizers identification will be designated as "A" and "B".

3.2 Equipment and methods

The samples described in **table 6** were analyzed through different techniques such as DSC, FTIR-ATR, AFM, SEM and EDX. Additionally, a thermal shrinkage and mechanical behavior evaluation was made to all samples.

3.2.1 Differential Scanning Calorimetry (DSC)

3.2.1.1 Brief theoretical introduction

The DSC is a thermal analysis technique that can be used in many industries like food, paper, polymers, and electronics. Every material has a heat capacity (Cp), expressed in J/g, J/Mol or calories/g, meaning that it can hold a certain amount of energy[68]. The Cp corresponds to the amount of energy needed to increase the materials temperature by 1°C[69]. When a material, like a thermoplastic polymer, is subjected to a temperature gradient, its heat capacity (Cp) changes. In a general way, the Cp of a material increases with the increasing temperature[68]. The Heat Flow DSC can measure the heat flow (amount of heat supplied per time) in the sample, detecting and quantifying the movement of heat that occurs[68,70,71]. In this way, it can quantify the enthalpy variations associated with the different structural changes a material undergoes. These changes allow the identification of transition states like glass transitions (Tg) and phase transitions (melt and recrystallization). The crystallinity of a polymer can also

be determined using the enthalpy associated with the melting of the material[68]. Comparing the heat involved in the melting of the polymeric material (ΔHf), obtained by DSC, with the heat of fusion of the same polymeric material but pure (100% crystalline) ($\Delta Hf_{100\%}$ (PP) = 207 J/g[72]) can give us information about the degree of crystallization of the sample in study[70,71]. Knowing the percentage of crystallinity of the sample, it is possible to study some mechanical properties like brittleness, toughness, or stiffness (modulus). To calculate the percentage of crystallinity (C%), the following equation can be used:

$$C(\%) = \frac{\Delta Hf}{\Delta Hf100\%} * 100 \qquad \textbf{Equation (7)}^{71}$$

To ensure that the values of crystallinity and glass transition of the polymer in study are trustworthy, a thermal treatment, usually two scans/heating runs, are used so that in the first run, the thermal history of the polymer is eliminated[70,71].

3.2.1.2 Equipment and method

At the present work, three specimens of each sample were analyzed through DSC with a PerkinElmer, model 6000, equipped with an intracooler. The equipment was purged with dry high purity nitrogen gas with a flow of 20 ml/min. Each specimen was weighted in an analytical balance of Sartorius, M-pact series, model AX224. Each specimen was added to an aluminum cap and introduced in the DSC equipment. The program used to perform the DSC analysis has temperature range of -20°C to 280°C with an initial temperature of -20°C and a heating and cooling rate of 10°C/min. Two scans were performed to all the samples. The program steps are described in **table 7**.

Table 7. Steps and characteristics of program 1.

Program	
Initial temperature (°C)	-20.00
N_2 (purge gas) flow rate (mL/min)	20.00
Step n°1 – Heat from -20.00°C to 280.00°C at 10.00°C/min;	
Step n°2 – Cool from 280.00°C to -20.00°C at 10.00°C/min;	
Step n°3 – Hold for 1.00 min at -20.00°C;	
Step n°4 – Heat from -20.00°C to 280.00°C at 10.00°C/min;	
Step n°5 – Cool from 280.00°C to -20.00°C at 10.00°C/min;	
Step n°6 – Hold for 1.00 min at -20.00°C;	

3.2.2 Fourier Transform Infrared Spectroscopy (FTIR) and the Attenuated Total Reflectance (ATR) technique

3.2.2.1 Brief theoretical introduction

The FTIR spectroscopy is a technique used in infrared spectroscopy. The infrared radiation (IR) is comprehended between the visible radiation and the microwave radiation[73]. The IR can be divided into three zones: NIR (Near infrared), MIR (middle infrared) and FIR (far infrared). The NIR, MIR and FIR includes wavenumber between 10 000 – 4000 cm^{-1}, 4000 – 200 cm^{-1} and 200 – 10 cm^{-1}, respectively[73,74].

When a sample is subjected to IR, this radiation will interact with the sample, leading to the absorption of part of the radiation by the chemical bonds of molecules present in the sample. The functional groups that absorb this radiation must be IR active, meaning that it must have a dipole moment. The IR interacting with the covalent bond of molecules with an electric dipole will promote the back-and-forth oscillation of the bond[74]. It is important to refer that every bond in molecules have their own natural vibration frequency so, depending on the bonds present in a molecule, a particular IR radiation frequency will be absorbed by each bond present. For instance, bonds like C-C, C-H, C-O and C=C can absorb IR radiation at a specific wavelength[74]. Since different functional groups like C=O, C-H or N-H show characteristic absorption/emission of IR radiation at different frequencies, they will appear in a certain region of the IR spectra[74]. Based on this, the FTIR technique his capable of giving qualitative information about the sample. The extent of the absorption of IR by the sample can also give a quantitative approach to the analysis, enabling the determination of the concentration of a component[73].

In order to address some issues related to sample preparation (reproducibility issues and time consuming) of FTIR, the Attenuated Total Reflectance (ATR) technique can be used[75]. In this technique, an IR beam travels onto an optically dense crystal. On hitting this crystal, the reflectance of the beam in the crystal creates an evanescence wave that propagates beyond the crystal surface (protrudes between 0.5 - 5µm), hitting the sample. The resulting attenuated energy from the evanescence wave travels back to the detector in the IR spectrometer which then generates the infrared spectra[75].

3.2.2.2 Equipment and method

At the present work, the samples illustrated in **table 7** were analyzed through Fourier Transform Infrared Spectroscopy – Attenuated Total Reflectance (FTIR-ATR) using a PerkinElmer, Frontier model, FT-IR spectrometer with a diamond crystal (figure 15).

Before the analysis of the samples, a background check was made from the ATR crystal. Then, a small portion of sample 1 was placed onto the small crystal area. After that, the pressure arm was

positioned and locked over the crystal/sample area. The pressure applied to the sample, pushing it closer to the crystal, was regulated through the pressure arm. Once the spectra is clearly visible on the computer, the data was collected. The same procedure was made to the remaining samples. The wavelength range of the spectra is comprehended between 4000 – 600 cm^{-1}.

3.2.3 Atomic Force Microscopy (AFM)

3.2.3.1 Brief theoretical introduction

The AFM technique can produce a 3D profile, at a nanoscale, of the materials surface, through the measure of the forces involved between a sharp probe, supported by a flexible cantilever, and a very short distant sample (0.2-10nm between the probe and the sample). The interaction between the probe and sample depends on the existing forces[76]. This technique enables the characterization of the samples surface topography, analyzing its roughness through height parameters (R), such as average roughness (R_a), root mean square roughness (R_q), maximum height of the profile (R_T), maximum profile valley depth (R_v), maximum profile peak height (R_p), ten-point average roughness (R_Z), third highest peak to third lowest valley height (R_{3Zi}), total roughness (R_t), average total roughness (R_{tm}), average maximum profile peak heights (R_{pm}) and average maximum profile valley depths (R_{vm}). The most used heigh parameters are R_a, which is the mean value of the height absolute values of the surface profile, and R_q that represents the standard deviation of surface heights[76,77]. In the following **figure 21**, some roughness parameters such as R_a and R_q are presented.

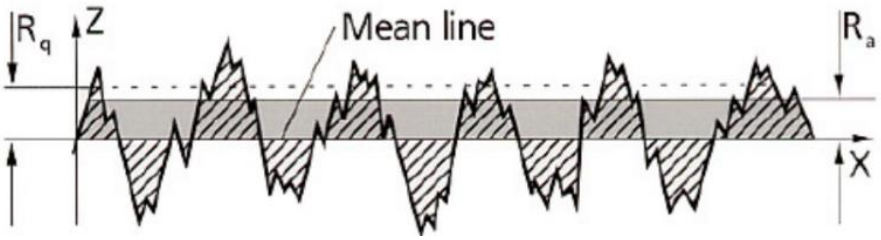

Figure 21 - R_x and R_q parameters obtainable by AFM technique analysis (adapted from[76]).

3.2.3.2 Equipment and method

The different samples topography was characterized through the Dimension Icon, Bruker, USA equipment. To measure the roughness, ScanAsyst mode, which is a PeakForce tapping based image optimization technique, was used through an ScanAsyst-air tip from Bruker with a linear scanning rate of 1Hz and a scan resolution of 512 samples/line.

Each studied sample has a metallization pattern like the one presented in **figure 13**. So, three sectors (A, B and C) were selected to perform this study. Sector A is localized at the one end of the film

that contains the demetallized edge, sector B corresponds to the zone between segments and sector C is the outer segment zone. In both sectors A and B, two areas were selected. Area A1 and A2, present in sector A, represents the non-metallized zone of the film and the inner segment metalized zone, respectively. Area B1 and B2, present in sector B, are the non-metallized segment area and the metallized area between segments, respectively.

This analysis was performed at 3B's Research Group.

3.2.4 Scanning Electron Microscopy (SEM) coupled with Energy Dispersive X-Ray (EDX)

To study the morphological aspects of the different samples, the SEM technique was performed. The qualitative and quantitative determination of the chemical elements present in these samples was executed through the EDX technique.

3.2.4.1 Brief theoretical introduction to SEM

Electron microscopy (EM) and optical microscopy (OM) have the same principle but while OM uses visible light, EM uses electron beam with shorter wavelength than the visible light[78].

In SEM analysis, a voltage accelerated electron beam scans the surface of the sample, where some electrons are backscattered due to elastic collisions with atoms while other electrons suffer inelastic collisions with the sample surface atoms, ionizing it, leading to the release of an outer layer electron, namely, secondary electron (SE). Since backscattered electrons come from deeper sample regions than the secondary electrons, they carry different type of information. These electrons will serve as a signal to build up a final high-resolution image[79].

Through this technique, it's possible to study the morphology of the sample in a quasi-three-dimensional perspective with a much better resolution, magnification and larger depth of field that of the optical microscopic, capable of reaching a resolving power better than one nanometer[78–80]. SEM can also give qualitative information about the materials composition, morphology, topography and crystallography[78].

3.2.4.2 Brief theoretical introduction to EDX

EDX is a standard method capable of giving qualitative and quantitative information about chemical elements present in a sample[81]. It can be used to identify contaminations, quality control screening and identify materials, for example[82].

It's usually coupled with SEM to detect the elemental composition of the studied sample. Through SEM analysis, an electron beam is directed into the sample surface, interacting with the nucleus of the

sample atoms present. The electron beam will excite the electron most proximate to the nucleus, leading to its ejection[82]. Then, to compensate the hole left from the ejected electron, another electron from the adjacent layers will move to its place, releasing a characteristic X-Ray radiation[81,82].

An energy dispersive detector will receive, analyze and quantify this radiation emitted by the sample atoms, enabling their qualitative and quantitative determination[81].

3.2.4.3 Equipment and sample preparation

Since the different samples surface needs to be electrically conductive for SEM imaging, they were coated, through sputtering, with a fine layer of gold with the Sputter Coater Cressington 108A equipment.

The different samples morphologies were characterized with the JEOL series JSM-6010LV (Japan) in high vacuum mode with an accelerating voltage of 10keV. The qualitative and quantitative characterization of the different chemical elements present in the different study areas of the different samples was performed with the EDX equipment INCAx-Act, PentaFET Precision (Oxford Instruments), which was coupled with the SEM equipment. The different study areas were the same as the ones mentioned in section 3.2.3.2..

This analysis was performed at 3B's Research Group.

3.2.5 Mechanical tests

3.2.5.1 Brief theoretical introduction

The mechanical tests allow the understanding of the materials behavior when a certain force is applied. When a certain stress/force is applied to a material, an internal reaction occurs to stablish the material equilibrium. A mean tension (σ) will act as an internal resistance to the applied force (F). It's mentioned as "mean tension" because its distribution is not uniform along the material due to the different mechanical properties of the different crystalline grains present in the material[83]. With the applied force, the material may start to stretch (Δl) in a proportional way. The material can display a reversible (plastic) and irreversible (deformation) behavior. The reversible behavior means that once the applied force is interrupted, the material will return to its initial dimensions[83]. The elastic modulus (E), or Young Modulus, which refers to the elastic behaviour of the material, is based on the ratio between the tension and the linear deformation[83–85], according with the following **equation 8**:

$$\sigma = E * \varepsilon \Leftrightarrow E = \frac{\sigma}{\varepsilon} \quad \textbf{Equation 8}^{[83]}$$

This elastic modulus, E, is an indicative of the materials stiffness. Higher values of E leads to lower elastic deformation under a certain applied stress, therefore, more force must be applied to the material to produce the same strain as in a less stiff material[83,85].

The mechanical tests performed for this dissertation bases on traction tests in which its possible to obtain a stress-strain curve. This curve presents three different regions, namely, the elastic region, plastic region and fracture zone. An example of the stress-strain curve is presented in the following **figure 22**.

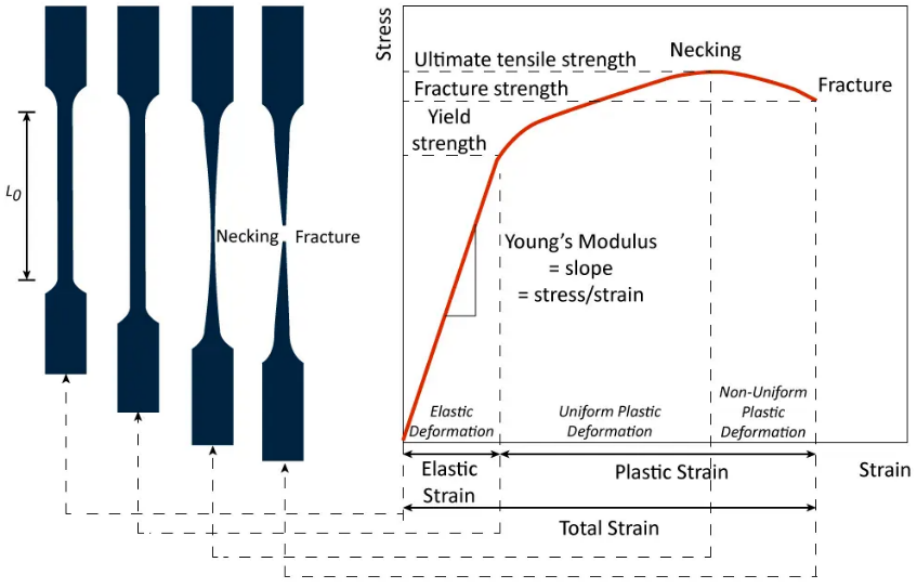

Figure 22 - Stress-strain curve with a schematic that represent the materials evolution along the traction test (adapted from[86]).

The slope of the linear portion of stress-strain curve corresponds to the elastic modulus of the material[85]. At a certain amount of stress, the materials will undergo plastic deformation. The point at which there's a passage from elastic behaviour to plastic behaviour is designed as Yield strength[84]. There will be a point in which the stress will start to decrease while the material continues to elongate. That point is described as ultimate tensile strength, also known as tensile strength, and corresponds to the ability of a material to resist a force pulling it apart[87]. Continuing the materials elongation will eventually lead to its fracture.

3.2.5.2 Equipment and methods

The mechanical behavior evaluation of the different samples was performed in accordance with the standard ISO 527-3, "Plastics – Determination of the tensile properties – Part 3: Test conditions for films or sheets"[88].

The Instron 4505 Universal Mechanical Testing Equipment with a 50N load cell, crosshead speed of 5mm/min and a distance between strips of 100 mm was used for tensile testing. The different samples were stretched in the machine direction. To standardize the different samples dimensions, all samples were cut to 25mm wide and 150 mm long and at least 6 specimens of each sample was tested.

This analysis was performed at 3B's Research Group.

3.2.6 Thermal shrinkage

With the intention of studying the thermal shrinkage behavior of the different samples, five replicates of each sample were cut from the respective main film roll and placed between two pre-dried papers (**figure 23**). To have a reference for the measurements of the shrinkage at length (machine direction (MD)) and width (transverse direction (TD)), each one of the specimens were marked in red with a permanent pen. To retain the samples on the pre-dried paper, small green stickers were used.

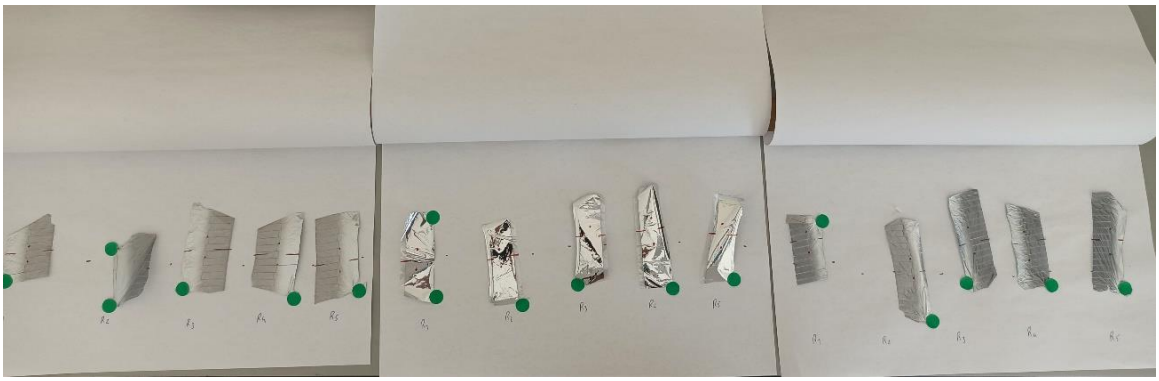

Figure 23 - Sample's specimens used to study the shrinkage behaviour.

All pre-dried papers with the specimens of the different samples were heated from 25°C to 125°C using a drying oven from the brand "Nahita", 632 plus model. Measurements of length and width of the replicates of different samples were done after they were exposed, for 30 min, at the temperature of 25, 70, 85, 105, 110 and 125°C.

To measure the length and width of each specimen, they were placed between two glass blades and were measured using a Leica microscope with a digital camera, EC3 model, with a C-thread adaptor coupled with a RSF Eletroniks, SZ 311 model. This microscope was connected to a computer to obtain a better display of the replicates image.

To calculate the sample shrinkage (%) in MD and TD, that occurred over the different temperatures, a comparison must be done between the first measurement (T=25°C) and the measurement at the following temperatures. The average of the specimen's measurements, for each sample, at different

temperatures, was used as a term of comparison. So, in the case of shrinkage (%) at MD for example, we must consider the average MD measure of specimens of a sample at 25°C (ΔL1) and the average MD measure of the same specimens at the following temperatures (25, 70, 85, 105, 110 and 125°C) (ΔL2). The following **equation 9** was used to calculate the shrinkage of the samples in MD and TD.

$$Shrinkage\ (\%) = \frac{\Delta L1 - \Delta L2}{\Delta L1} * 100 \quad \textbf{Equation 9}$$

Chapter 4 - Results and discussion

In this chapter, the results of the different analysis will be presented and discussed. On each analysis, the influence of three factors such as the base film type, the metallization and the film thickness on the obtained results will be studied. This study will be done comparing sample 1 with sample 4 and sample 2 with sample 5 for the base film effect factor, sample 1 with sample 2 and sample 4 with sample 5 for the metallization effect factor and sample 2 with sample 3 for thickness effect factor.

4.1 Differential Scanning Calorimetry

The thermal analysis was conducted via DSC. The following **table 8** presents the mean weights of each sample's specimens subjected to DSC analysis.

Table 8. Mean weights of the different samples subjected to the DSC analysis.

Sample	Mean weight (± 0.1 mg)
1	7.2
2	7.0
3	7.2
4	7.0
5	7.0

Three thermograms where obtained for each sample. These thermograms allowed the observation the different samples behaviour while subjected to thermal gradient and the determination of various parameters. The following **figure 24** shows, as an example, one of the thermograms of sample 1 where two different peaks are clearly visible corresponding to the melting (endothermic peak) and crystallization (exothermic peak) of the crystalline structure. Since two scans were performed, two endothermic and exothermic peaks are present. The remaining thermograms are present in the **annex I** of the present dissertation.

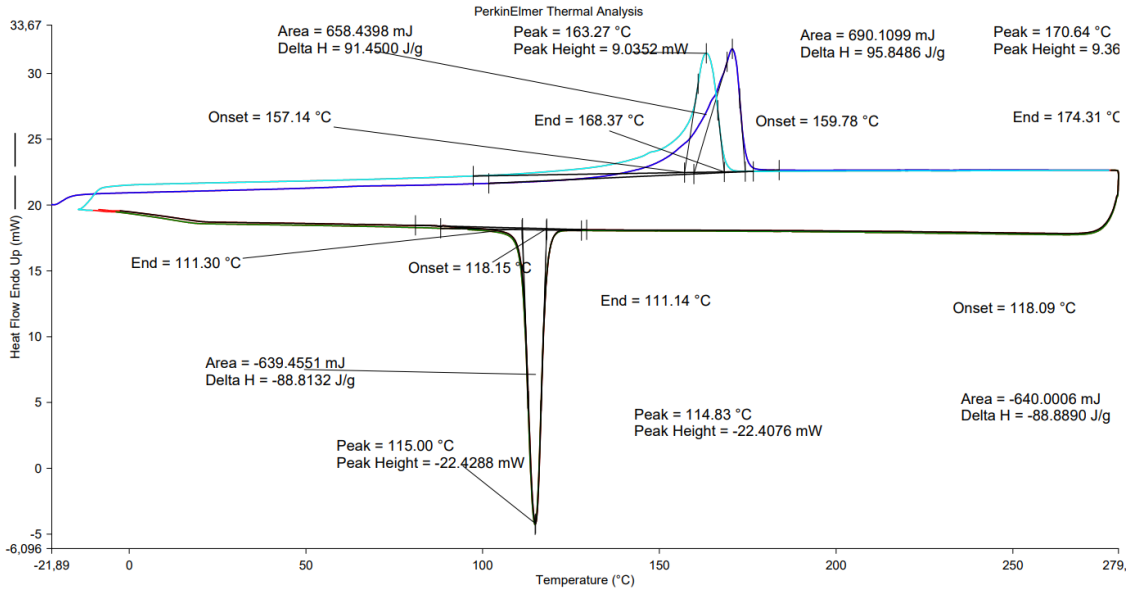

Figure 24- One of the DSC thermograms of sample 1.

Through the different thermograms of the different samples in study, parameters such as the onset temperature, end temperature, peak of melt and crystallization, enthalpy of melt and crystallization and the crystallinity are obtained. In the following **table 9**, the results of each samples, in the first scan, are presented. The results of the second scan are shown in **table 10**.

Table 9. Mean values of the different parameters related to the melt and crystallization phase of the different samples during the first run of DSC analysis.

Sample	Melt					Crystallization			
	Onset (°C)	End (°C)	Peak (°C)	ΔHm (J/g)	Crystallinity (%)	Onset (°C)	End (°C)	Peak (°C)	ΔHc (J/g)
1	162.0	174.1	170.7	95.4	46.1	117.5	110.6	114.3	-93.4
2	162.7	175.0	171.2	99.4	48.0	117.7	110.0	113.6	-95.5
3	161.8	175.1	171.8	85.7	41.4	117.4	110.0	113.6	-86.6
4	164.9	174.3	169.5	117.9	56.9	120.8	111.3	115.5	-116.9
5	164.8	173.2	168.3	114.1	55.1	123.4	112.7	117.5	-117.8

Table 10. Mean values of the parameters related to the melt and crystallization phase of the different samples during the second run of DSC analysis.

Sample	Melt					Crystallization			
	On set (°C)	End (°C)	Peak (°C)	ΔHm (J/g)	Crystallinity (%)	On set (°C)	End (°C)	Peak (°C)	ΔHc (J/g)
1	157.1	168.6	163.4	95.3	46.0	117.7	110.8	114.4	-93.1
2	156.4	168.5	163.0	93.4	45.1	118.0	110.2	113.9	-95.6
3	156.9	168.8	163.4	85.2	41.1	117.6	110.2	113.7	-86.4
4	157.5	169.1	164.2	120.7	58.3	120.7	111.1	115.3	-116.8
5	157.7	168.6	164.3	124.6	60.2	123.3	112.7	117.4	-117.1

Through the previous **table 9** and **table 10**, it's possible to observe that all samples present a melting peak between 168-172°C in the first scan and 163-164°C in the second scan. As previously mentioned, a perfectly isotactic polypropylene has a melting peak of 171°C. Meanwhile, the commercial iPP has a melting temperature range between 160 and 166°C, depending on the atactic portion present in the material[10,89]. In this perspective, the different samples in study might contain isotactic polypropylene in their molecular structure. The major melting peak might be related with the melt of the crystalline structure of the polymer, namely the α-phase[61]. In some thermograms, a subtle peak appeared around 150°C which might indicate the presence of a β-phase structure which usually appears at a somewhat lower temperature than α-phase[90,91].

It's clear that sample 1, 2 and 3 have lower crystallinity compared with sample 4 and 5. Also, the enthalpy values associated with the melt and crystallization process of samples 1, 2 and 3 are lower than the ones occurred in samples 4 and 5. Samples with higher crystallinity have higher endothermic enthalpy since more energy is required to melt the crystalline phase of the material. To study the effect of the base film on the previously mentioned parameters, only the second scan will be considered. Comparing sample 1 with sample 4 and sample 2 with sample 5, the base film has a significative effect on the crystallinity (**figure 25**), crystallization enthalpy and melting enthalpy. No significant effect was observed on the remaining parameters. The BOPP/X present in samples 1, 2 and 3 led to a reduced crystallinity, which might indicate that the added compound X has an amorphous nature.

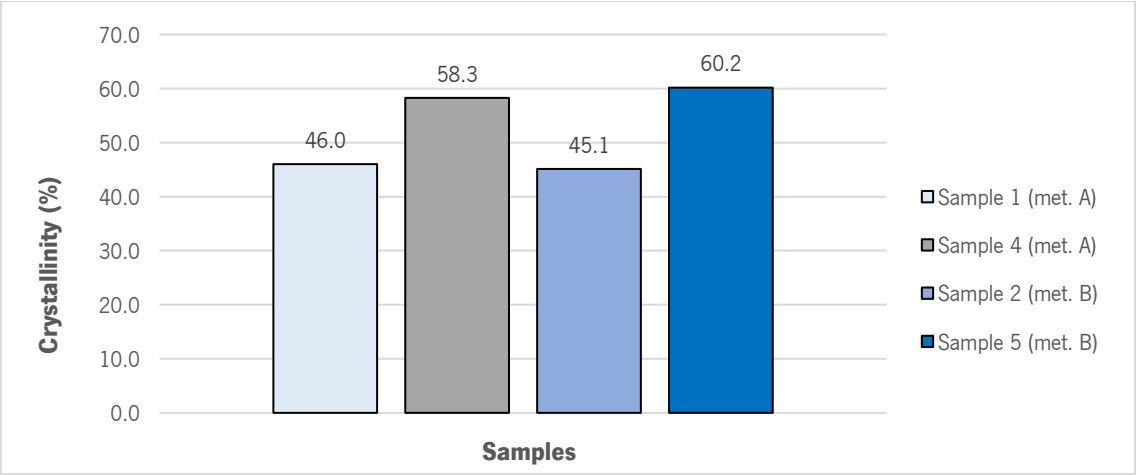

Figure 25- Compound X effect on sample 1 and sample 2 crystallinity.

The thickness effect can be observed through comparison between sample 2 and sample 3 since they have the same base film and metallizer (B). Only the second scan results of DSC will be used to study the thickness effect. Sample 3 had the lowest crystallinity (41.1%) value of all the samples while sample 2 has a higher crystallinity value (45.1%) than sample 3 (**figure 26**). This may indicate that the thickness of the sample has a negative effect on the crystallinity. A similar behaviour was observed in Xiong J. et al.[61]. Due to the higher crystallinity of sample 2 compared with sample 3, its exothermal and endothermal enthalpies will also be greater than sample 3. Thickness had no significant effect on the remaining parameters.

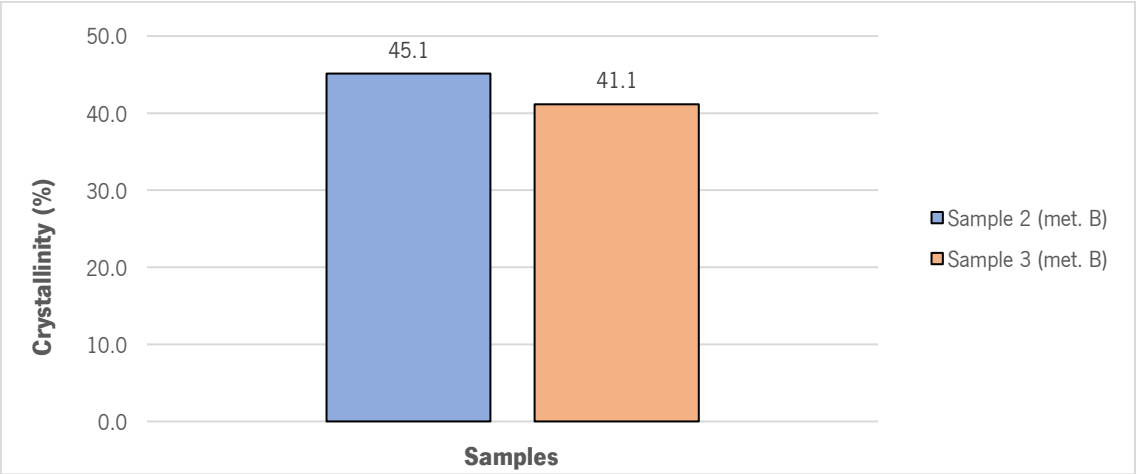

Figure 26- Crystallinity of sample 2 and 3.

Comparing samples that suffered a metallization process from different metallizers will enable the study of the metallizer effect on the thermal behaviour of these samples. Considering that sample 1 and sample 4 suffered a metallization process from metallizer A and sample 2 and sample 5 suffered a metallization process from metallizer B, a comparison of sample 1 with sample 2 and sample 4 with

sample 5 can be done to achieve such study. Since the metallizer effect is related to the productive process of the samples, only the first scan results (**table 9**) of the DSC analysis shall be considered.

Through **table 9**, sample 1 has a slightly lower crystallinity (46.1%) than sample 2 (48.0%). The melting and crystallization enthalpy are also slightly different, being greater for sample 2. Meanwhile, comparing sample 4 with sample 5, the results are a little different. Sample 4 has a somewhat higher crystallinity (56.9%) than sample 5 (55.1%). Also, the melting enthalpy of sample 4 is higher than sample 5 but, the crystallization enthalpy is slightly higher in sample 5 than sample 4. No clear trend was observed regarding the effect of the metallizer on the samples thermal behaviour.

4.2 FTIR-ATR

The FTIR-ATR spectra in the range of 650-4000 cm^{-1} of sample 4 is presented in **figure 27**. The obtained spectra has six intense peaks where four of them are present between the wavenumber range of 3000 and 2800 cm^{-1} and the remaining two peaks are in the wavenumber range 1400 and 1300cm^{-1}. Also, about six peaks with lower intensity are present in the wavenumber range of 1200 and 800cm^{-1}. Sample 4 absorption peaks in the IR region and their vibrational characteristics are displayed in the **table 11**. Since sample 4 and sample 5 have the same base film, the obtained spectra is similar to the sample 5 spectra which is present in **annex II** of the present dissertation.

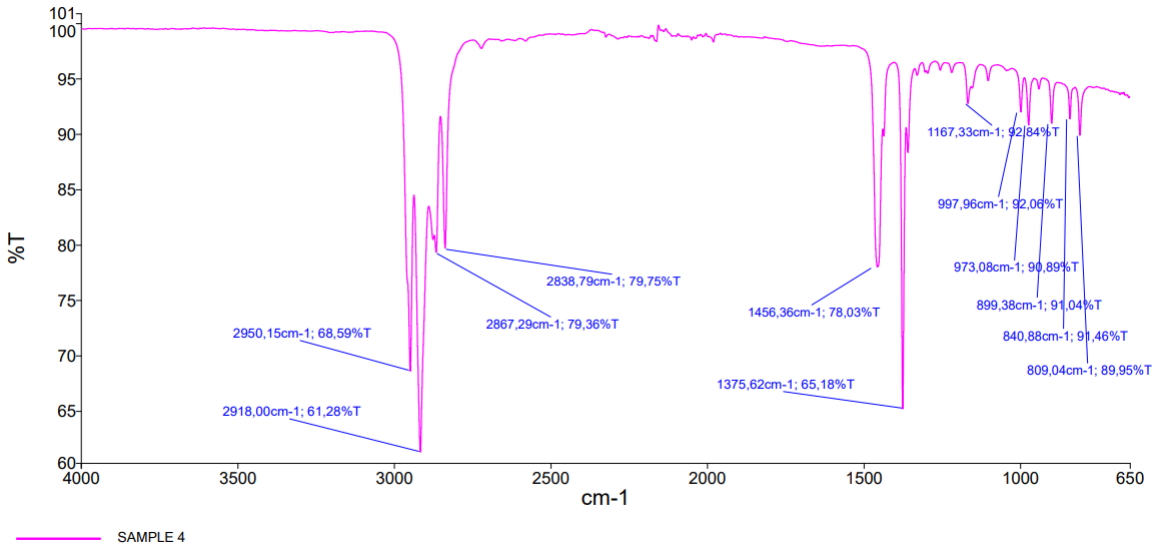

Figure 27- FTIR-ATR spectra of sample 4.

Table 11. Identification and description of the sample 4 bands obtained through FTIR-ATR analysis.

Band (cm^{-1})	Assignment	Reference
2950	Asymmetric stretching vibration of CH_3	10,48,92
2918	Asymmetric stretching vibration of CH_2	10,92
2867	Symmetric stretching vibration of CH_3	10,92
2838	Symmetric stretching vibration of CH_2	92
1456	Asymmetric deformation vibration of CH_3 or scissor vibration of CH_2	10,92
1375	Symmetric bending vibration mode of CH_3	10,48,92
1167	Asymmetric stretching vibration of C-C, asymmetric rocking vibration of CH_3 and asymmetric wagging vibration of C-H	10,92
997	Asymmetric rocking vibration of CH_3	10,92
973	Asymmetric rocking vibration of CH_3 and asymmetric stretching vibration of C-C	10,92
899	Asymmetric rocking vibration of CH_3 and asymmetric and symmetric stretching vibrations of C-C	10,92
840	C-CH_3 stretching vibration or rocking vibrations of CH_2	10,48,92
809	Rocking vibrations of CH_2	10,92

The following **figure 28** shows the FTIR-ATR spectra of sample 2. The number, position and intensity of peaks are very similar to the ones illustrated in figure 33. Since sample 1 and 3 have the same base film as sample 2, the obtained spectra are similar and are shown in **annex II** of the present dissertation.

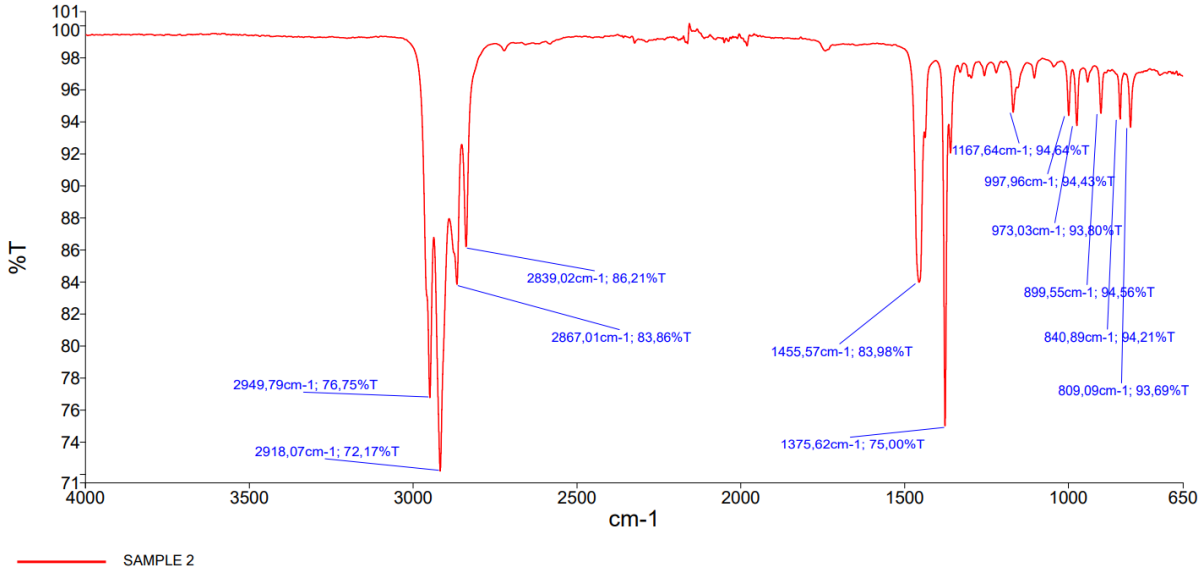

Figure 28- FTIR-ATR spectra of sample 2.

Looking at the FTIR-ATR results, all the samples consist in a base film of PP. Since sample 1, 2 and 3 has a modified BOPP where compound X was added in their base material, their spectra should have some indication regarding the presence of this substance. It was expected some peaks situated at 1017 cm^{-1} and 1596 cm^{-1} and a higher intensity of peak 1017cm^{-1}, depending on the substance quantity on the BOPP, according with previous studies[·]. So, one reason for the absence of these bands might be related to the amount of the added compound X present in the samples, which might be inferior to the detection capability of FTIR-ATR equipment.

4.3 Mechanical results

The following **table 12** shows the mean values (μ) and standard deviation (σ) of each mechanical parameter obtained for the different samples.

Table 12. Mean values (μ) and standard deviation (σ) of each mechanical parameter results of the different samples.

Sample		Young Modulus (MPa)	Tensile Stress at Yield (Offset 0.2%) (MPa)	Maximum tensile strength (MPa)	Strain at maximum load (%)	Strain at break (%)
1	**μ**	3968.8	45.2	88.8	29.5	29.5
	σ	206.2	4.9	14.8	13.4	13.4
2	**μ**	3742.8	42.2	80.1	24.7	24.7
	σ	391.0	2.1	19.5	16.2	16.2
3	**μ**	3484.3	39.8	95.2	56.1	56.1
	σ	146.7	0.9	4.6	5.6	5.6
4	**μ**	4249.2	42.7	141.2	38.3	38.3
	σ	225.4	2.1	15.2	7.8	7.8
5	**μ**	4209.6	44.9	133.5	35.6	35.6
	σ	356.9	1.3	12.4	8.1	8.1

Through the Dixon's Q-test, it was possible to analyse the presence of outliers in the different results and remove them. Additionally, various boxplots were made via "Rstudio" software which enabled a better comparison of the mechanical parameters between the different samples.

The following **figure 29** shows a general perspective of the obtained young modulus of each sample in study. In terms of capacitor application, a dielectric with high modulus is desired since it helps achieving higher breakdown strength[61]. It's clear that sample 4 and sample 5 have higher young modulus in comparison with the remaining samples. Sample 3, on the other hand, has the lowest young modulus.

[·] For confidentiality reasons, the studies references will not be shown.

It's known that the crystallinity of a semicrystalline polymer has a significant effect on their physical and mechanical behaviour[93]. In fact, mechanical properties such as tensile impact strength, yield strength and young modulus are higher in the direction of molecular orientation[27,94]. So, the crystallinity of these samples might explain the observed differences in the obtained young modulus.

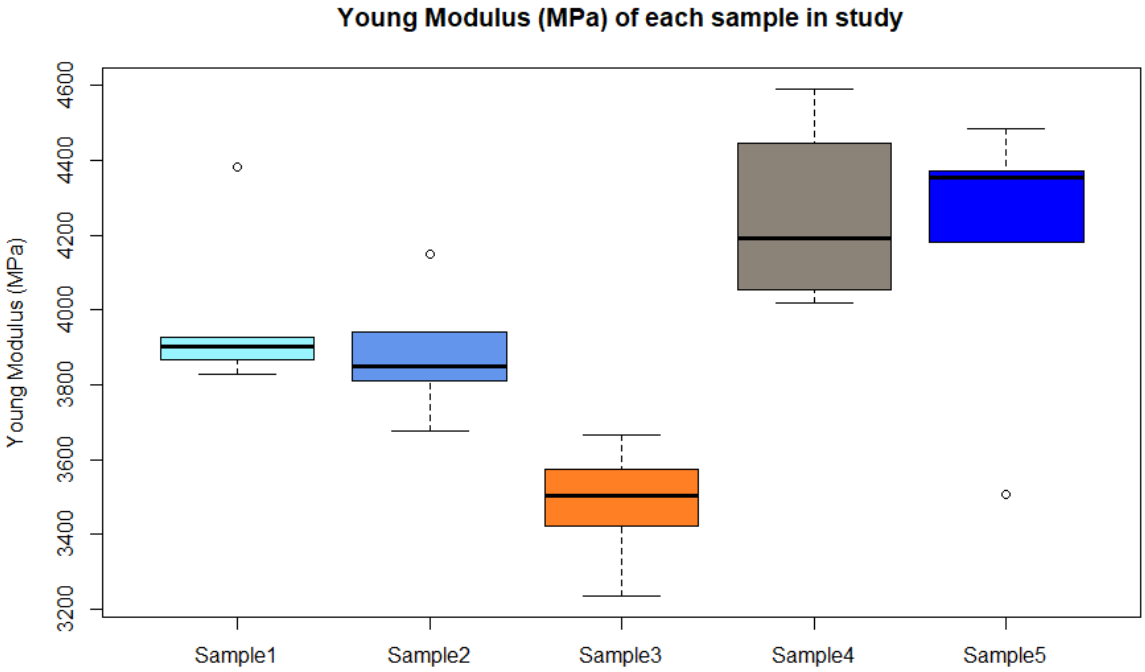

Figure 29- Young modulus (MPa) of each sample in study.

Through **figure 30**, a general perspective of all samples maximum tensile strength is shown. Apparently, samples only containing BOPP have higher tensile strength than BOPP/X samples, meaning that they can withstand a higher amount of stress before fracture. Also, the higher crystallinity of these samples might be responsible for the higher tensile strength[95].

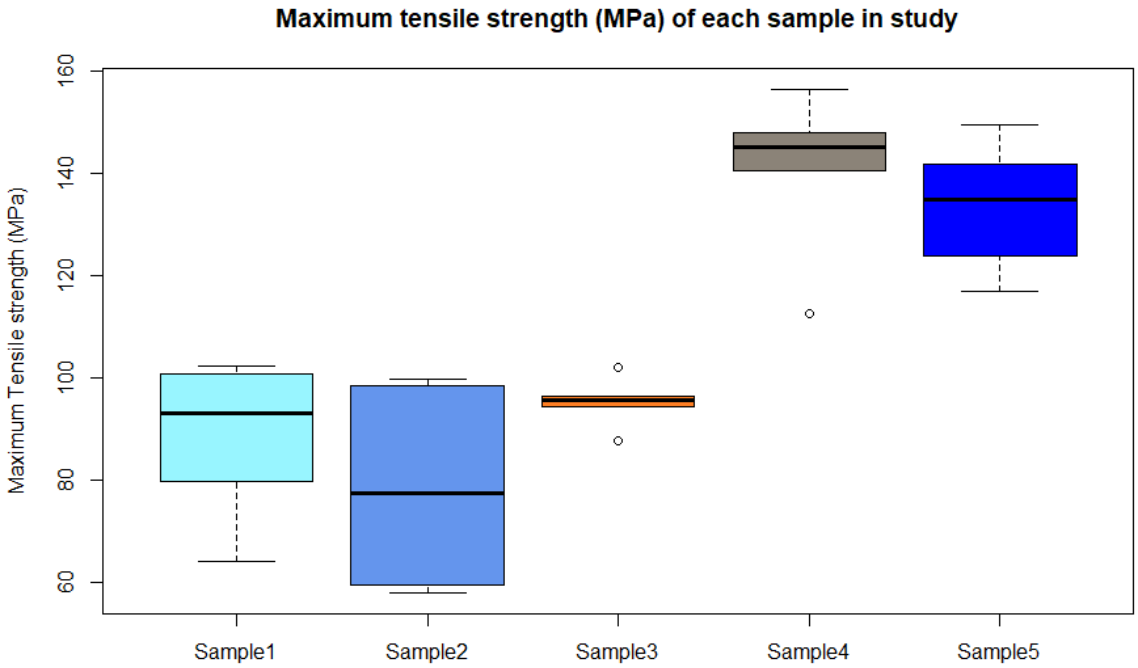

Figure 30- Maximum tensile strength (MPa) of each sample in study.

Figure 31 shows the different samples strain at break. It's clear that the sample 3 has a significantly higher strain at break, having a more ductile behaviour than the remaining samples, meaning that it's capable of achieving higher elongation before being fractured. The higher thickness of sample might be responsible for the higher strain at failure[96]. Also, the lower crystallinity of this sample can also influence its stretching capability[97].

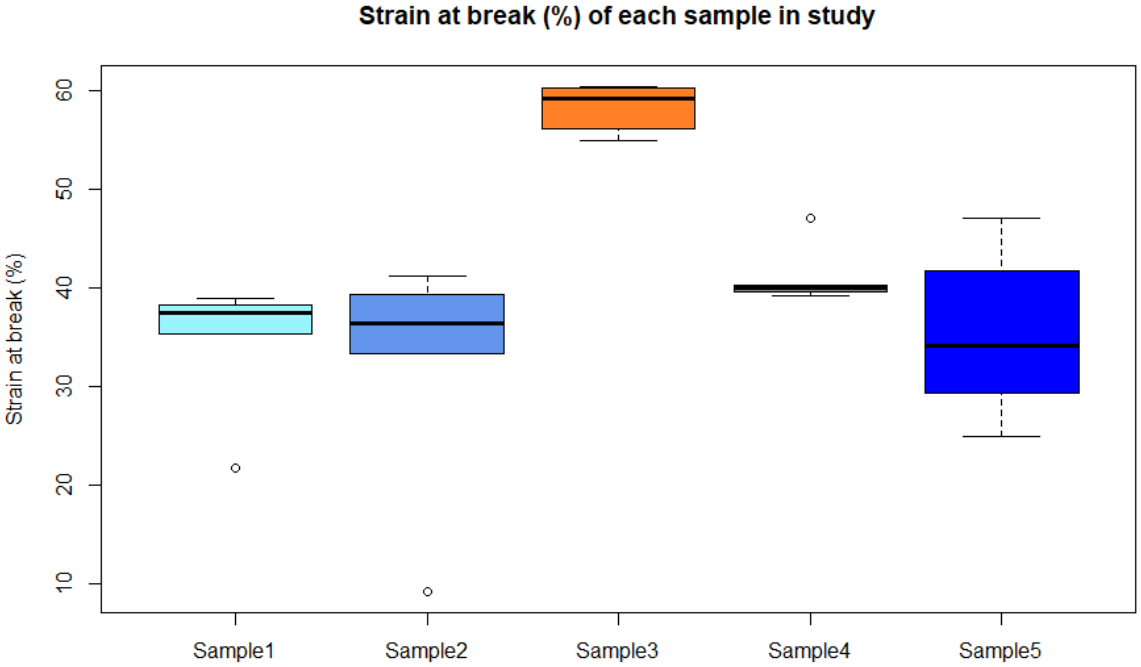

Figure 31- Strain at break (%) of each sample in study.

Through **figure 32** and **figure 33**, it's possible to observe the impact of BOPP modification on the studied mechanical properties. Sample 1 and sample 2 have lower young modulus and lower maximum tensile strength when compared with sample 4 and sample 5, respectively. The addition of compound X on BOPP may lead to an increase in various mechanical properties, such as the Young Modulus and tensile strength, according with previous studies[·]. On the present research, the opposite behaviour was observed. Also, when comparing sample 1 with sample 4, the tensile stress at yield is higher for sample 1, indicating that compound X presence might have a positive effect on this parameter but, comparing sample 2 with sample 5, the opposite behaviour is observed. It would be expected that the tensile strength at yield would be higher in sample 4 than sample 1 due to the higher crystallinity[98]. The modification of BOPP did not promote significant changes in the strain at break parameter.

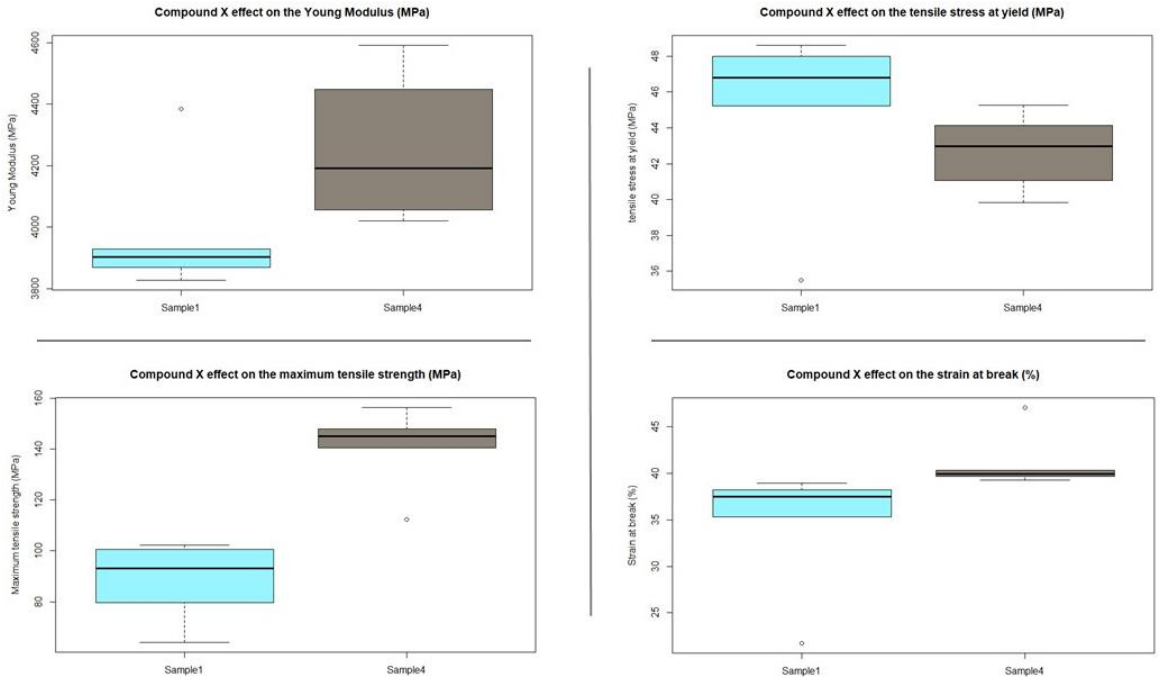

Figure 32- Comparison between sample 1 and sample 4 mechanical properties.

[·] For confidentiality reasons, the studies references will not be shown.

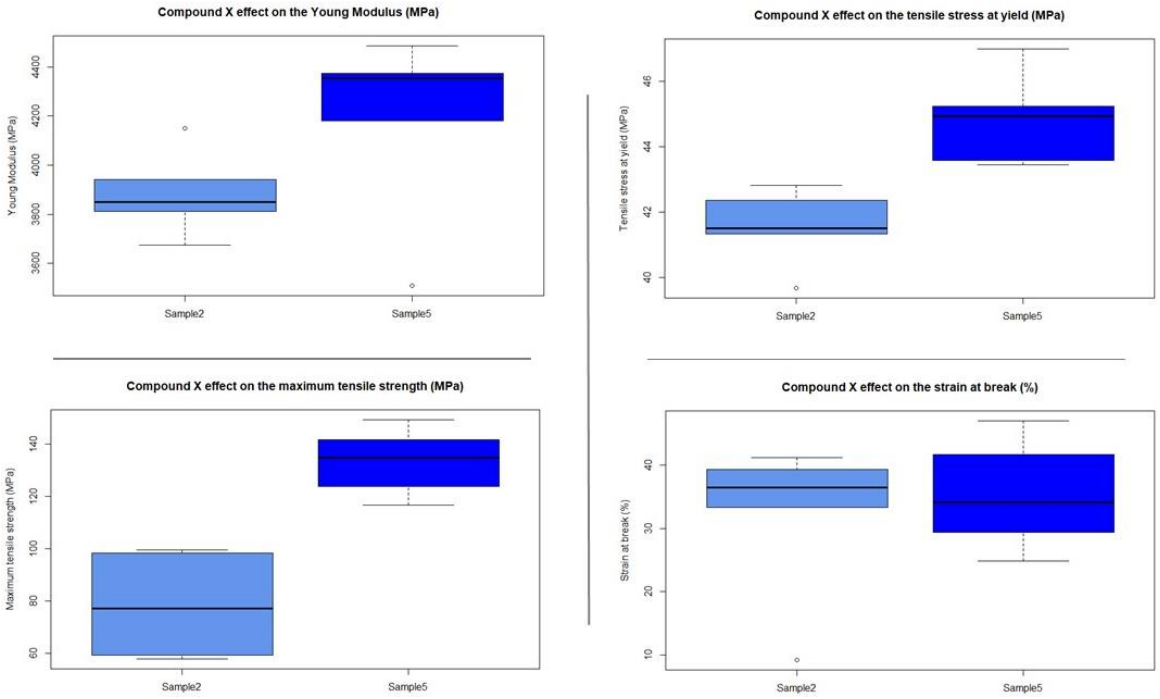

Figure 33- Comparison between sample 2 and sample 5 mechanical properties.

A t-test was performed to check if the observed mechanical properties differences between samples are statistically significant. The results of the t-test are shown in the following **table 13**.

Table 13. Comparison of sample 1 with sample 4 and sample 2 with sample 5 through the statistical t values and respective t-critical values.

	Young Modulus (MPa)		**Tensile strength at yield (MPa)**		**Maximum tensile strength (MPa)**		**Strain at break (%)**	
	Stat t	*T-critical*	*Stat t*	*T-critical*	*Stat t*	*T-critical*	*Stat t*	*T-critical*
Sample 1 vs Sample 4	3.9	2.6	4.1	2.3	8.2	2.3	2.8	3.2
Sample 2 vs Sample 5	8.0	2.3	4.6	2.3	5.6	2.2	0.5	2.4

Through **table 13**, it's possible to see that stat t is higher than T-critical for the young modulus, tensile strength at yield and maximum tensile strength properties, meaning that they're affected by the presence of compound X. On the other hand, comparing the stat t to the T-critical value, the strain at break parameter is not affected by the compound X presence.

To study the thickness effect on the mechanical properties, sample 2 and 3 mechanical results are compared in the following **figure 34**. It's possible to observe that sample 3 has lower young modulus and lower tensile stress at yield than sample 2, indicating a negative effect of thickness on these

parameters. On the other hand, sample 3 has a higher strain at break compared with sample 2. In the case of the maximum tensile strength parameter, sample 2 has a wider variability of the results but no clear differences are observed when compared with sample 3 through t-test.

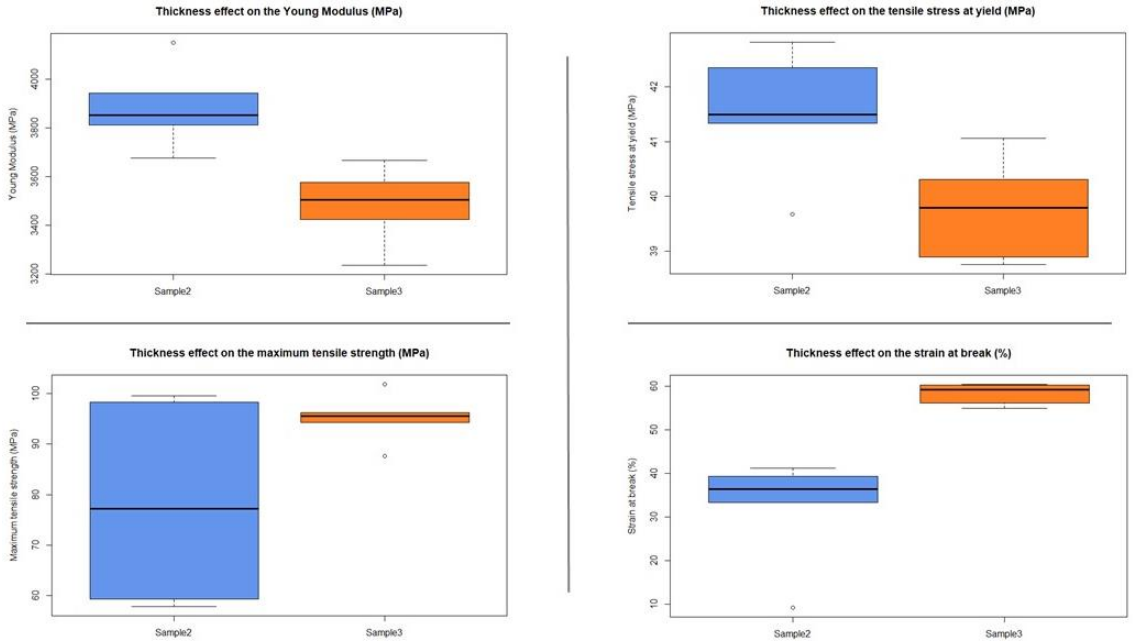

Figure 34- Comparison between sample 2 and sample 3 mechanical properties.

The following **table 14** shows the results of the t-test that was performed at the different mechanical parameters of sample 2 and sample 3.

Table 14. Comparison between sample 2 and sample 3 through the statistical t values and respective t-critical values.

	Young Modulus (MPa)		**Tensile strength at yield (MPa)**		**Maximum tensile strength (MPa)**		**Strain at break (%)**	
	Stat t	*T-critical*	*Stat t*	*T-critical*	*Stat t*	*T-critical*	*Stat t*	*T-critical*
Sample 2 vs Sample 3	4.4	2.3	4.5	2.3	2.0	2.6	10.5	2.3

Through **table 14**, it's possible to see that the differences between sample 2 and sample 3 young modulus, tensile strength and strain at break are statistically significative since stat t is higher than T-critical. On the contrary, no differences are observed in the maximum tensile strength parameter since the value of stat t is inferior to the T-critical value.

To study the metallizer effect on the mechanical properties, sample 1 and 2 mechanical results are compared in the following **figure 35** and sample 4 and sample 5 are compared in **figure 36**.

Looking at both figures, no clear differences are observed in both samples mechanical properties except for the tensile stress at yield of sample 1 which seems to be higher than sample 2.

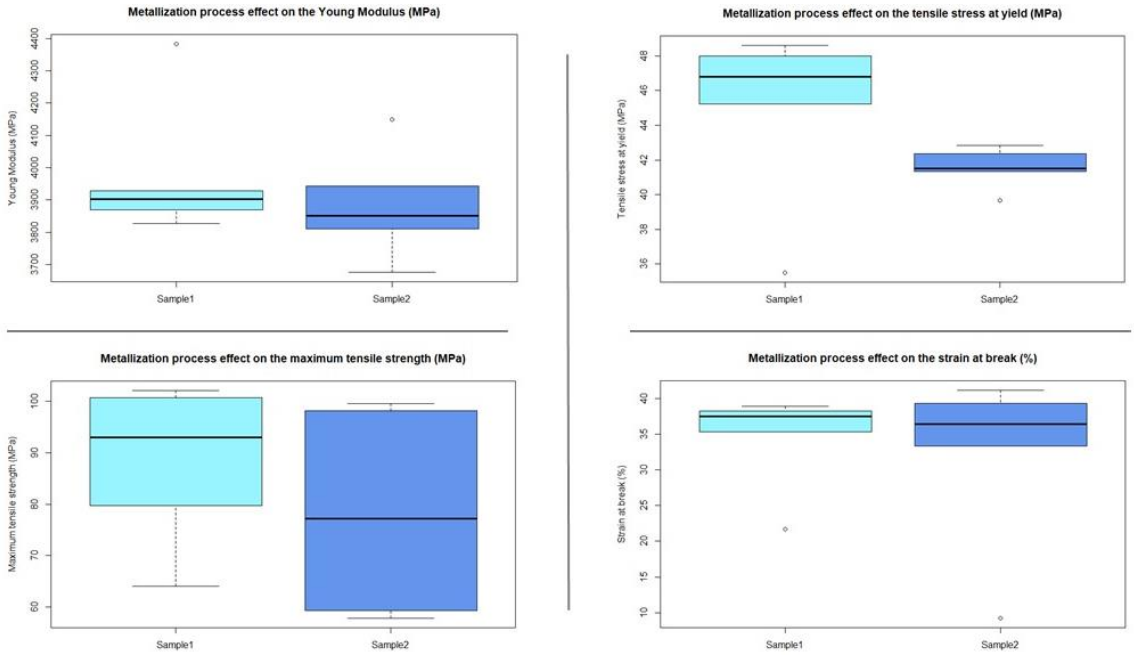

Figure 35- Comparison between sample 1 and sample 2 mechanical properties.

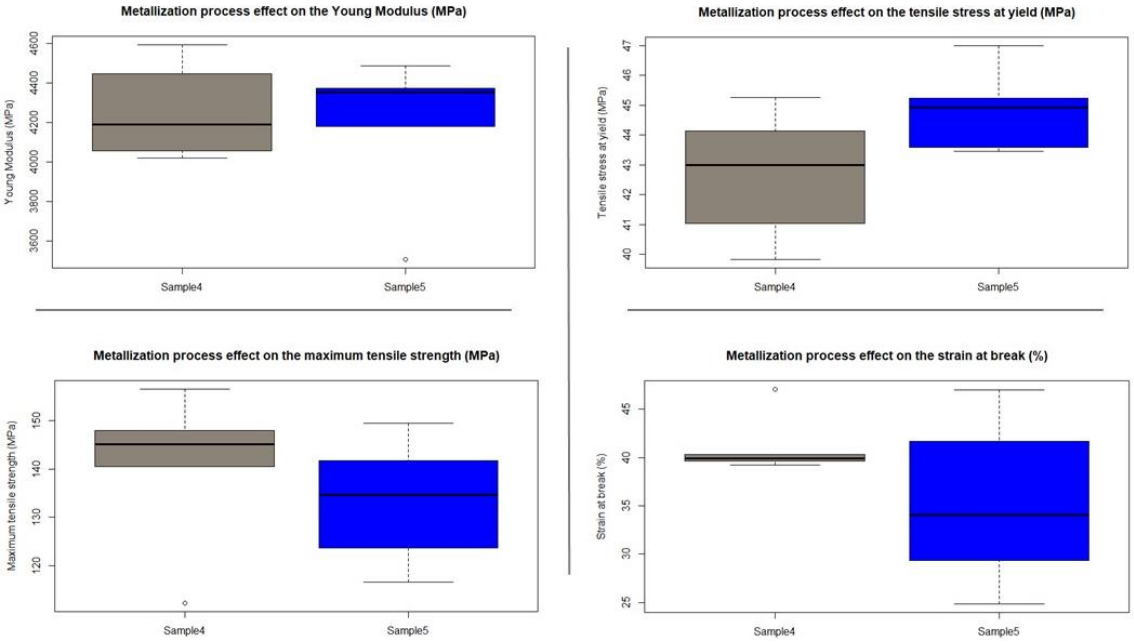

Figure 36- Comparison between sample 4 and sample 5 mechanical properties.

A t-test was again performed to check if the observed mechanical properties differences between samples are statistically significant. The results of the t-test are shown in the following **table 15**.

Table 15. Comparison of sample 1 with sample 2 and sample 4 with sample 5 through the statistical t values and respective t-critical values.

	Young Modulus (MPa)		**Tensile strength at yield (MPa)**		**Maximum tensile strength (MPa)**		**Strain at break (%)**	
	Stat t	*T-critical*	*Stat t*	*T-critical*	*Stat t*	*T-critical*	*Stat t*	*T-critical*
Sample 1 vs Sample 2	1.3	2.3	7.9	2.3	1.0	2.2	0.03	2.4
Sample 4 vs Sample 5	0.9	2.3	2.1	2.2	2.2	2.3	1.1	2.8

Through **table 15**, no significant differences were observed in the young modulus, maximum tensile strength and strain at break between sample 1 and sample 2 and between sample 4 and sample 5 since stat t is lower than T-critical. Concerning the tensile strength at yield parameter, different behaviours were observed. Sample 1 has a substantially higher tensile strength at yield than sample 2, which might indicate that the metallizer A has a positive influence in this mechanical parameter compared with metallizer B. But, comparing sample 4 with sample 5, no statistical differences were observed considering this mechanical parameter.

4.4 SEM

In the present section the morphological aspects of the different samples areas will be discussed. It's clear that, depending on the presence or absence of compound X, different morphologies are observed. In samples 1, 2 and 3, it's possible to observe the presence of long fibers oriented in the machine direction on the different analysed sectors. Also, narrower strands are seen coming out of larger veins such as on sample 1, sector A. This might be a clear evidence of the stretching in transversal direction[99]. **Figure 37** shows, as an example, the different morphological aspects, on sector A, between samples with and without compound X (sample 1 and sample 4, respectively).

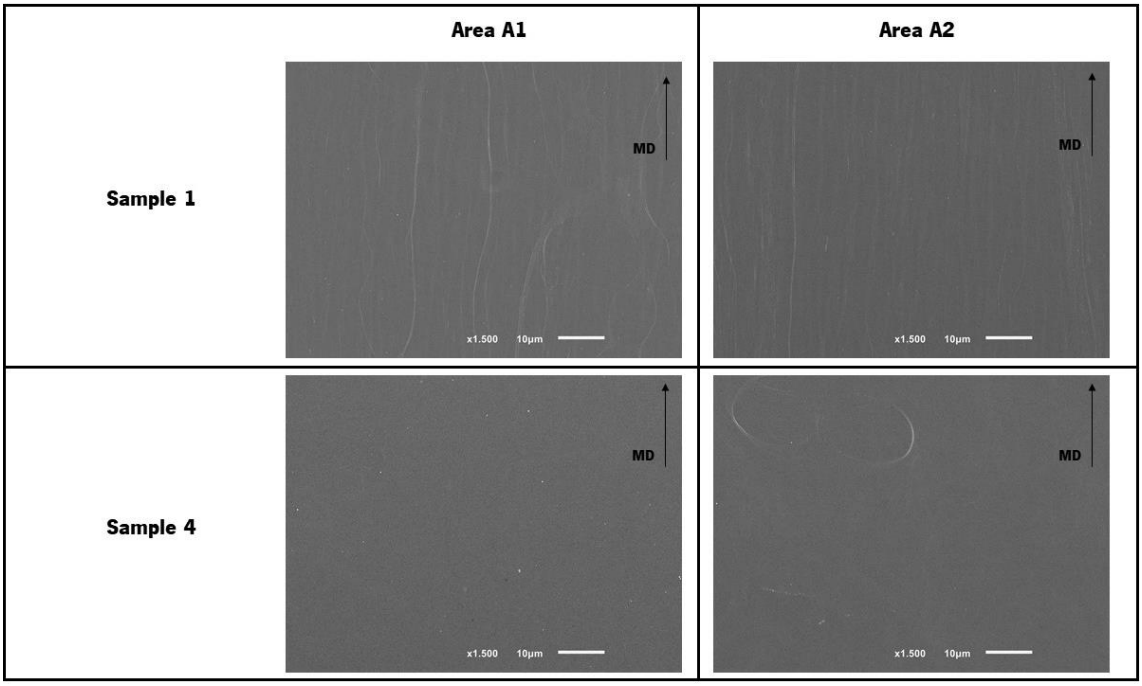

Figure 37- SEM images of sector A, areas A1 and A2, of sample 1 and sample 4.

The addition of compound X in polypropylene might lead to the development of fibrous structures, according with previous studies[·]. In this case, since compound X is present in a lesser quantity than PP, it's possible to assume that these fibers correspond to this compound. Crater-like structures are also formed on these samples. Of all the samples containing compound X, these structures are more easily observed in sample 3. The formation of these craters might be related with the PP crystal dislocation system where stretching causes the lower density β crystals to change into higher density α crystals, leading to the formation of crater-like structures where previously β crystals existed[64,100]. This β to α crystal transition might also promote the formation of microvoids/porosity on the film, influencing its breakdown strength[101]. The fact that these structures are more visible on the thicker sample might be related with the

[·] For confidentiality reasons, the studies references will not be shown.

fact that thicker samples have larger crystal grain sizes and spherulites[100]. The following **figure 38** shows, as an example, the sector B of sample 1, sample 2 and sample 3 where morphological structures such as fibers and craters can be observed.

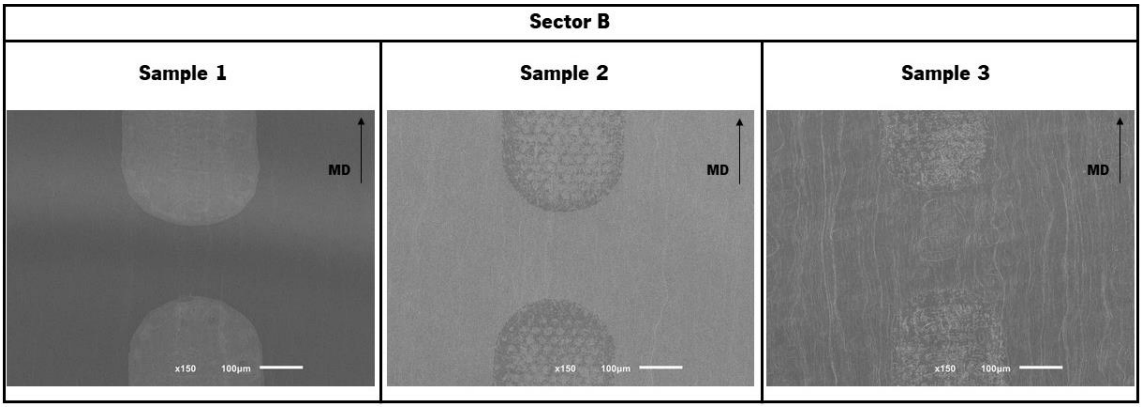

Figure 38- SEM images of the sector B of samples 1, sample 2 and sample 3.

Samples 4 and 5 morphologies consists in crater-like structures only. No long fibrous structures are observed, which reinforces the statement that the fibers correspond to presence of compound X in the samples. Another curious observation is related with the metallization present in the different samples. Samples which suffered a metallization process from metallizer B, have the same metallization pattern, in the form of clusters, on the segmented areas of the film while samples that have been metallized by metallizer A do not show this metallization pattern. This difference in metallization patterns is present in samples with compound X, as its possible to see through **figure 38**, and samples without compound X, which can be observed on the following **figure 39**. The remaining SEM images are present on **annex III** of the present dissertation.

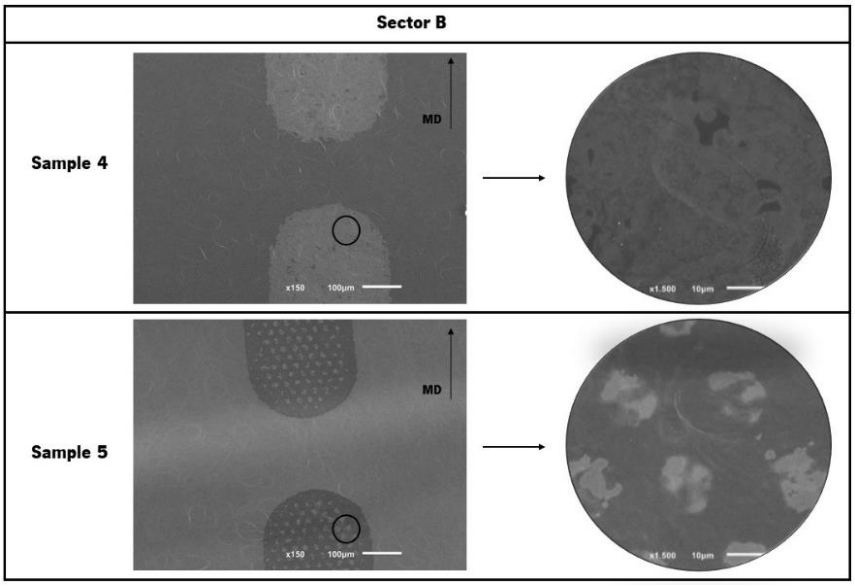

Figure 39- SEM images of the sector B of sample 4 and sample 5.

4.5 EDS

The qualitative and quantitative characterization of the chemical elements present on each study areas was performed through EDS and graphical representation of the results is shown in **figure 40**. The EDS spectrum of the different areas of each sample are present on **annex IV** of the present dissertation.

From the EDS analysis performed on the different samples, five elements were identified such as carbon (C), oxygen (O), gold (Au), aluminium (Al) and Zinc (Zn). The element weight total percentage (Wt%) of each one of these elements is different on the different areas of the sample. The presence of gold (Au) is due to the sample's preparation and will not be considered in the present discussion.

The molecular structure of compound X and PP are composed, mainly, by carbon atoms and this can be observed through EDS analysis results where, on the different areas of each sample, carbon is the main element with a percentual weight varying between 99.6% and 78.4%, with emphasis for area A1 and area B1.

Zinc and aluminium are the metals present on the analysed samples, but their weight and distribution vary across the different areas of the samples. Area A1 doesn't have any metals presents. Low quantities of aluminium (≈1.2 – 1.8 wt%) was detected in the area A2 of the different samples. No metals were detected on area B1 except in sample 1 and sample 2 where very low quantities of aluminium were present (0.5 and 0.6 wt%, respectively). Although metallization clusters were observed in area B1 of samples 2, 3 and 5, only Al was detected on sample 2 but in very low quantities (≈0.6 wt %) and neither aluminium nor zinc were detected in sample 3 and 5. In addition to aluminium, zinc started to be detected in area B2 except for sample 4. Higher quantities of zinc were detected in area C in all samples, ranging between 5.4 to 15.9 wt%. Sample 3 has the higher amount of zinc in area C while sample 2 has the lower amount of zinc although they were both metallized by the same metallizer, which might indicate that the amount of zinc and aluminium present on the different areas of the sample can be optimized according to the client requirements. The addition of a very thin layer of aluminium on the surface of PP dielectric can lead to an increase in the energy density of the capacitor of, approximately, 75% compared with the rated breakdown voltage of the dielectric[102].

Oxygen is also present in the different samples. In fact, like carbon, this element is present in all the analysed areas of the samples, having a more significant presence in the metallized areas, evidencing the oxidation of metal layer of the film. The electrode oxidation, which might have occurred due to atmospheric exposure during storage, can lead to its corrosion, causing capacitance losses of the

capacitor[103,104]. The presence of air between the metallized dielectric layers of the capacitor will also affect its self-healing process capabilities, increasing the duration and area of this process, and provide the required conditions to induce electrochemical corrosion when the capacitor is subjected to AC or pulse electrical field[104]. Nonetheless, higher electrode thickness can be used to supress the oxidation[103] and usually Al/Zn alloy with, higher wt% of zinc, can be used to supress the oxidation of aluminium when under AC[105].

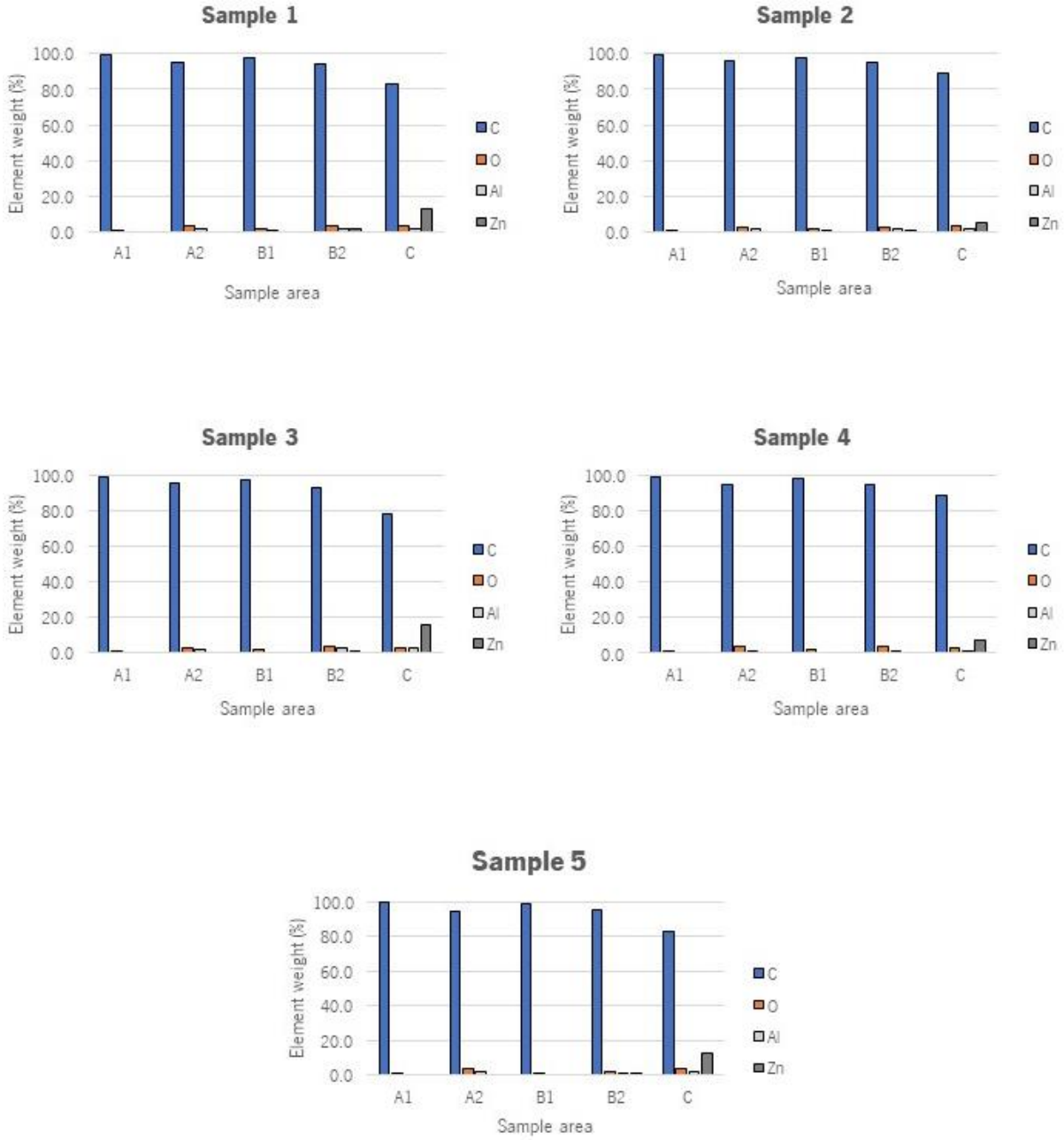

Figure 40- Chemical elements weight distribution along the different areas of the samples in study.

4.6 AFM

The AFM images and surface roughness parameters, of each area of the different samples, are presented from **figures 41** to **45** and **table 16** to **table 20**, respectively. The scanned area corresponds to 25μm². Long fibre structures, mainly oriented in MD, can be observed in samples containing compound X. TD stretching influence on fibres orientation is also visible since they're not perfectly oriented on MD. Some examples of this are sample 2, area A2 and sample 3, areas A2 and B2, where most structures are oriented towards TD. All samples also show a smaller fibre-like network structure forming surface-craters which is the result of biaxially stretching PP cast film as previously mentioned. In sample 1, area A1, sample 2, area B1 and sample 3, area B1, a higher point can be detected which might be a surface defect that was probably created during the film manufacture.

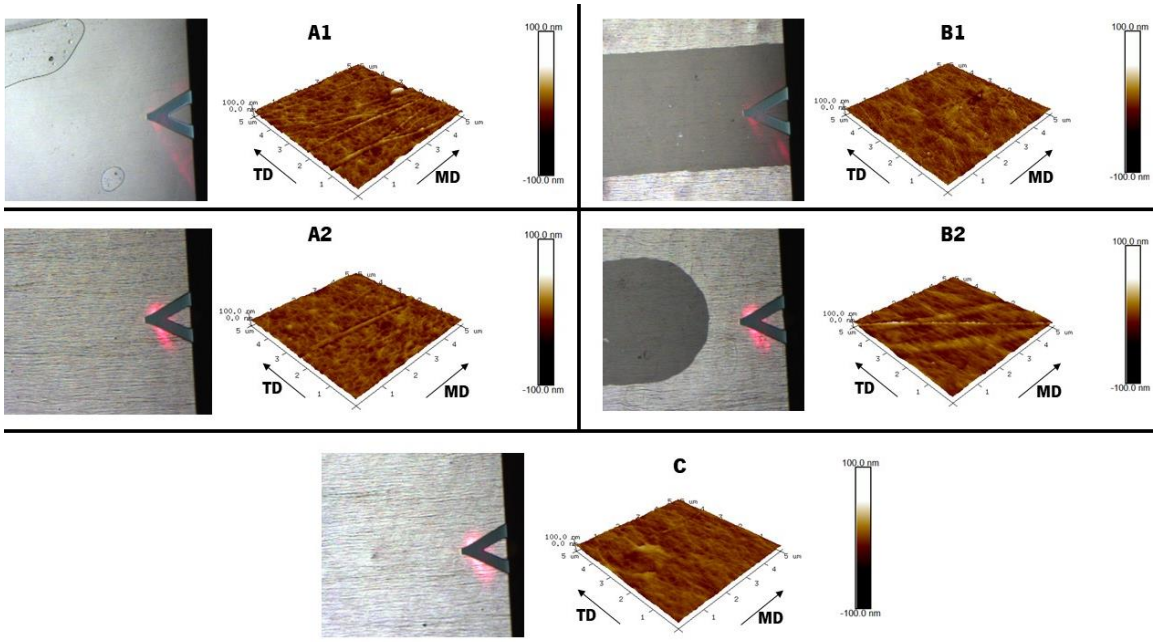

Figure 41- AFM images of the different study areas of sample 1.

Table 16. Surface roughness parameters of each area in study of sample 1 and the standard deviation of each parameter.

Sample 1 areas	A1	A2	B1	B2	C1	σ
Rq (nm)	7.83	6.09	6.98	7.36	5.78	0.86
Ra (nm)	5.87	4.83	5.53	5.71	4.50	0.59
Rmax (nm)	92.40	51.60	86.20	69.00	52.40	18.79

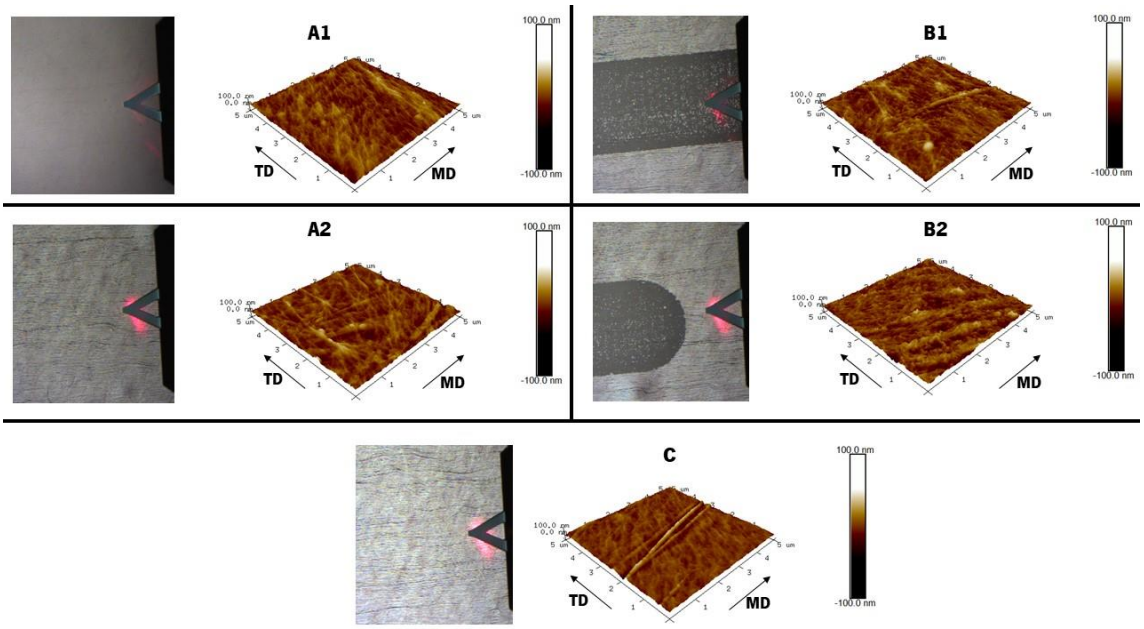

Figure 42- AFM images of the different study areas of sample 2.

Table 17. Surface roughness parameters of each area in study of sample 2 and the standard deviation of each parameter.

Sample 2 areas	A1	A2	B1	B2	C1	σ
Rq (nm)	8.49	8.06	8.82	8.70	6.81	0.82
Ra (nm)	6.73	6.21	6.86	6.75	4.97	0.79
Rmax (nm)	68.60	84.90	85.20	84.80	79.10	7.13

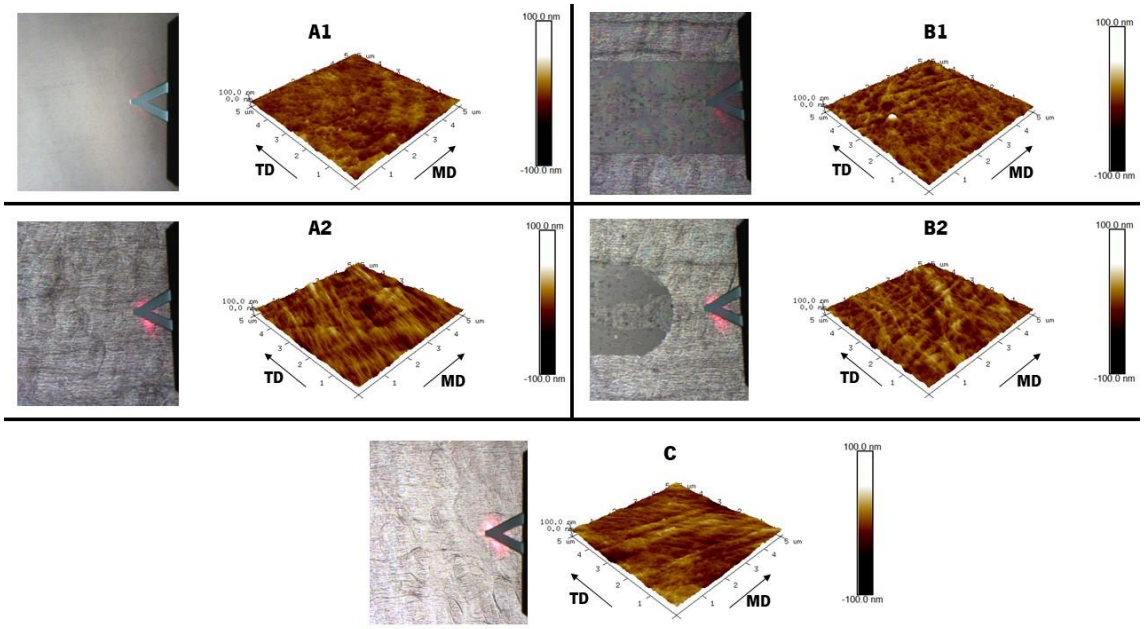

Figure 43- AFM images of the different study areas of sample 3.

Table 18. Surface roughness parameters of each area in study of sample 3 and the standard deviation of each parameter.

Sample 3 areas	A1	A2	B1	B2	C1	σ
Rq (nm)	7.36	10.60	8.93	10.00	10.20	1.31
Ra (nm)	5.76	8.27	6.93	7.96	8.11	1.06
Rmax (nm)	60.30	94.10	106.00	86.60	87.00	16.76

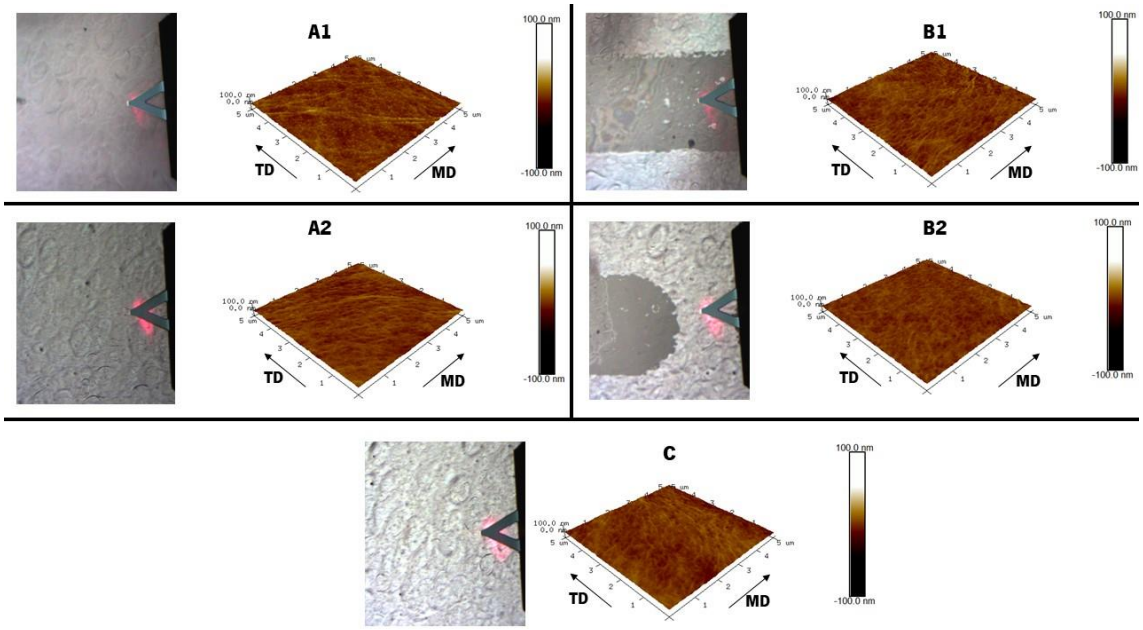

Figure 44- AFM images of the different study areas of sample 4.

Table 19. Surface roughness parameters of each area in study of sample 4 and the standard deviation of each parameter.

Sample 4 areas	A1	A2	B1	B2	C1	σ
Rq (nm)	4.89	4.58	4.71	3.66	4.72	0.49
Ra (nm)	3.81	3.62	3.75	2.91	3.78	0.38
Rmax (nm)	49.30	41.70	43.20	33.50	38.60	5.83

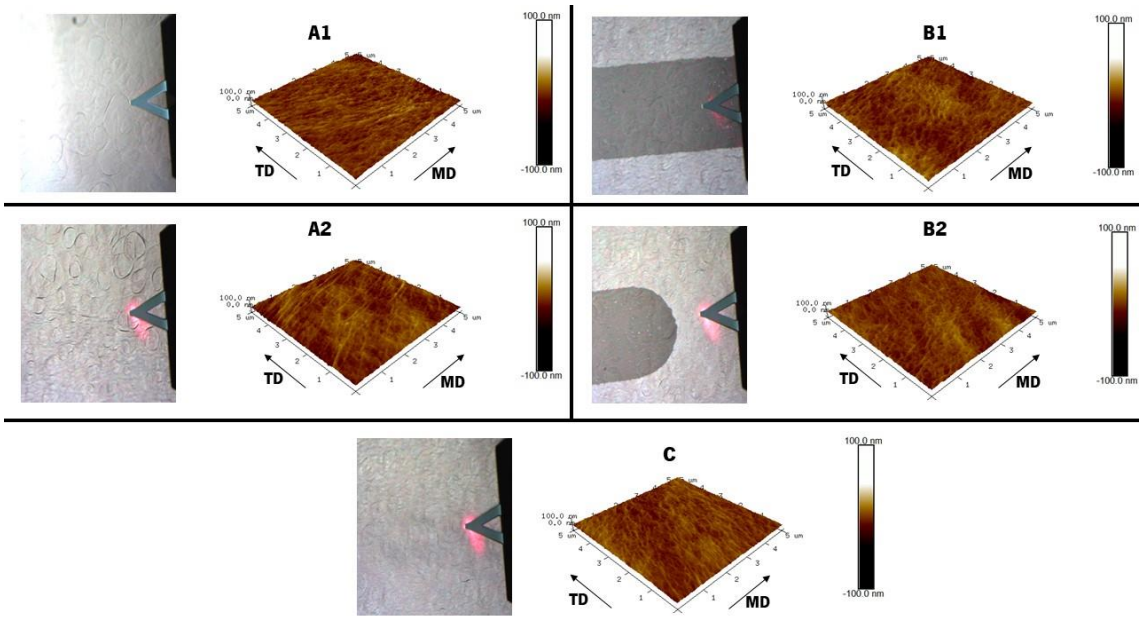

Figure 45- AFM images of the different study areas of sample 5.

Table 20. Surface roughness parameters of each area in study of sample 5 and the standard deviation of each parameter.

Sample 5 areas	A1	A2	B1	B2	C1	σ
Rq (nm)	6.28	6.89	6.67	5.64	5.22	0.70
Ra (nm)	4.91	5.55	5.31	4.42	4.19	0.57
Rmax (nm)	67.70	58.30	57.10	46.50	43.80	9.67

According to the obtained results regarding the AFM analysis and observing **figure 46**, the root means square roughness (Rq) of all samples vary between 3.66 and 10.60nm. Sample 3 has as an overall higher Rq along the different areas of the sample when compared with the remaining samples, except for area A1. It also has the higher variation between all areas, with a standard variation equal to 1.31. Sample 2 has higher Rq values for the different areas when compared with sample 1 but they have similar variations along the different areas. The standard variation between the different areas corresponds to 0.86 for sample 1 and 0.82 for sample 2, having a more uniform topography along the different areas when compared with sample 3. Sample 5 has lower values Rq then sample 1, 2 and 3 except for area A2, where it has a slightly higher Rq than sample 1. The standard deviation between all areas of sample 5 is 0.70, which is lower than sample 1, sample 2 and sample 3. Sample 4 is the sample in with the lowest Rq values in all areas. It also has the lowest standard deviation of Rq (0.49) between the different areas, meaning that it presents a more uniform topography along the different areas. The same behaviour can be observed through the obtained average roughness (Ra) values (**figure 47**).

Comparing the obtained Ra values with the typical Ra values for capacitor applications (0.1 - 0.9 µm)[101], they're acceptable.

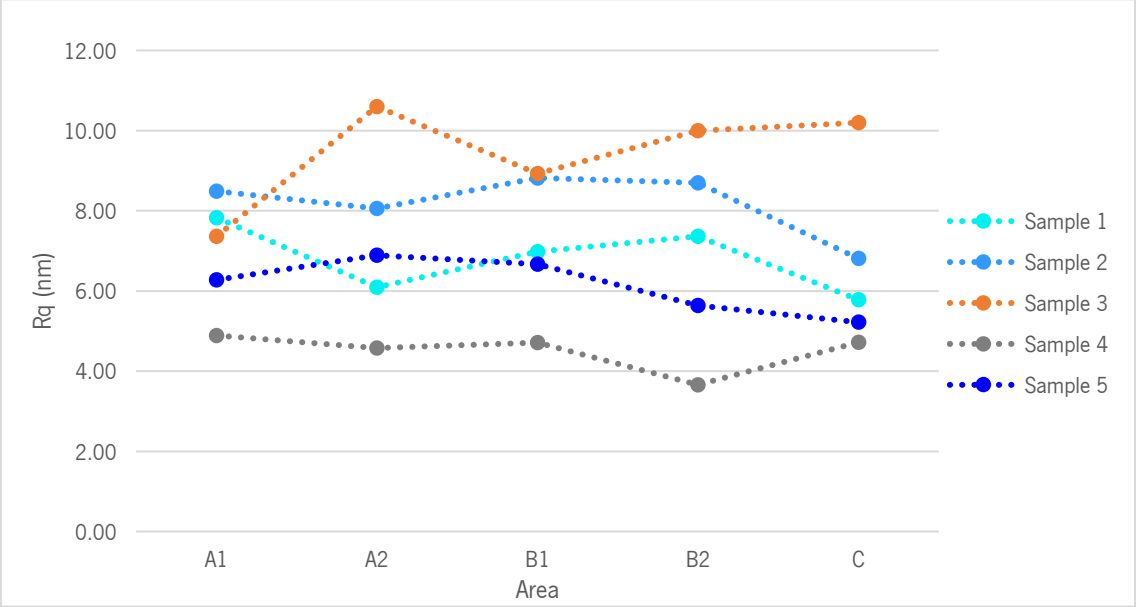

Figure 46- Rq value along the different areas of each sample.

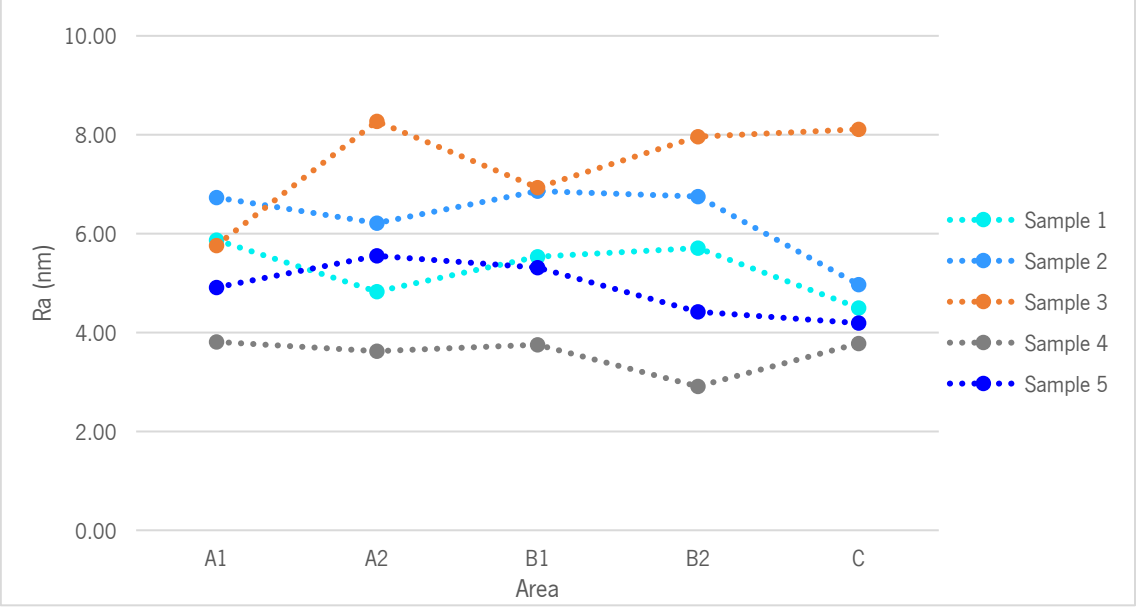

Figure 47- Ra values along the different areas of each sample.

Through **figures 48** and **49**, it's possible to observe that the presence of compound X led to an overall higher Rq and Ra, respectively, on all the analysed areas.

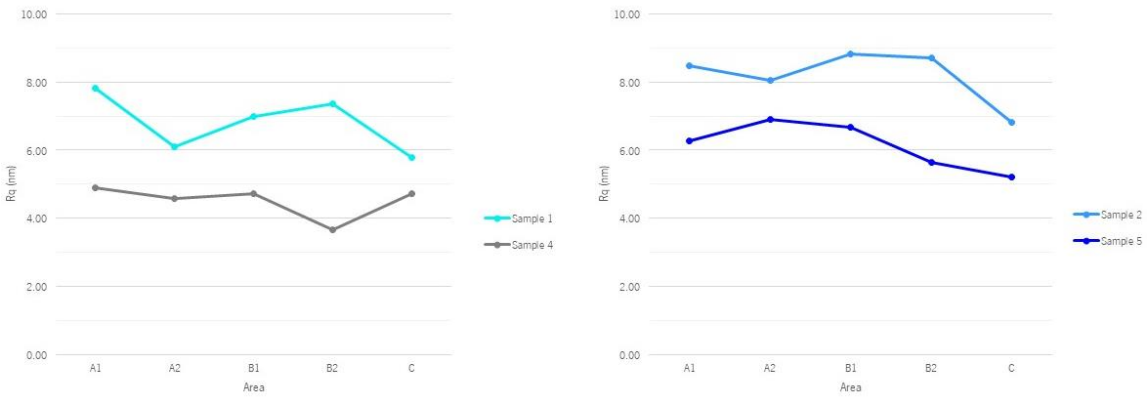

Figure 48- Base film effect on the Rq values.

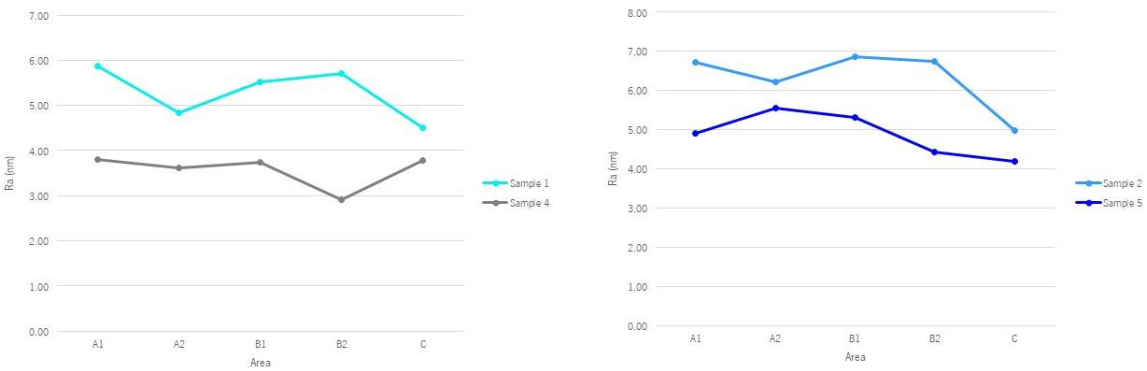

Figure 49- Base film effect on the Ra values.

According to **figures 50** and **51**, samples with greater thickness, such as sample 3, have an overall higher Rq and Ra values than samples with lesser thickness, respectively. Sample 3 is also less homogeneous since a higher standard variation value (σ (Rq) =1.31 and σ (Ra) =1.06) was obtained compared with sample 2 (σ (Rq) =0.82 and σ (Ra) =0.79).

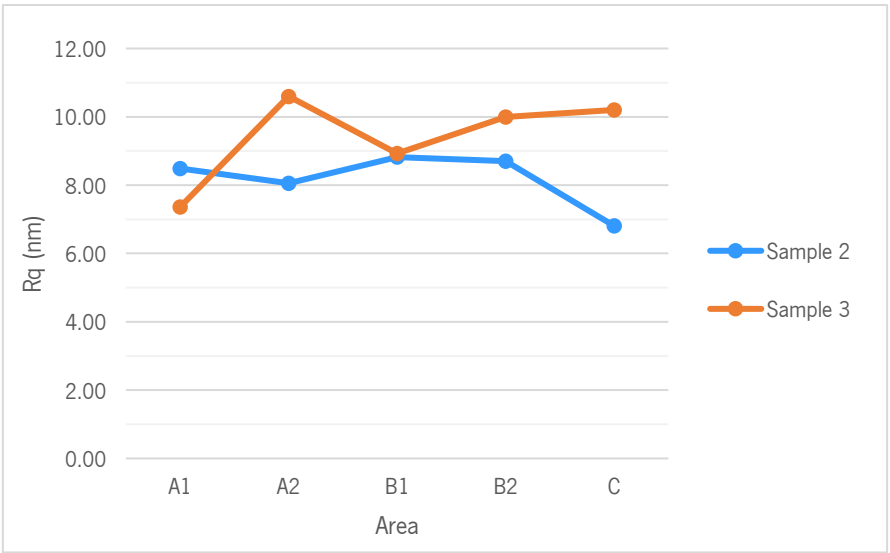

Figure 50- Thickness effect on the Rq values.

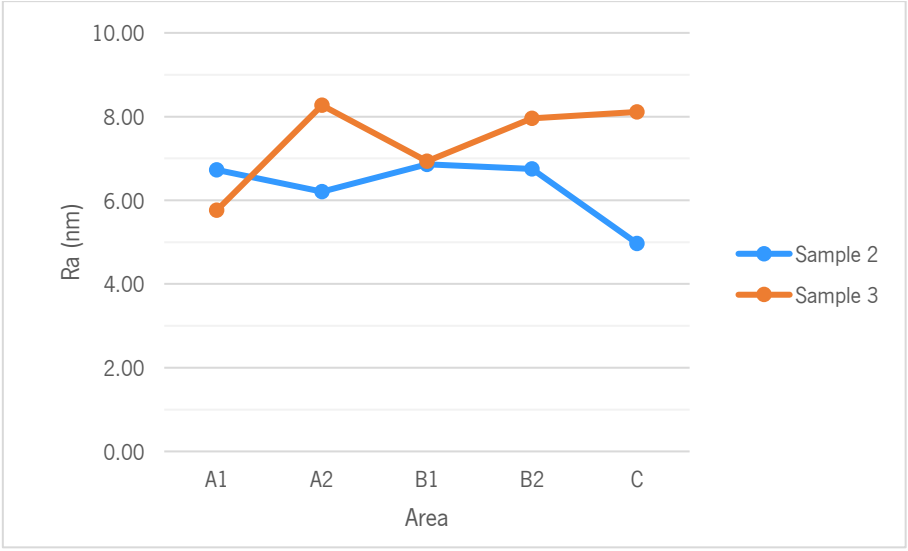

Figure 51- Thickness effect on the Ra values.

Analysing the following **figures 52** and **53**, it's possible to understand what effect the type of metallizer has in the Rq and Ra of samples with similar thickness and same base film. It's possible to observe that samples that have been metallized through metallizer A (sample 1 and sample 4) have an overall lower Rq and Ra values on all areas than samples that were metallized from metallizer B (sample 2 and sample 5).

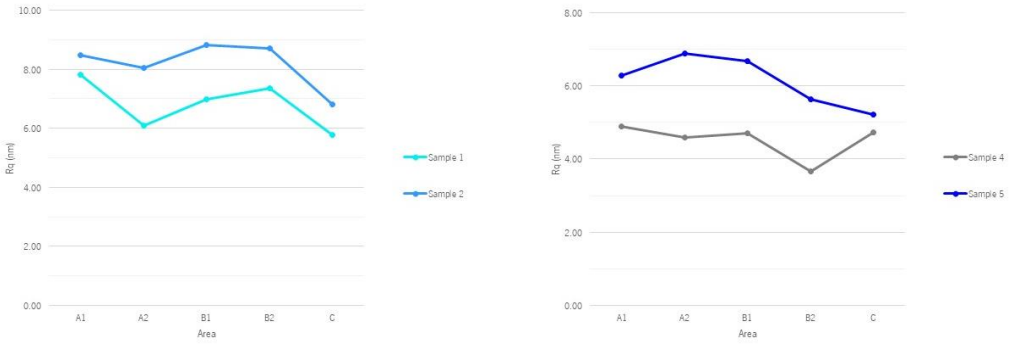

Figure 52- Metallizer effect on the samples Rq.

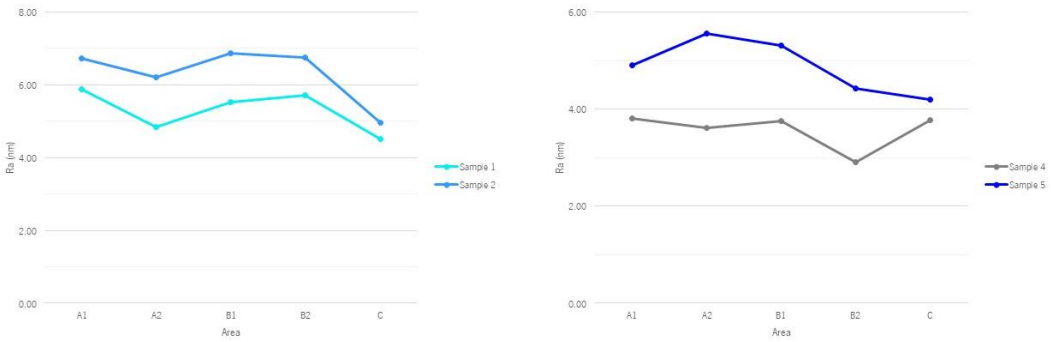

Figure 53- Metallizer effect on the samples Ra.

The roughness of a film influences the correct junction between the metallic layer and the dielectric. Higher roughness can lead to a non-conforming contact between these layers, promoting the appearance of air gaps. These gaps have an active participation during the higher voltages breakdown processes where partial discharges occur, leading to the occurrence of more self-clearing processes in capacitors, reducing its capacitance[106]. Also, the presence of surface defects on the dielectric may negatively affect its voltage withstanding capability, that is, reduces its dielectric strength[106]. At the same time, a certain amount of roughness is needed for some capacitor manufacturing such as the winding of film during metalization[101].

4.7 Shrinkage

The results regarding the shrinkage of the films in TD and MD, along the different temperature range, are presented in the following **table 21** and **table 22**, respectively. The graphical representation of the shrinkage behaviour in TD and MD is presented on **figures 54** and **55**, respectively.

Table 21- TD shrinkage (%) obtained for the different samples, using equation 9, throughout the the temperature range of 25-125°C.

T (°C)	TD shrinkage (%)				
	Sample 1	**Sample 2**	**Sample 3**	**Sample 4**	**Sample 5**
25	0.00	0.00	0.00	0.00	0.00
70	-0.01	0.23	0.06	0.06	-0.04
85	-0.04	0.09	0.00	-0.45	0.00
105	-0.21	-0.42	-0.36	-0.74	-0.21
110	-0.29	-0.17	-0.24	-1.09	-0.69
125	-0.32	-1.07	-0.31	-1.90	-2.15

Sample 3 suffered the lowest TD shrinkage during the exposure to the temperature range, having a shrinkage of, approximately, -0.31%. It was followed by sample 1 and sample 2 which had TD shrinkages of -0.32% and -1.07%, respectively. Sample 4 and sample 5 had the most TD shrinkage, reaching values of, approximately, -2%. The positive values present on **table 26** might probably correspond to random errors produced during the measurements of the different samples.

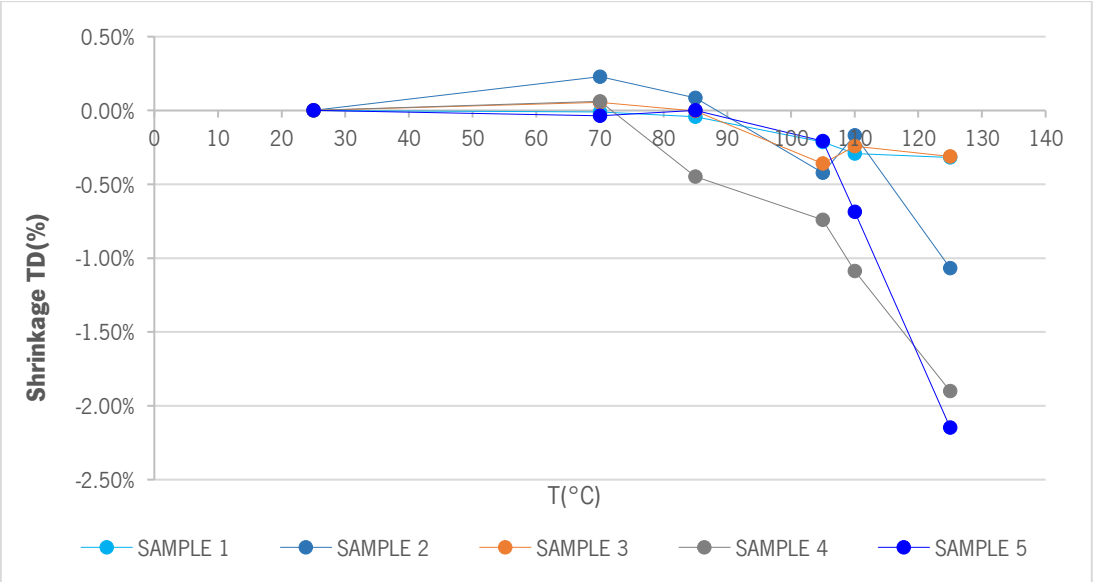

Figure 54- TD shrinkage (%) of the different samples between a temperature range of 25-125°C.

Table 22- MD shrinkage (%) obtained for the different samples, using equation 9, throughout the the temperature range of 25-125°C.

T (°C)	MD shrinkage (%)				
	Sample 1	Sample 2	Sample 3	Sample 4	Sample 5
25	0.00	0.00	0.00	0.00	0.00
70	-0.05	-0.10	0.10	-0.70	0.12
85	-0.26	-0.28	-0.22	-0.73	-0.23
105	-0.78	-0.82	-0.48	-1.29	-1.02
110	-0.92	-0.95	-0.46	-2.10	-1.31
125	-1.67	-1.52	-1.05	-2.73	-2.47

The sample that had the least MD shrinkage (%) at the 125°C was sample 3 (-1.05%), followed by sample 2 and sample 1 with MD shrinkage values of -1.52% and -1.67%, respectively. Sample 4 and 5 had the highest recorded MD shrinkage values, standing between 2.50-2.70%, approximately.

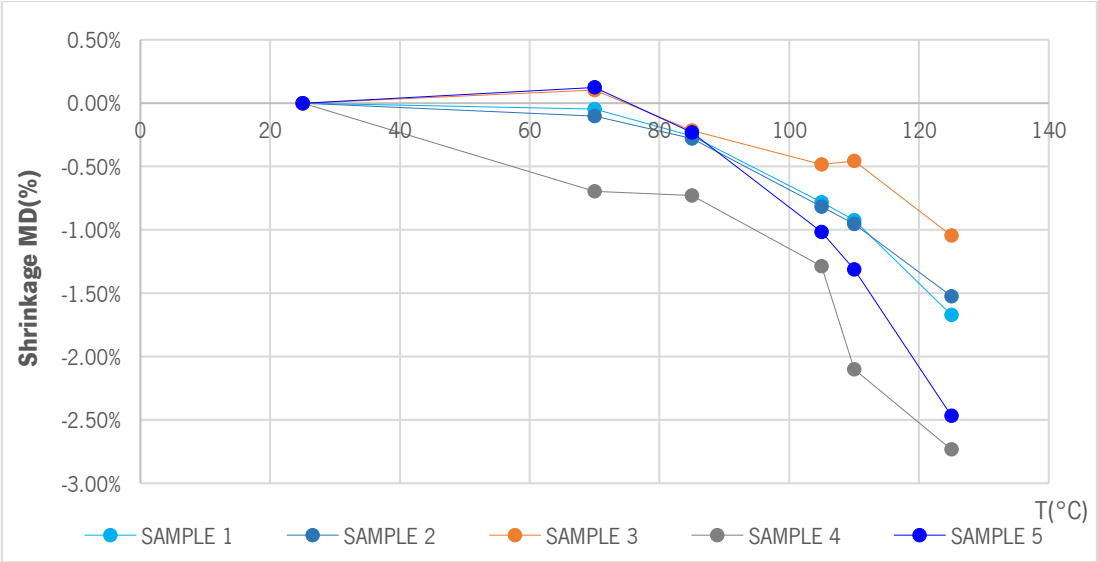

Figure 55- MD shrinkage (%) of the different samples between a temperature range of 25-125°C.

According to the shrinkage results in both TD and MD, it's clear that samples containing compound X have a better performance in high temperature, in terms of dimensional stability, when compared with samples that only contain BOPP. According to previous studies[·], this behaviour was expected since the presence of compound X tends to increase the dimensional stability of PP films when exposed to elevated temperatures. All samples suffered greater shrinkage in MD than TD.

The preferable shrinkage of BOPP films for MD and TD are comprehended between 1.8 – 2.5% at a temperature of 120°C[107]. At 125°C, the obtained values are within this range except the MD shrinkage of sample 4 (-2.73%).

The results also show that the sample 3 greater thickness had a positive effect on the shrinkage, leading to reduced values in TD and MD when compared with sample 2. The metallization effect does not seem to influence the obtained results since different since different behaviours are observed depending on the shrinkage direction. Considering TD, samples with the same thickness and base film that suffered a metallization process from metallizer A seem to suffer slightly lower shrinkage than samples with the same thickness and base film metallized from metallizer B. On the contrary, when analysing the results on MD, the opposite behaviour is observed, where samples metallized by metallizer B suffer lower shrinkage when compared with samples metallized by metallizer A.

In capacitors, the shrinkage of films is needed in a manufacturing perspective where a heat treatment is applied to the film so that they gain more tightness. Subjecting the film to exceeding

[·] For confidentiality reasons, the studies references will not be shown.

temperatures may lead to excessive shrinkage of film which can cause reduction of the capacity of the capacitor or even destruction of the film[107].

Chapter 5 - Conclusions

Several techniques were used to study the different samples in terms of calorimetry, morphology, chemical structure, mechanical performance, surface roughness and dimensional stability towards a high temperature exposure. Many differences were observed depending on the base film, thickness and metallizer process used in the samples.

Unmodified films possess a higher crystallinity and enthalpy energies regarding the melting and crystallization than samples where compound X was present, which might demonstrate the amorphous nature of this compound. Also, according with the melting temperature of the second scan, it was possible to verify that all samples contain commercial iPP. The main melting peak that probably corresponds to the melting of the α-phase crystal structure while the subtle peak around 150°C can be due to the melting of the β-phase. The increased thickness sample 3 led to a reduced crystallinity. No effect was observed regarding the type of metallizer at which the sample was submitted.

Through FTIR-ATR, polypropylene characteristic peaks were detected in all samples. Sample 1, 2 and 3 spectra did not show any clear evidence of compound X presence. This might be due to the low quantity of this material present on these samples which might be below the equipment detection limit.

The mechanical test showed an increased young modulus on samples that doesn't contain compound X in which the increased crystallinity of sample 4 and sample 5 might be responsible for this behaviour. Sample 3 had the lowest young modulus value in which its higher thickness and lower crystallinity can explain this observation. Samples with compound X also have a lower maximum tensile strength than simple BOPP samples. In terms of strain at break, thickness had a positive effect on this parameter since longer strains were obtained for sample 3. Through t-test method, it was possible to conclude that the presence of compound X on BOPP/X significantly affected the young modulus, tensile stress at yield and maximum tensile strength while strain at break parameter wasn't, statistically, affected. The thickness had significant effect on all studied parameters except the maximum tensile strength. Regarding the metallizer effect, the results show that this factor does not affect the young modulus, maximum tensile strength and strain at break parameters, but no clear trend was observed regarding the tensile strength at yield.

SEM evidenced different morphologies regarding the type of base film. Sample 1, 2 and 3 possess long fibres oriented in machine direction and crater-like structures on all the studied sectors. The fibres might correspond to the presence of compound X. The crater-like structures are related to the PP crystal dislocation system occurred during the stretching of the films were lower density β crystals change into α crystals. Sample 4 and 5 possess a crater-like surface structures and no fibers were observed since only PP is present. Sample 3 structures were clearer and easier to be observed which might be due to the larger crystals grain sizes and spherulites due to its higher thickness. It was possible to distinguish the metallizer through this technique since metallizer B produced metallized clusters along the segments of the films that were absent on samples metallized through metallizer A.

Through EDS technique, elements such as carbon, oxygen, aluminium, and zinc were detected in all samples. The wt% of these elements is different along the different studied sectors. Carbon was the element present in higher quantity since PP and compound X are molecularly composed by carbon and hydrogen. The presence of oxygen, mainly on metallized areas, are a result of oxidation that might have occurred during atmospheric exposure during storage of the samples. The fact that Al and Zn only appeared on certain areas and with different wt% regarding the same metallizer shows that the metallization process can be optimised according to the client requirements.

The surface roughness of samples, that were analysed through AFM, are different depending on the base film, thickness and metallizer of the samples. The addition of compound X led to an increased surface roughness when compared with samples 4 and 5. Sample 3 had the higher roughness of all samples on almost all areas, which might be due to the higher thickness of this sample. Samples metallized through metallizer A have lower surface roughness on all areas when compared with samples metallized through metallizer B.

Regarding the dimensional stability of the samples subjected to a thermal gradient, it's clear that depending on the base film and thickness of the samples, different shrinkage behaviours are observed. Samples containing compound X have a better shrinkage performance in machine direction and transverse direction than samples containing only PP at 125°C. Sample 3 had the best performance, indicating that higher shrinkage has a positive effect on dimensional stability of the film when subjected to a high thermal environment. All samples suffered greater shrinkage in MD than TD.

References

(1) Vishay. *History - We believe our past powers our future*. https://jobs.vishay.com/content/History/?locale=en_US (accessed 2022-01-03).

(2) Vishay. *Applications | Vishay*. https://www.vishay.com/applications/ (accessed 2022-01-03).

(3) Vishay. *Quality and Environmental | Vishay*. https://www.vishay.com/quality/ (accessed 2022-01-03).

(4) Vishay. *Vishay Intertechnology Mourns the Loss of Its Founder, Dr. Felix Zandman*. VISHAY INTERTECHNOLOGY MOURNS THE LOSS OF ITS FOUNDER, DR. FELIX ZANDMAN. https://ir.vishay.com/news/news-details/2011/Vishay-Intertechnology-Mourns-the-Loss-of-Its-Founder-Dr-Felix-Zandman/default.aspx (accessed 2022-01-03).

(5) Carvalhal, D. Caracterização iónica de resinas epóxi utilizando técnicas cromatográficas. Dissertação de Mestrado, Universidade do Minho, 2019.

(6) International Organization for Standardization. *Occupational health and safety management systems — Requirements with guidance for use (ISO 45001:2018)*. ISO. https://www.iso.org/cms/render/live/en/sites/isoorg/contents/data/standard/06/37/63787.html (accessed 2022-03-31).

(7) International Organization for Standardization. *Environmental management systems — Requirements with guidance for use (ISO 14001:2015)*. ISO. https://www.iso.org/cms/render/live/en/sites/isoorg/contents/data/standard/06/08/60857.html (accessed 2022-03-31).

(8) International Organization for Standardization. *Quality management systems — Requirements (ISO 9001:2015)*. ISO. https://www.iso.org/cms/render/live/en/sites/isoorg/contents/data/standard/06/20/62085.html (accessed 2022-03-31).

(9) International Automotive Task Force. *About – International Automotive Task Force*. https://www.iatfglobaloversight.org/iatf-169492016/about/ (accessed 2022-03-31).

(10) Santos, S. Characterization of metallized polypropylene films. Dissertação de Mestrado, Universidade do Minho, 2021.

(11) Kemet Corporation. *Introduction to Capacitor Technologies*; Technical document; 2013; p 16.

(12) Lima, A. B. P. de. Study of the Tightness of the Metallization Used on Top of a Thin Film Capacitor Cell. Dissertação de Mestrado, Universidade do Minho, 2015.

(13) Kuriakose, A. *Parallel Plate Capacitors and Their Properties*; Scholarly project (Electronics-Electromagnetism); Ahmedabad University, 2020; p 19.

(14) TDK Corporation. Film Capacitors - General Technical Information. **2018**, 41.

(15) Ling, S.; Sanny, J.; Moebs, W. Chapter 8 - Capacitance. In *University physics*; 2016; Vol. 2, p 339.

(16) Hartlein, R.; Hampton, N.; Perkel, J.; Hernandez, J.; Elledge, S.; del Valle, Y.; Grimaldo, J.; Deku, K. *Applying Diagnostics to Enhance Cable System Reliability (Cable Diagnostic Focused Initiative, Phase II)*; 2016; pp 162–163. https://doi.org/10.2172/1255949.

(17) Roederstein, V. Radio Interference Supression Capacitors. In *General Technical Information*; 2002; p 7.

(18) Schimanski, T. High-Performance Polypropylene Structures for Eco-Friendly, Fully Recyclable Composites. PhD Thesis, Technische Universiteit Eindhoven, 2002.

(19) Maddah, H. Polypropylene as a Promising Plastic: A Review. *2163-1352* **2016**, *2016*, 1–11. https://doi.org/10.5923/j.ajps.20160601.01.

(20) Raka, L.; Bogoeva-Gaceva, G. CRYSTALLIZATION OF POLYPROPYLENE: APPLICATION OF DIFFERENTIAL SCANNING CALORIMETRY PART II. CRYSTAL FORMS AND NUCLEATION. *Contrib. Sect. Nat. Math. Biotech. Sci.* **2017**, *29* (1–2). https://doi.org/10.20903/csnmbs.masa.2008.29.1-2.14.

(21) Gopanna, A.; Thomas, S. P.; Rajan, K. P.; Rajan, R.; Rainosalo, E.; Zavašnik, J.; Chavali, M. Investigation of Mechanical, Dynamic Mechanical, Rheological and Morphological Properties of Blends Based on Polypropylene (PP) and Cyclic Olefin Copolymer (COC). *Eur. Polym. J.* **2018**, *108*, 439–451. https://doi.org/10.1016/j.eurpolymj.2018.09.030.

(22) Heath, D. E.; Cooper, S. L. Polymers: Basic Principles. In *Biomaterials Science: An Introduction to Materials in Medicine*; Elsevier, 2013; pp 64–79. https://doi.org/10.1016/B978-0-08-087780-8.00008-5.

(23) Sastri, V. R. 6 - Commodity Thermoplastics: Polyvinyl Chloride, Polyolefins, and Polystyrene. In *Plastics in Medical Devices (Second Edition)*; Sastri, V. R., Ed.; William Andrew Publishing: Oxford, 2014; pp 73–120. https://doi.org/10.1016/B978-1-4557-3201-2.00006-9.

(24) Raka, L.; Bogoeva-Gaceva, G. CRYSTALLIZATION OF POLYPROPYLENE: APPLICATION OF DIFFERENTIAL SCANNING CALORIMETRY PART I. ISOTHERMAL AND NON-ISOTHERMAL CRYSTALLIZATION. *Contrib. Sect. Nat. Math. Biotech. Sci.* **2017**, *29* (1–2). https://doi.org/10.20903/csnmbs.masa.2008.29.1-2.13.

(25) Baur, E.; Osswald, T. A.; Rudolph, N. 5 - Plastic Materials. In *Plastics Handbook - The resource for plastic engineers*; Baur, E., Osswald, T. A., Rudolph, N., Eds.; Hanser, 2019; pp 337–578. https://doi.org/10.3139/9781569905609.005.

(26) Galli, P.; Danesi, S.; Simonazzi, T. Polypropylene Based Polymer Blends: Fields of Application and New Trends. *Polym. Eng. Sci.* **1984**, *24* (8), 544–554. https://doi.org/10.1002/pen.760240807.

(27) Meer, D. W. van der. Structure-Property Relationships in Isotactic Polypropylene: The Influence of Chain Architecture and Nucleation on Crystallization, Morphology and Mechanical Properties, Twente University Press, Enschede, 2003.

(28) Shubhra, Q. T.; Alam, A.; Quaiyyum, M. Mechanical Properties of Polypropylene Composites: A Review. *J. Thermoplast. Compos. Mater.* **2013**, *26* (3), 362–391. https://doi.org/10.1177/0892705711428659.

(29) Kotek, J.; Kelnar, I.; Baldrian, J.; Raab, M. Tensile Behaviour of Isotactic Polypropylene Modified by Specific Nucleation and Active Fillers. *Eur. Polym. J.* **2004**, *40* (4), 679–684. https://doi.org/10.1016/j.eurpolymj.2003.12.004.

(30) Kotek, J.; Kelnar, I.; Baldrian, J.; Raab, M. Structural Transformations of Isotactic Polypropylene Induced by Heating and UV Light. *Eur. Polym. J.* **2004**, *40* (12), 2731–2738. https://doi.org/10.1016/j.eurpolymj.2004.07.017.

(31) Belko, V.; Ivanov, I.; Plotnikov, A.; Belanov, V. Energy Characteristics of Self-Healing Process in Metallized Film Capacitors. *E3S Web Conf.* **2019**, *140*, 02006. https://doi.org/10.1051/e3sconf/201914002006.

(32) Makdessi, M.; Sari, A.; Venet, P. Metallized Polymer Film Capacitors Ageing Law Based on Capacitance Degradation. *Microelectron. Reliab.* **2014**, *54* (9–10), 1823–1827. https://doi.org/10.1016/j.microrel.2014.07.103.

(33) Montanari, D.; Saarinen, K.; Scagliarini, F.; Zeidler, D.; Niskala, M. Film Capacitors for Automotive and Industrial Applications. **2009**, 11.

(34) Kerrigan, R. M.; Kropiewnicki, B. Film Capacitor Thermal Strategies Increase Power Density. **2008**, 5 (and references therein).

(35) Gupta, A.; Yadav, O. P.; DeVoto, D.; Major, J. A Review of Degradation Behavior and Modeling of Capacitors. In *ASME 2018 International Technical Conference and Exhibition on Packaging and Integration of Electronic and Photonic Microsystems*; American Society of Mechanical Engineers: San Francisco, California, USA, 2018; p V001T04A004. https://doi.org/10.1115/IPACK2018-8262.

(36) Wu, X.; Tang, S.; Song, G.; Zhang, Z.; Tan, D. Q. High-Temperature Resistant Polypropylene Films Enhanced by Atomic Layer Deposition. *Nano Express* **2021**, *2* (1), 010025. https://doi.org/10.1088/2632-959X/abe518.

(37) Montanari, G. C.; Fabiani, D. Searching for the Factors Which Affect Self-Healing Capacitor Degradation under Non-Sinusoidal Voltage. *IEEE Trans. Dielectr. Electr. Insul.* **1999**, *6* (3), 319–325. https://doi.org/10.1109/94.775617.

(38) Li, H.; Li, H.; Li, Z.; Lin, F.; Wang, W.; Wang, B.; Huang, X.; Guo, X. Temperature Dependence of Self-Healing Characteristics of Metallized Polypropylene Film. *Microelectron. Reliab.* **2015**, *55* (12), 2721–2726. https://doi.org/10.1016/j.microrel.2015.09.007.

(39) Flicker, J.; Kaplar, R.; Marinella, M.; Granata, J. Lifetime Testing of Metallized Thin Film Capacitors for Inverter Applications. In *2013 IEEE 39th Photovoltaic Specialists Conference (PVSC)*; IEEE: Tampa, FL, USA, 2013; pp 3340–3342. https://doi.org/10.1109/PVSC.2013.6745166.

(40) Qin, S.; Ho, J.; Rabuffi, M.; Borelli, G.; Jow, T. Implications of the Anisotropic Thermal Conductivity of Capacitor Windings. *IEEE Electr. Insul. Mag.* **2011**, *27* (1), 7–13. https://doi.org/10.1109/MEI.2011.5699442.

(41) Schneuwly, A.; Gröning, P.; Schlapbach, L.; Brüesch, P.; Carlen, M. W.; Gallay, R. Temperature-Dependent Dielectric Breakdown Strength of Oil Impregnated Polypropylene Foils. *Mater. Sci. Eng. B* **1998**, *54* (3), 182–188. https://doi.org/10.1016/S0921-5107(98)00161-5.

(42) Qi, X.; Zheng, Z.; Boggs, S. Computation of Electro-Thermal Breakdown of Polymer Films. In *2003 Annual Report Conference on Electrical Insulation and Dielectric Phenomena*; IEEE: Albuquerque, NM, USA, 2003; pp 337–340. https://doi.org/10.1109/CEIDP.2003.1254862.

(43) Kong, M. G.; Lee, Y. P. Electrically Induced Heat Dissipation in Metallized Film Capacitors. *IEEE Trans. Dielectr. Electr. Insul.* **2004**, *11* (6), 1007–1013. https://doi.org/10.1109/TDEI.2004.1387824.

(44) Steinerfilm Germany. *Segmentierung - Steinerfilm a step ahead - Masking/Segment Metallization*. https://www.steinerfilm.de/en/our-strong-points/segment-metallization/ (accessed 2022-02-11).

(45) Paloniemi, P. Theory of Equalization of Thermal Ageing Processes of Electrical Insulating Materialsin Thermal Endurance Tests I: Review of Theoretical Basis of Test Methods and Chemical and Physical Aspects of Ageing. *IEEE Trans. Electr. Insul.* **1981**, *EI-16* (1), 1–6. https://doi.org/10.1109/TEI.1981.298388.

(46) Brown, R. W. Linking Corrosion and Catastrophic Failure in Low-Power Metallized Polypropylene Capacitors. *IEEE Trans. Device Mater. Reliab.* **2006**, *6* (2), 326–333. https://doi.org/10.1109/TDMR.2006.876612.

(47) Ho, J. S.; Greenbaum, S. G. Polymer Capacitor Dielectrics for High Temperature Applications. *ACS Appl. Mater. Interfaces* **2018**, *10* (35), 29189–29218. https://doi.org/10.1021/acsami.8b07705.

(48) Gopanna, A.; Mandapati, R. N.; Thomas, S. P.; Rajan, K.; Chavali, M. Fourier Transform Infrared Spectroscopy (FTIR), Raman Spectroscopy and Wide-Angle X-Ray Scattering (WAXS) of Polypropylene (PP)/Cyclic Olefin Copolymer (COC) Blends for Qualitative and Quantitative Analysis. *Polym. Bull.* **2019**, *76* (8), 4259–4274. https://doi.org/10.1007/s00289-018-2599-0.

(49) Shah, H. C.; Nema, S. K. The Effect Of Cyclic Olefin Copolymer Loading On Linear Low Density Polyethylene Blends: Characterization By Fourier-Transform Infrared Spectroscopy And X-Ray Diffraction. **2019**, *8* (08), 7.

(50) Shin, J. Y.; Park, J. Y.; Liu, C.; He, J.; Kim, S. C. Chemical Structure and Physical Properties of Cyclic Olefin Copolymers (IUPAC Technical Report). *Pure Appl. Chem.* **2005**, *77* (5), 801–814. https://doi.org/10.1351/pac200577050801.

(51) Šlouf, M.; Kolarˇı´k, J.; Fambri, L. Phase Morphology of PP/COC Blends. *J. Appl. Polym. Sci.* **2004**, *91* (1), 253–259. https://doi.org/10.1002/app.13253.

(52) Fambri, L.; Kolarik, J.; Pegoretti, A.; Penati, A. Thermal, Thermo-Mechanical, and Dynamic Mechanical Properties of Polypropylene/Cycloolefin Copolymer Blends. *J. Appl. Polym. Sci.* **2011**, *122* (5), 3406–3414. https://doi.org/10.1002/app.34426.

(53) Zaremba, D.; Evert, R. Materials, Chemical Properties and Analysis. In *Polymer Optical Fibres*; Elsevier, 2017; pp 153–186. https://doi.org/10.1016/B978-0-08-100039-7.00005-1.

(54) TOPAS Advanced Polymers. *Markets | TOPAS*. https://topas.com/markets (accessed 2022-01-28).

(55) TOPAS Advanced Polymers; Polyplastics. *TOPAS COC - Cycle Olefin Copolymer*. Brochures. https://topas.com/tech-center/brochures (accessed 2021-10-29).

(56) *APEL™ ,Cyclo Olefin Copolymer (COC)| Business and Products | MITSUI CHEMICALS AMERICA, INC.* https://us.mitsuichemicals.com/service/product/apel.htm (accessed 2022-01-28).

(57) Fambri, L.; Kolarik, J.; Pasqualini, E.; Penati, A.; Pegoretti, A. Rheological Study on Polypropylene/Cycloolefin Copolymer Blends. *Macromol. Symp.* **2008**, *263* (1), 114–120. https://doi.org/10.1002/masy.200850314.

(58) Alba, C.; Pelaez, D.; Cabo, L. High-Temperature Metallized Polymer Film Capacitors Based on Blends of Polypropylene and Cyclic Olefin Copolymers. In *2020 IEEE 3rd International Conference on*

Dielectrics (ICD); IEEE: Valencia, Spain, 2020; pp 669–672. https://doi.org/10.1109/ICD46958.2020.9342006.

(59) Ritamaki, M.; Rytoluoto, I.; Lahti, K. Performance Metrics for a Modern BOPP Capacitor Film. *IEEE Trans. Dielectr. Electr. Insul.* **2019**, *26* (4), 1229–1237. https://doi.org/10.1109/TDEI.2019.007970.

(60) Kahouli, A.; Gallot-Lavallée, O.; Rain, P.; Lesaint, O.; Guillermin, C.; Lupin, J.-M. Dielectric Features of Two Grades of Bi-Oriented Isotactic Polypropylene. *J. Appl. Polym. Sci.* **2015**, *132* (28), n/a-n/a. https://doi.org/10.1002/app.42224.

(61) Xiong, J.; Wang, X.; Zhang, X.; Xie, Y.; Lu, J.; Zhang, Z. How the Biaxially Stretching Mode Influence Dielectric and Energy Storage Properties of Polypropylene Films. *J. Appl. Polym. Sci.* **2021**, *138* (11), 50029. https://doi.org/10.1002/app.50029.

(62) Díez, F. J.; Alvariño, C.; López, J.; Ramírez, C.; Abad, M. J.; Cano, J.; García-Garabal, S.; Barral, L. Influence of the Stretching in the Crystallinity of Biaxially Oriented Polypropylene (BOPP) Films. *J. Therm. Anal. Calorim.* **2005**, *81* (1), 21–25. https://doi.org/10.1007/s10973-005-0739-x.

(63) Yuksekkalayci, C.; Yilmazer, U.; Orbey, N. Effects of Nucleating Agent and Processing Conditions on the Mechanical, Thermal, and Optical Properties of Biaxially Oriented Polypropylene Films. *Polym. Eng. Sci.* **1999**, *39* (7), 1216–1222. https://doi.org/10.1002/pen.11508.

(64) Laihonen, S. J. Polypropylene: morphology, defects and electrical breakdown. PhD Thesis, KTH Royal Institute of Technology, Stockholm, 2005.

(65) Reed, C. W.; Cichanowskil, S. W. The Fundamentals of Aging in HV Polymer-Film Capacitors. *IEEE Trans. Dielectr. Electr. Insul.* **1994**, *1* (5), 904–922. https://doi.org/10.1109/94.326658.

(66) Mackey, M. ENHANCED DIELECTRIC PROPERTIES OF MICRO AND NANOLAYERED FILMS FOR CAPACITOR APPLICATIONS. PhD Thesis, Case Western Reserve University, 2012. https://doi.org/10.13140/RG.2.2.20754.58564.

(67) Ju, T.; Chen, X.; Langhe, D.; Ponting, M.; Baer, E.; Zhu, L. Enhancing Breakdown Strength and Lifetime of Multilayer Dielectric Films by Using High Temperature Polycarbonate Skin Layers. *Energy Storage Mater.* **2022**, *45*, 494–503. https://doi.org/10.1016/j.ensm.2021.12.009.

(68) PerkinElmer. Differential Scanning Calorimetry (DSC) - Frequently Asked Questions.

(69) HUMBOLDT UNIVERSITÄT ZU BERLIN. *Investigation of Polymers with Differential Scanning Calorimetry*. https://docplayer.net/23045605-Investigation-of-polymers-with-differential-scanning-calorimetry.html (accessed 2021-12-28).

(70) Blaine, R. L. *Determination of Polymer Crystallinity by DSC*; Technical document TA123; 2010; p 3.

(71) Technische Universität München. *Characterization of Polymers with Differential Scanning Calorimetry*; Technical document; 2019.

(72) Gee, D. R.; Melia, T. P. Thermal Properties of Melt and Solution Crystallized Isotactic Polypropylene. *Makromol. Chem.* **1970**, *132* (1), 195–201. https://doi.org/10.1002/macp.1970.021320117.

(73) Maria, C. Application of FTIR Spectroscopy in Environmental Studies. In *Advanced Aspects of Spectroscopy*; Akhyar Farrukh, M., Ed.; InTech, 2012. https://doi.org/10.5772/48331.

(74) Khan, S. A.; Khan, S. B.; Khan, L. U.; Farooq, A.; Akhtar, K.; Asiri, A. M. Fourier Transform Infrared Spectroscopy: Fundamentals and Application in Functional Groups and Nanomaterials Characterization. In *Handbook of Materials Characterization*; Sharma, S. K., Ed.; Springer International Publishing: Cham, 2018; pp 317–344. https://doi.org/10.1007/978-3-319-92955-2_9.

(75) PerkinElmer. FTIR Spectroscopy: Attenuated Total Reflectance (ATR) - Technical Note. 5.

(76) De Oliveira, R. R. L.; Albuquerque, D. A. C.; Cruz, T. G. S.; Yamaji, F. M.; Leite, F. L. Measurement of the Nanoscale Roughness by Atomic Force Microscopy: Basic Principles and Applications. In *Atomic Force Microscopy - Imaging, Measuring and Manipulating Surfaces at the Atomic Scale*; Bellitto, V., Ed.; InTech, 2012. https://doi.org/10.5772/37583.

(77) Raposo, M.; Ferreira, Q.; Ribeiro, P. A. A Guide for Atomic Force Microscopy Analysis of Soft-Condensed Matter. *Mod. Res. Educ. Top. Microsc.* **2007**, *1*, 758–769.

(78) Akhtar, K.; Khan, S. A.; Khan, S. B.; Asiri, A. M. Scanning Electron Microscopy: Principle and Applications in Nanomaterials Characterization. In *Handbook of Materials Characterization*; Sharma, S. K., Ed.; Springer International Publishing: Cham, 2018; pp 113–145. https://doi.org/10.1007/978-3-319-92955-2_4.

(79) ThermoFisher Scientific. *Electron Microscopy | Scanning Electron Microscopy - PT*. //www.thermofisher.com/uk/en/home/materials-science/learning-center/applications/sem-electrons.html (accessed 2022-01-11).

(80) Nixon, W. C. The General Principles of Scanning Electron Microscopy. *Philos. Trans. R. Soc. Lond. B. Biol. Sci.* **1971**, *261* (837,), 45–50.

(81) Ebnesajjad, S.; Ebnesajjad, C. F. Chapter 4 - Energy Dispersive X-Ray Spectroscopy (EDS). In *Surface treatment of materials for adhesive bonding*; William Andrew, an imprint of Elsevier: Amsterdam, 2014; p 49.

(82) Mutalib, M.; Rahman, M.; Othman, M.; Ismail, A.; Jaafar, J. Chapter 9 - Scanning Electron Microscopy (SEM) and Energy-Dispersive X-Ray (EDX) Spectroscopy. In *Membrane characterization*; Hilal, N., Ismail, A. F., Matsuura, T., Oatley-Radcliffe, D., Eds.; Elsevier: Amsterdam, Netherlands, 2017; pp 167–168.

(83) Davim, J. P.; Magalhães, A. G. Capitulo 2 - Ensaio de tracção. In *Ensaios Mecânicos e Técnológicos - Inclui exercícios resolvidos e propostos*; Publindústria, Edições Técnicas: Porto, 2004; pp 17–29.

(84) Kazanowski, P.; Dickson, R. Evaluation of Process Mechanism and Parameters for Automated Stretching Line. **2012**, 17.

(85) Sharir, A.; Barak, M. M.; Shahar, R. Whole Bone Mechanics and Mechanical Testing. *Vet. J.* **2008**, *177* (1), 8–17. https://doi.org/10.1016/j.tvjl.2007.09.012.

(86) Yalcin, D. *Effect of Specimen Geometry on Tensile Testing Results | iMechanica*. Effect of Specimen Geometry on Tensile Testing Results. https://imechanica.org/node/21939 (accessed 2022-01-13).

(87) Ismail, A. F.; Khulbe, K. C.; Matsuura, T. Chapter 3 - RO Membrane Characterization. In *Reverse osmosis*; Elsevier: Amsterdam, Netherlands ; Cambridge, MA, 2019; p 84.

(88) International Organization for Standardization. *Plastics — Determination of tensile properties — Part 3: Test conditions for films and sheets (ISO 527-3:2018)*. ISO. https://www.iso.org/cms/render/live/en/sites/isoorg/contents/data/standard/07/03/70307.html (accessed 2022-03-29).

(89) Delta Engineering. *PP*. Delta Engineering Belgium. https://delta-engineering.be/pp (accessed 2022-03-02).

(90) Chen, H. B.; Karger-Kocsis, J.; Wu, J. S.; Varga, J. Fracture Toughness of α- and β-Phase Polypropylene Homopolymers and Random- and Block-Copolymers. *Polymer* **2002**, *43* (24), 6505–6514. https://doi.org/10.1016/S0032-3861(02)00590-6.

(91) Fujiyama, M.; Kawamura, Y.; Wakino, T.; Okamoto, T. Study on Rough-Surface Biaxially Oriented Polypropylene Film. II. Influence of Stretching Conditions. *J. Appl. Polym. Sci.* **1988**, *36* (5), 995–1009. https://doi.org/10.1002/app.1988.070360502.

(92) Morent, R.; De Geyter, N.; Leys, C.; Gengembre, L.; Payen, E. Comparison between XPS- and FTIR-Analysis of Plasma-Treated Polypropylene Film Surfaces. *Surf. Interface Anal.* **2008**, *40* (3–4), 597–600. https://doi.org/10.1002/sia.2619.

(93) Li, J.; Zhu, Z.; Li, T.; Peng, X.; Jiang, S.; Turng, L. Quantification of the Young's Modulus for Polypropylene: Influence of Initial Crystallinity and Service Temperature. *J. Appl. Polym. Sci.* **2020**, *137* (16), 48581. https://doi.org/10.1002/app.48581.

(94) Fujiyama, M.; Awaya, H.; Kimura, S. Mechanical Anisotropy in Injection-Molded Polypropylene. *J. Appl. Polym. Sci.* **1977**, *21* (12), 3291–3309. https://doi.org/10.1002/app.1977.070211209.

(95) Physical, Thermal, and Mechanical Properties of Polymers. In *Biosurfaces*; John Wiley & Sons, Inc: Hoboken, NJ, USA, 2015; pp 329–344. https://doi.org/10.1002/9781118950623.app1.

(96) Lu, N.; Suo, Z.; Vlassak, J. J. The Effect of Film Thickness on the Failure Strain of Polymer-Supported Metal Films. *Acta Mater.* **2010**, *58* (5), 1679–1687. https://doi.org/10.1016/j.actamat.2009.11.010.

(97) Tamura, S.; Kuramoto, I.; Kanai, T. The Effect of Molecular Structure of Polypropylene on Stretchability for Biaxially Oriented Film. *Polym. Eng. Sci.* **2012**, *52* (6), 1383–1393. https://doi.org/10.1002/pen.22180.

(98) Chivers, R.; Moore, D. The Effect of Molecular Weight and Crystallinity on the Mechanical Properties of Injection Moulded Poly(Aryl-Ether-Ether-Ketone) Resin. *Polymer* **1994**, *35* (1), 110–116. https://doi.org/10.1016/0032-3861(94)90057-4.

(99) Nie, H.-Y.; Walzak, M. J.; McIntyre, N. S. Draw-Ratio-Dependent Morphology of Biaxially Oriented Polypropylene Films as Determined by Atomic Force Microscopy. *Polymer* **2000**, *41* (6), 2213–2218. https://doi.org/10.1016/S0032-3861(99)00397-3.

(100) Tamura, S.; Takino, K.; Yamada, T.; Kanai, T. Crater Formation Mechanism on the Surface of a Biaxially Oriented Polypropylene Film. *J. Appl. Polym. Sci.* **2012**, *126* (S2), E501–E512. https://doi.org/10.1002/app.36803.

(101) Rytöluoto, I.; Gitsas, A.; Pasanen, S.; Lahti, K. Effect of Film Structure and Morphology on the Dielectric Breakdown Characteristics of Cast and Biaxially Oriented Polypropylene Films. *Eur. Polym. J.* **2017**, *95*, 606–624. https://doi.org/10.1016/j.eurpolymj.2017.08.051.

(102) Kerrigan, R. M. Metallized Polypropylene Film Energy Storage Capacitors For Low Pulse Duty. **2007**, 6.

(103) Li, H.; Lewin, P.; Fothergill, J. C. Aging Mechanisms of X2 Metallized Film Capacitors in a High Temperature and Humidity Environment. In *2016 IEEE International Conference on Dielectrics (ICD)*; IEEE: Montpellier, France, 2016; pp 804–807. https://doi.org/10.1109/ICD.2016.7547738.

(104) Chen, Y.; Li, H.; Lin, F.; Lv, F.; Li, Z.; Zhang, M. Effect of Interlayer Air on Performance of Dry-Type Metalized Film Capacitor in DC, AC and Pulsed Applications. *IEEE Trans. Dielectr. Electr. Insul.* **2011**, *18* (4), 1301–1306. https://doi.org/10.1109/TDEI.2011.5976131.

(105) Lackey, D. V. A Versatile Capacitor Web Coater with Multiple Source Capability. *Anti-Corros. Methods Mater.* **1992**, *39* (2), 4–8. https://doi.org/10.1108/eb007303.

(106) Tan, D. Q. Differentiation of Roughness and Surface Defect Impact on Dielectric Strength of Polymeric Thin Films. *IET Nanodielectrics* **2020**, *3* (1), 28–31. https://doi.org/10.1049/iet-nde.2019.0031.

(107) Nagai I.; Ueda T.; Tanaka S. Biaxially oriented polypropylene film and condenser. JPH10119127A, May 12, 1998.

Annexes

Annex I – DSC thermograms

Sample 1:

1. Sample 1, specimen n° 2;

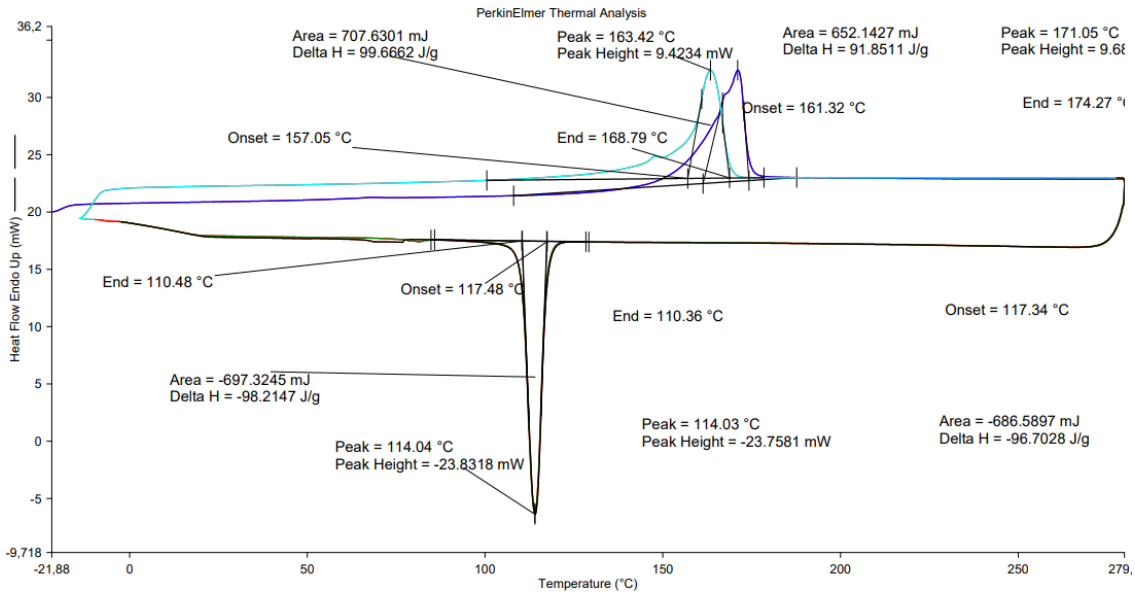

2. Sample 1, specimen n°3;

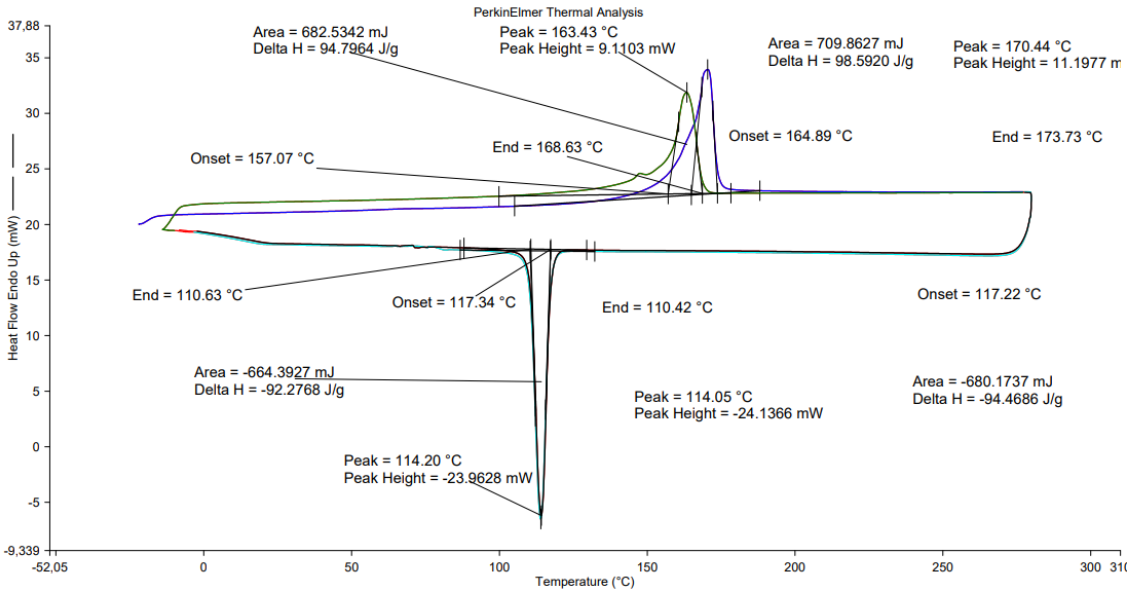

Sample 2:

1. Sample 2, specimen n°1;

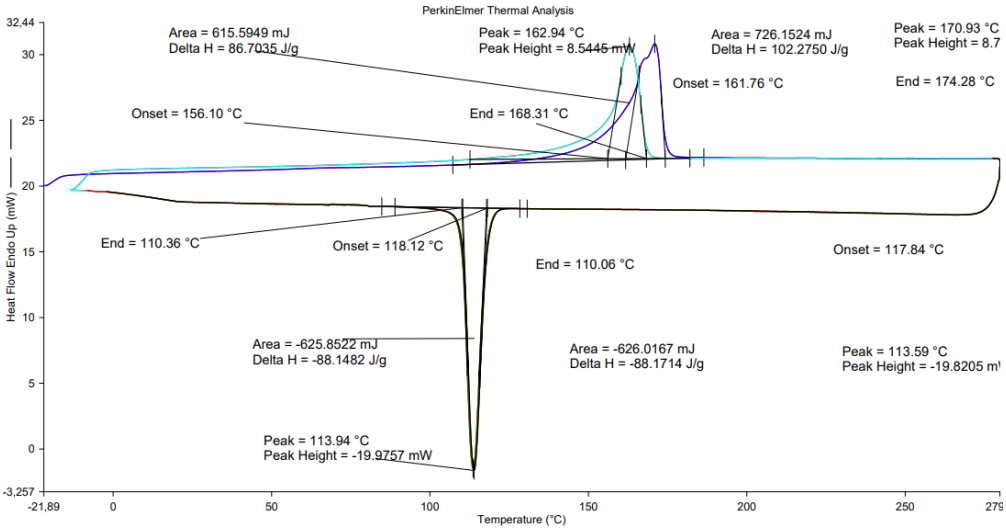

2. Sample 2, specimen n°2;

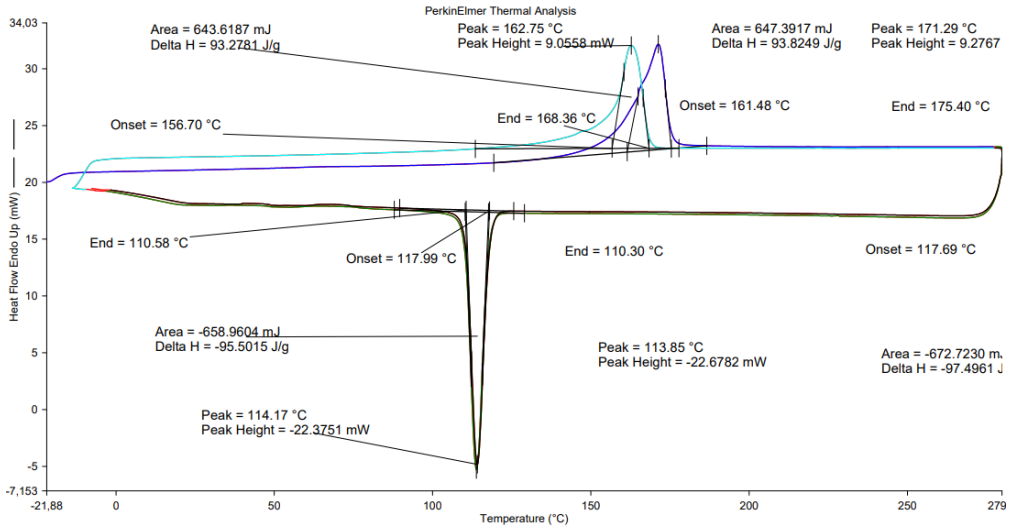

3. Sample 2, specimen n°3;

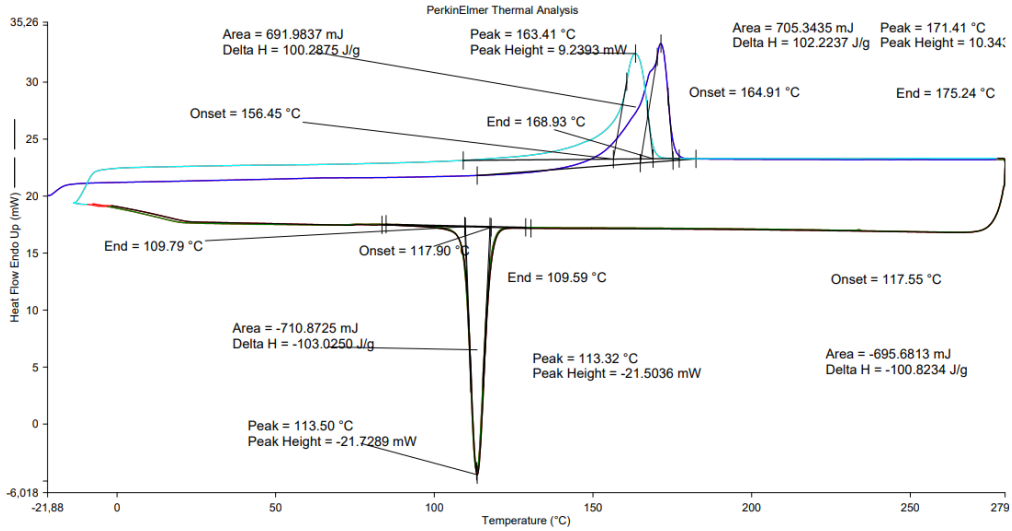

Sample 3:

1. Sample 3, specimen n°1;

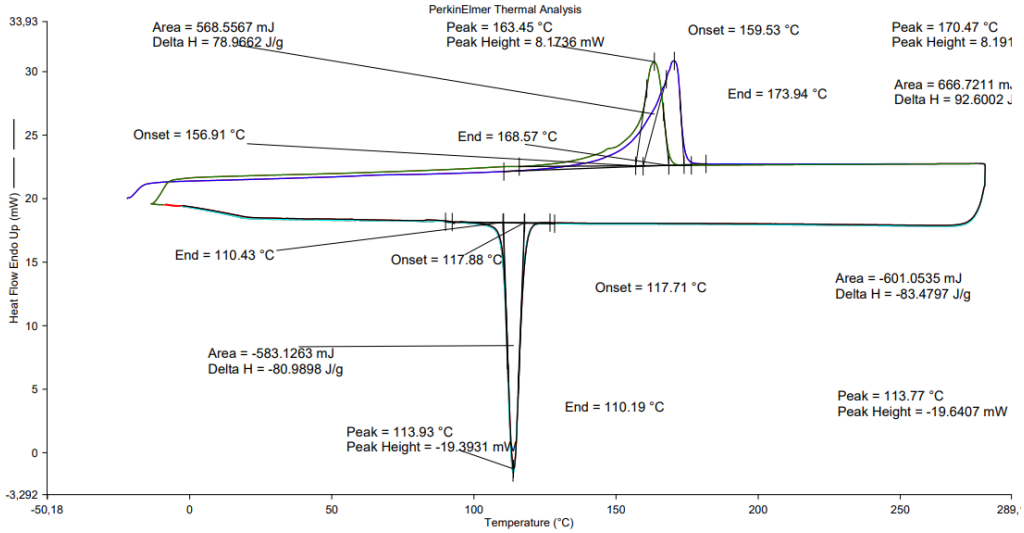

2. Sample 3, specimen n°2;

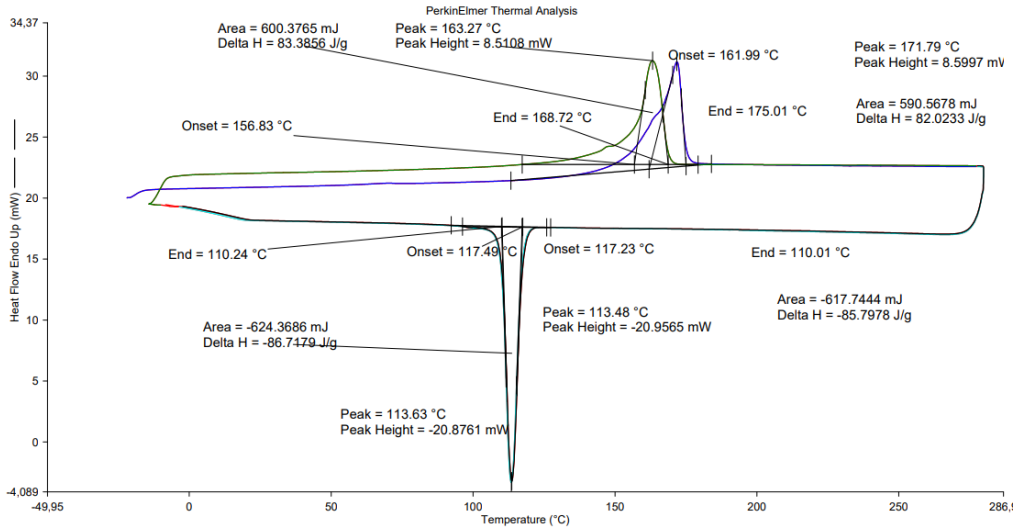

3. Sample 3, specimen n°3;

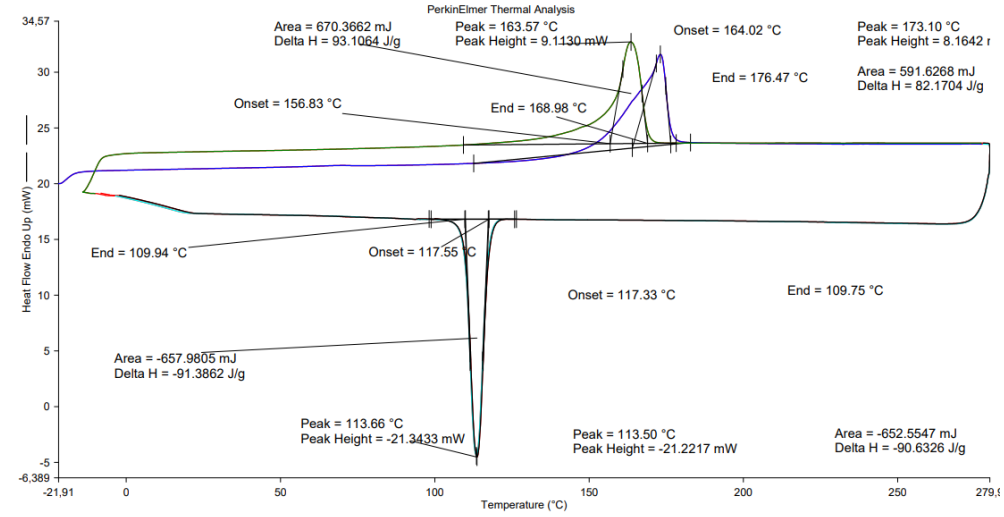

Sample 4:

1. Sample 4, specimen n°1;

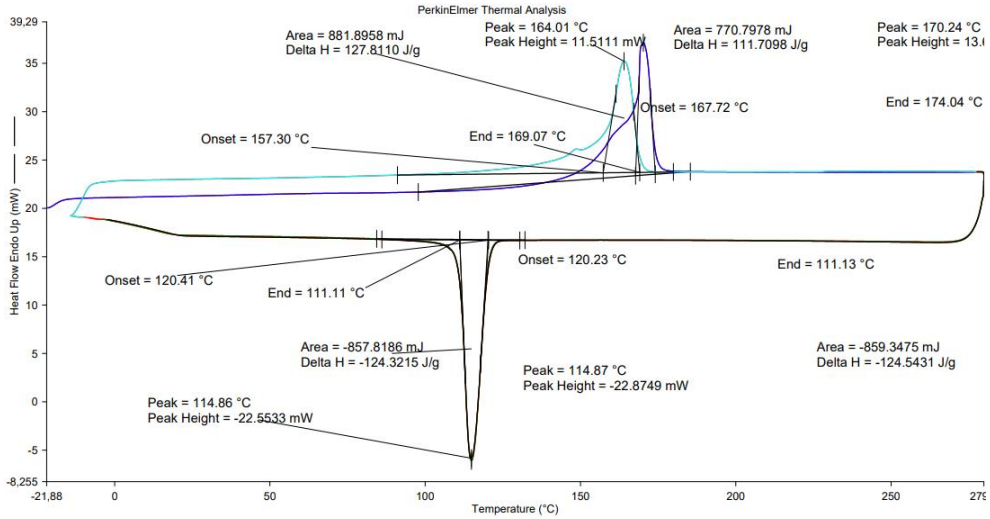

2. Sample 4, specimen n°2;

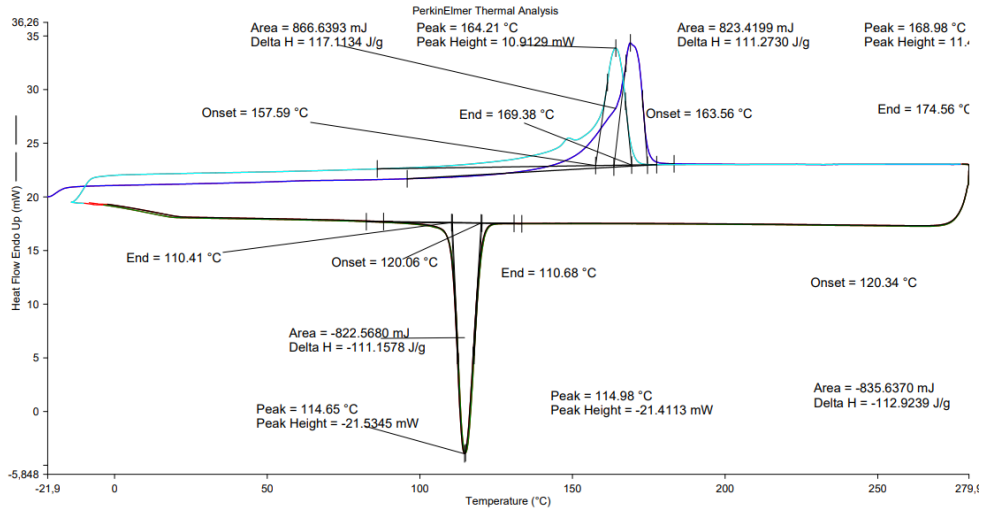

3. Sample 4, specimen n°3;

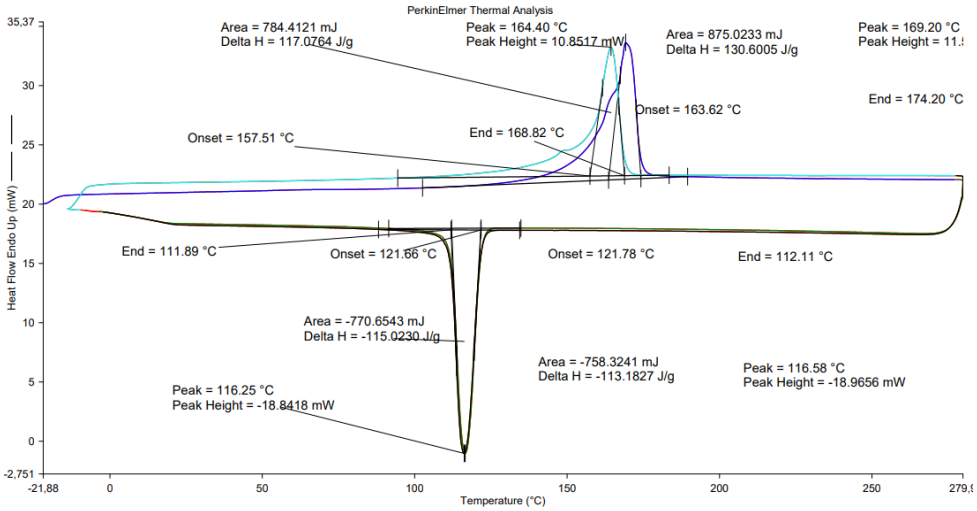

Sample 5:

1. Sample 5, specimen n°1;

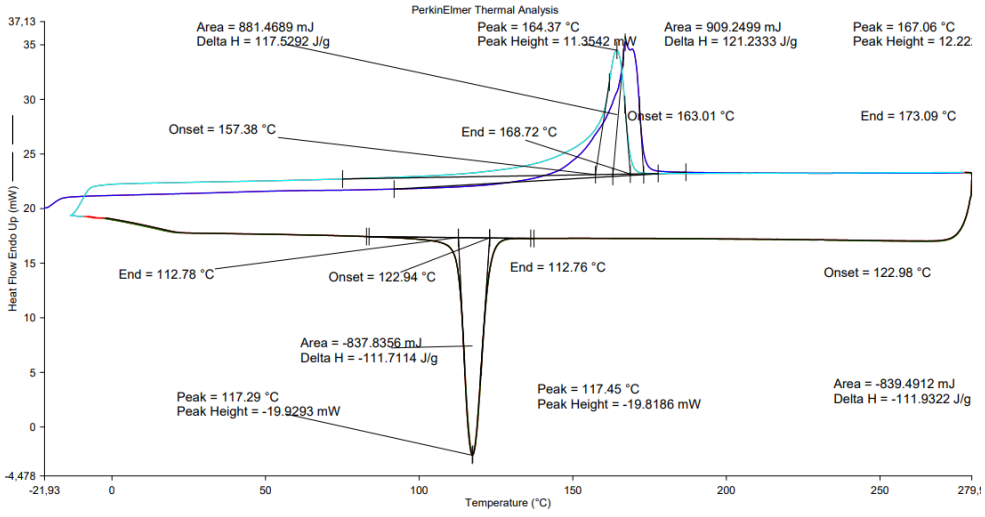

2. Sample 5, specimen n°2;

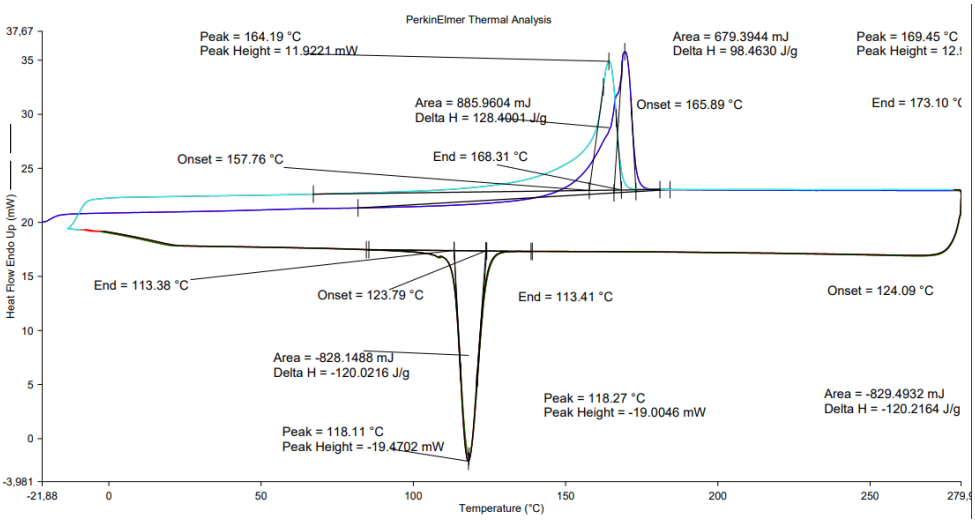

3. Sample 5, specimen n°3;

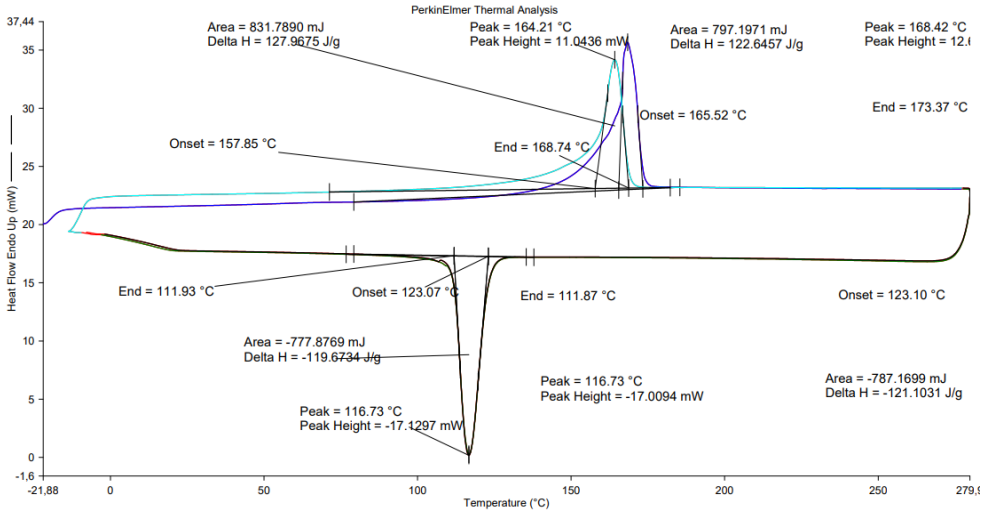

Annex II – FTIR-ATR

1. Sample 1;

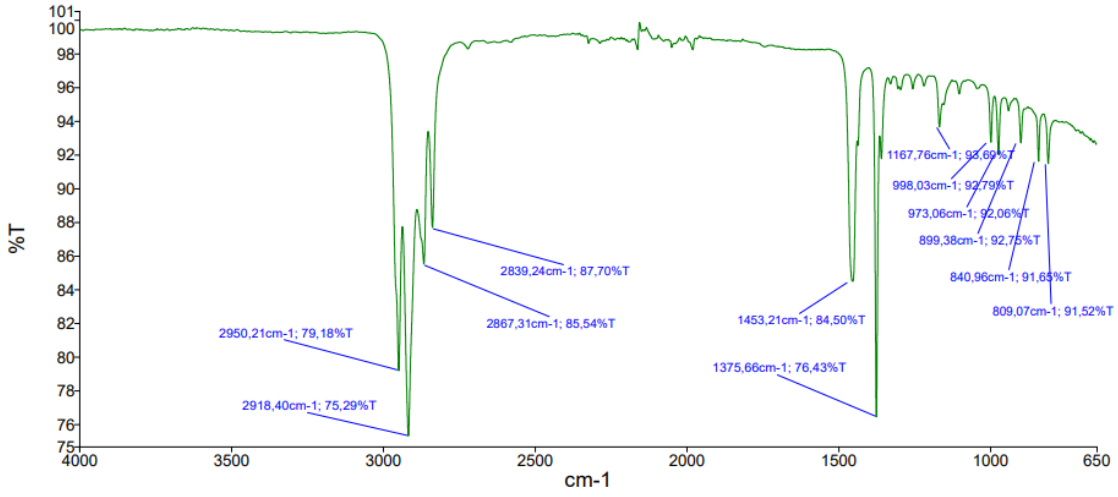

2. Sample 3;

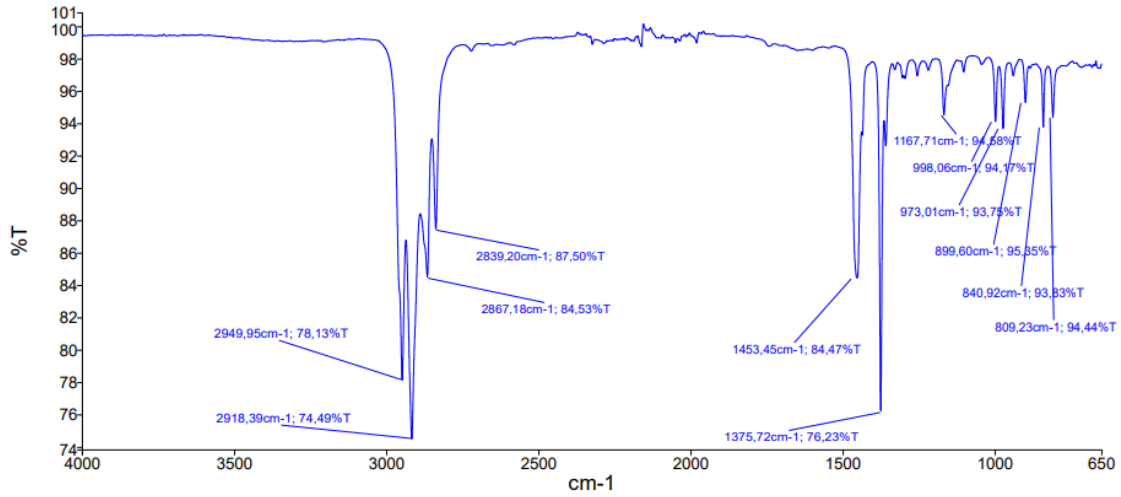

3. Sample 5;

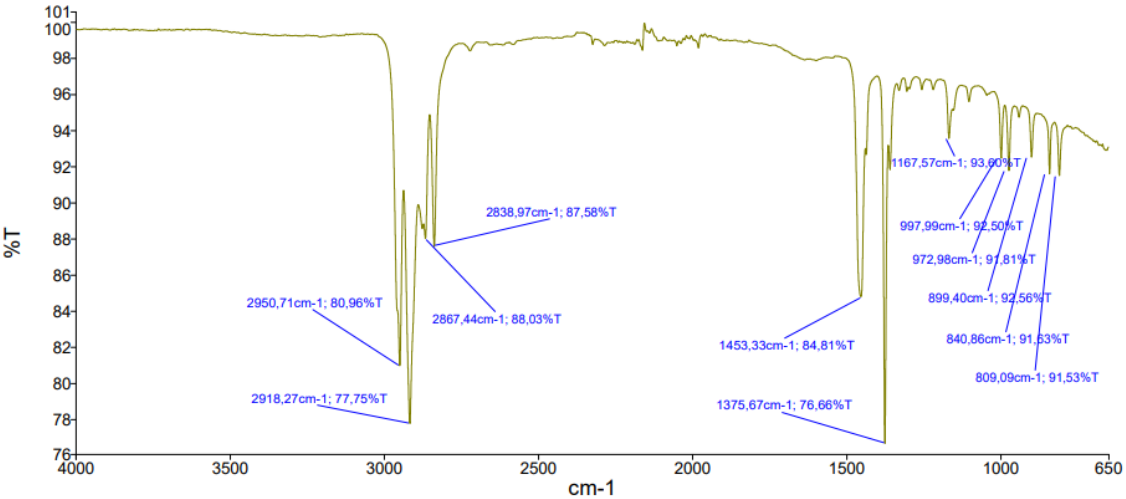

Annex III – SEM

Sample 1:

1. Sample 1, sector A;

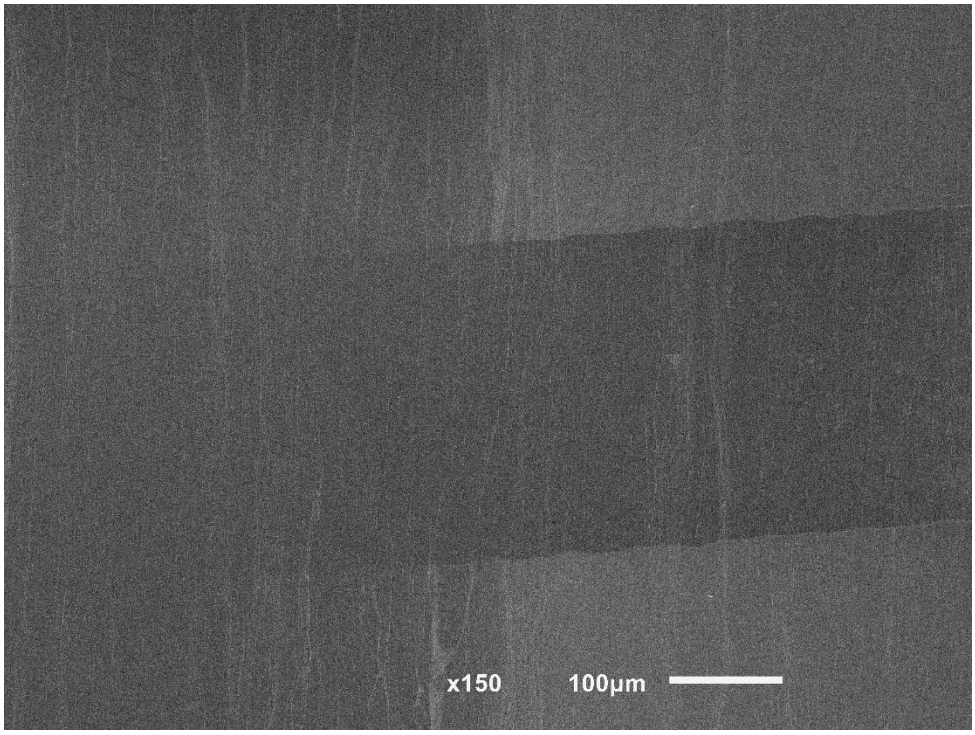

2. Sample 1, area B1;

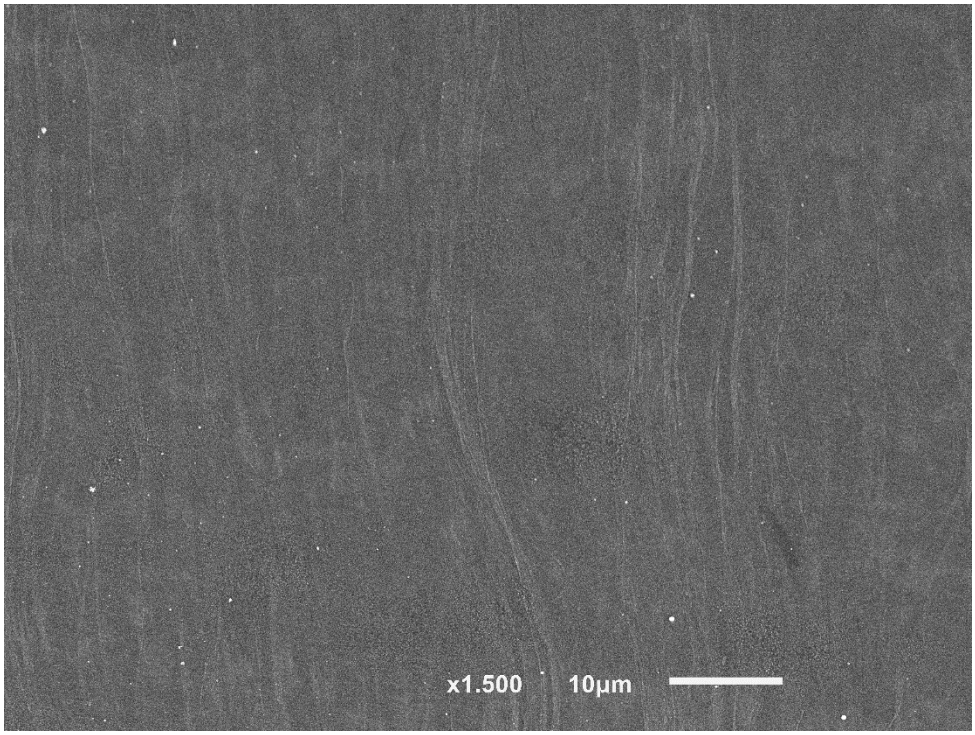

3. Sample 1, area B2;

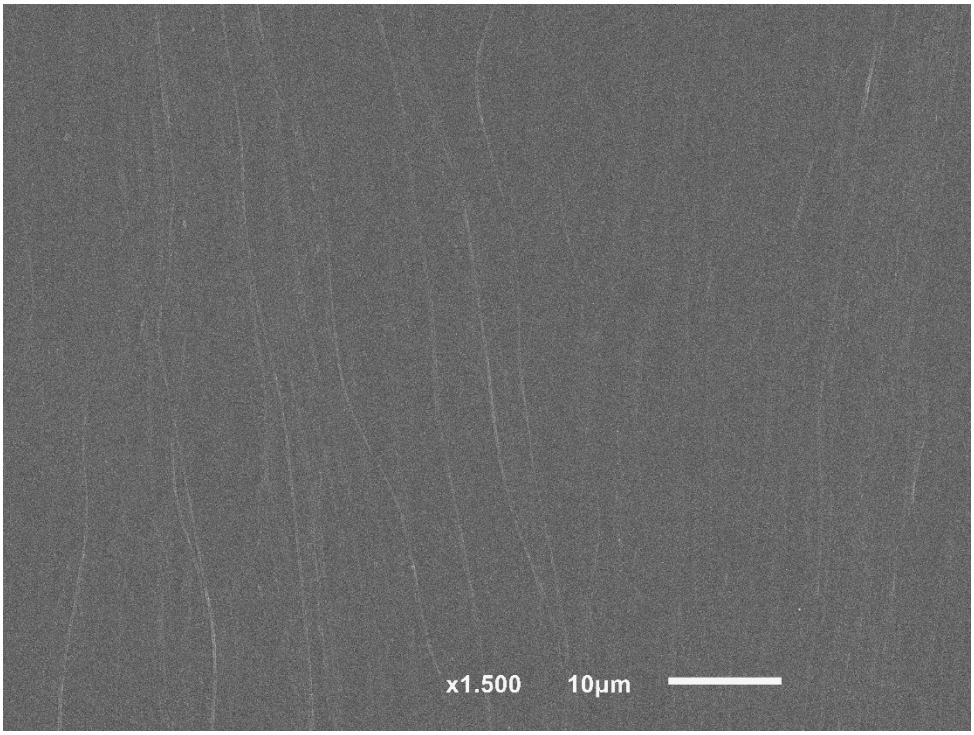

4. Sample 1, sector C;

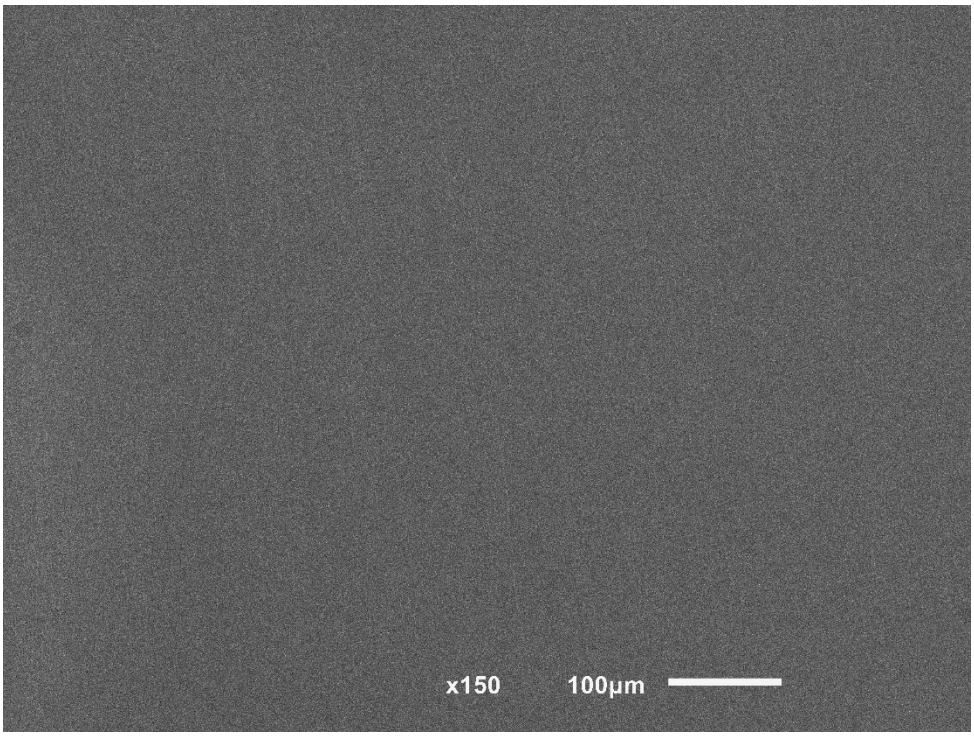

5. Sample 1, area C;

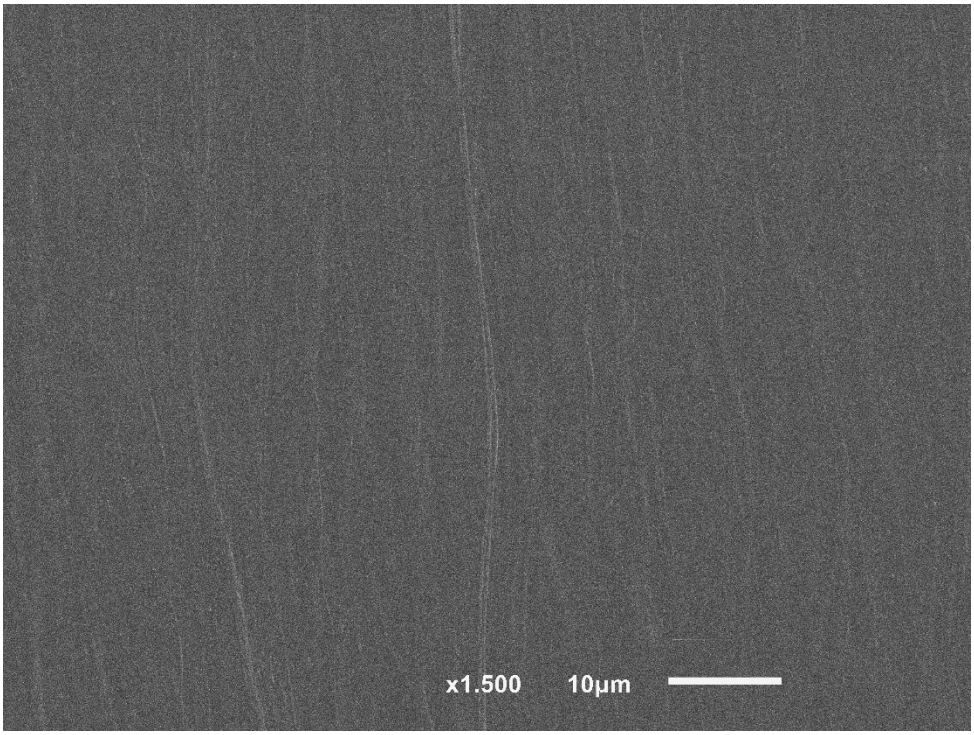

Sample 2:

1. Sample 2, sector A;

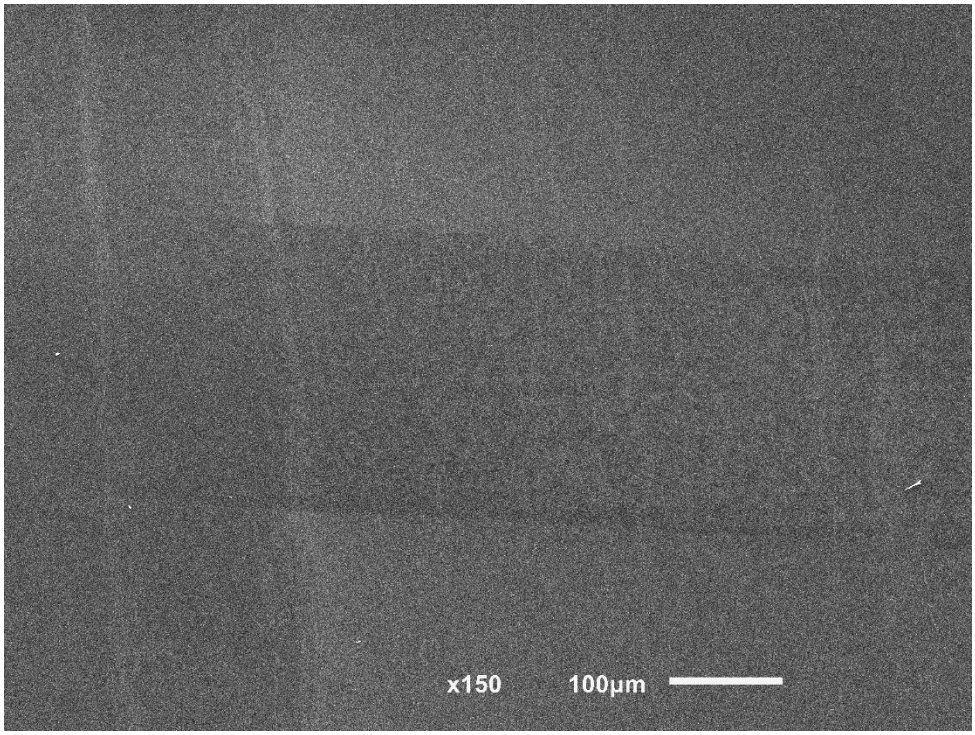

2. Sample 2, area A1;

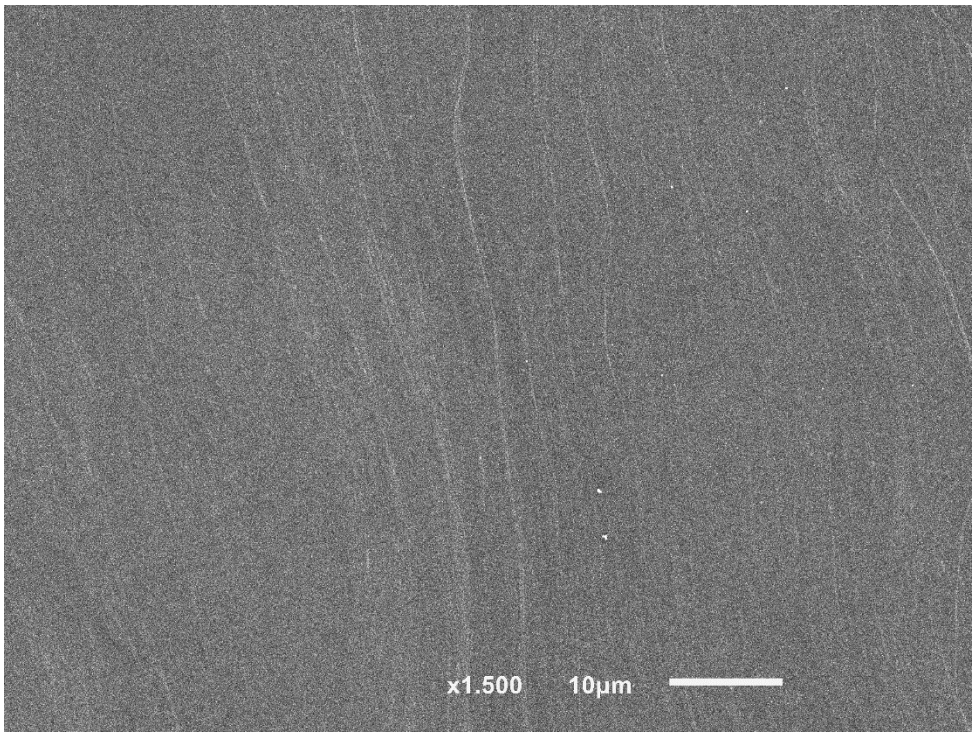

3. Sample 2, area A2;

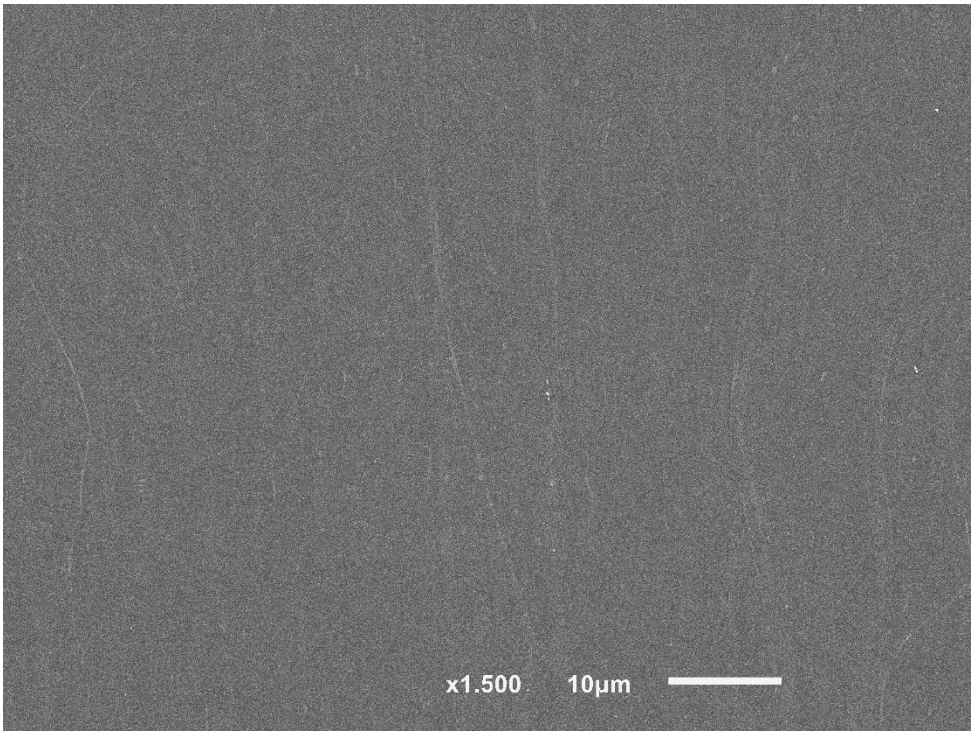

4. Sample 2, area B1;

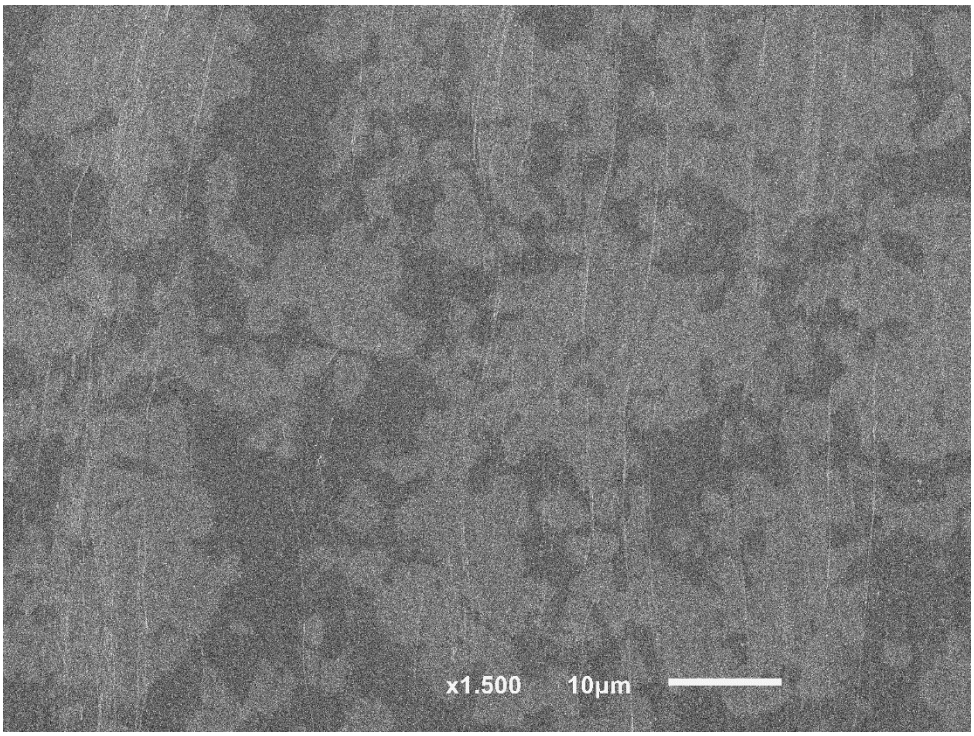

5. Sample 2, area B2;

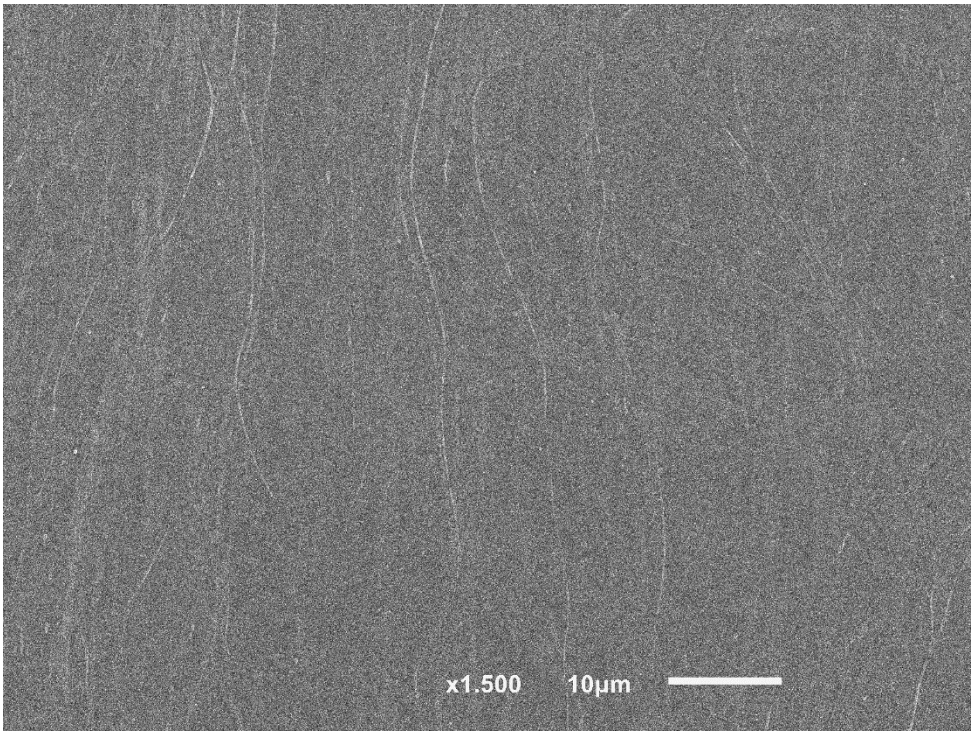

6. Sample 2, sector C;

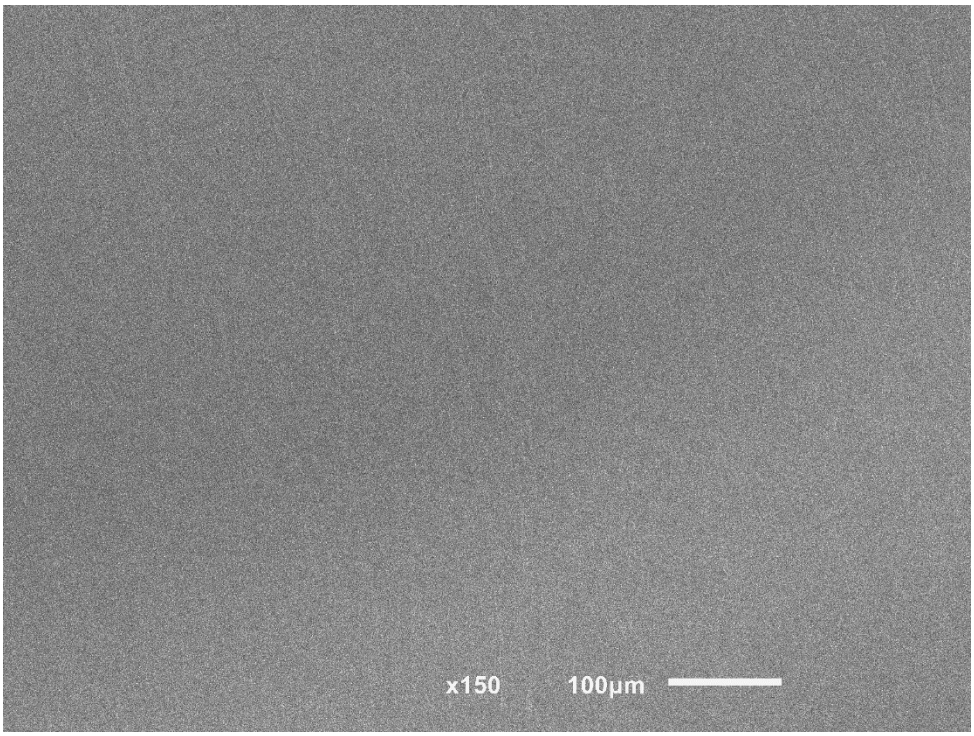

7. Sample 2, area C;

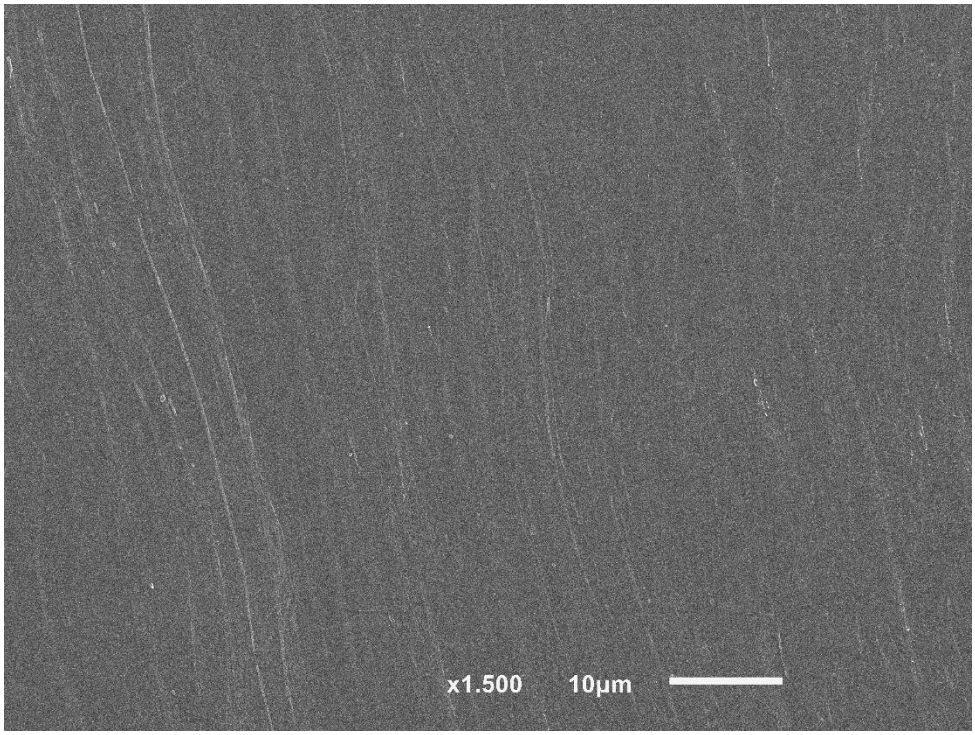

Sample 3:

1. Sample 3, sector A;

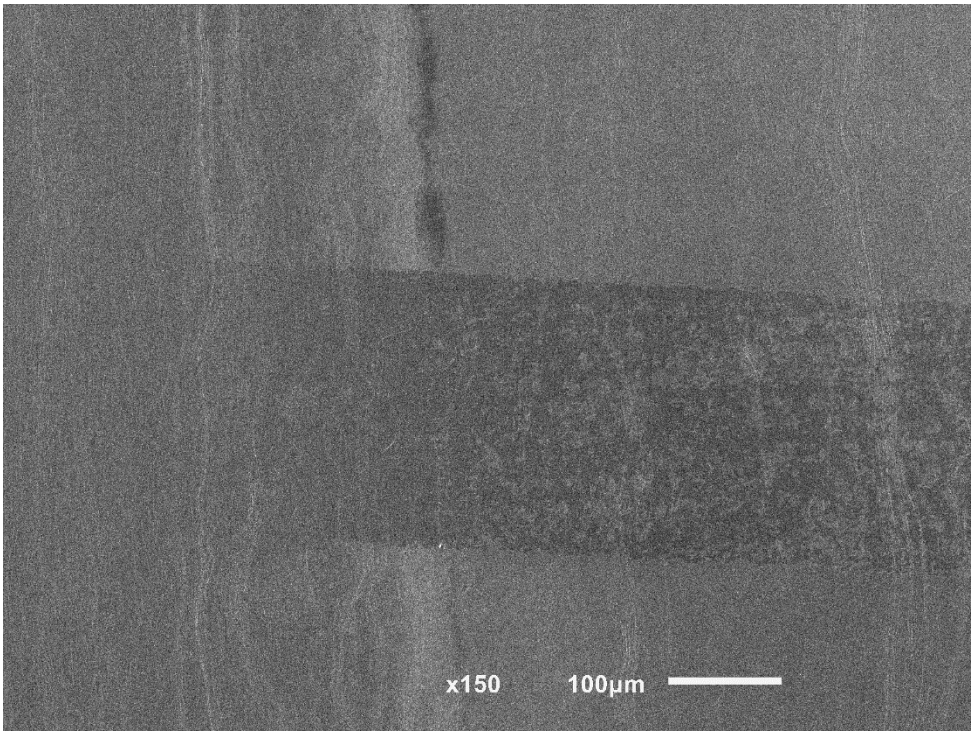

2. Sample 3, area A1;

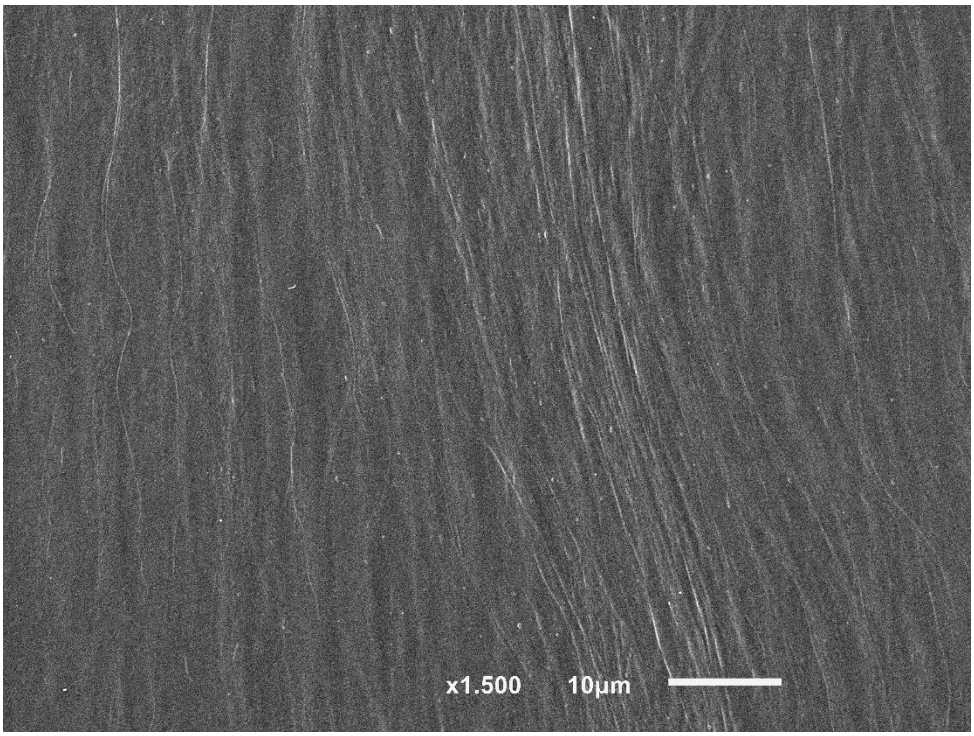

3. Sample 3, area A2;

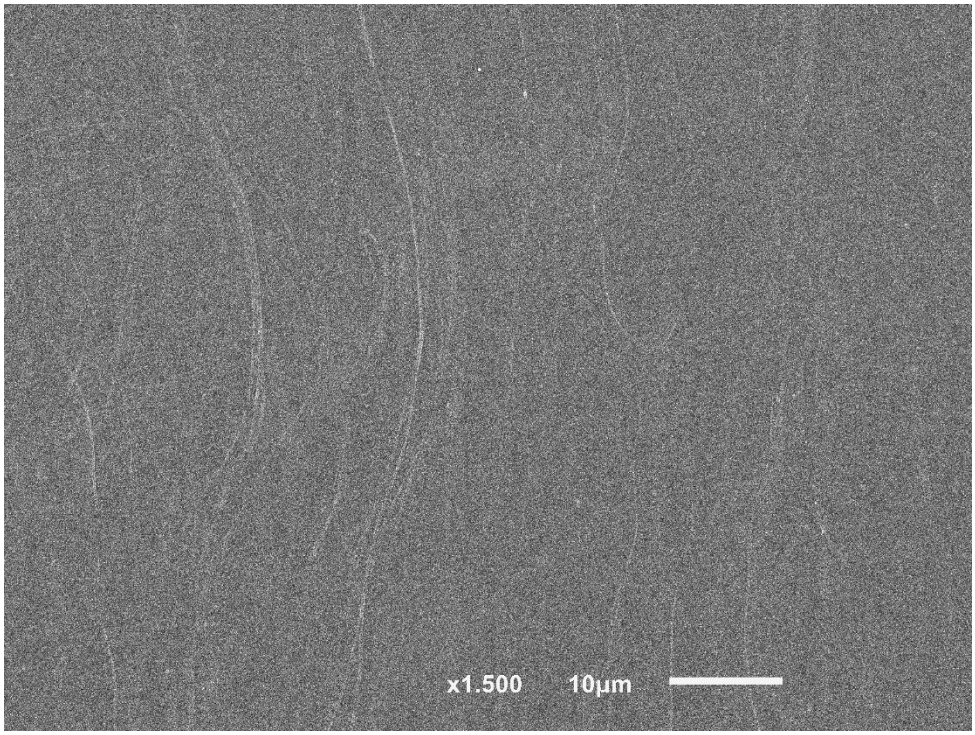

4. Sample 3, area B1;

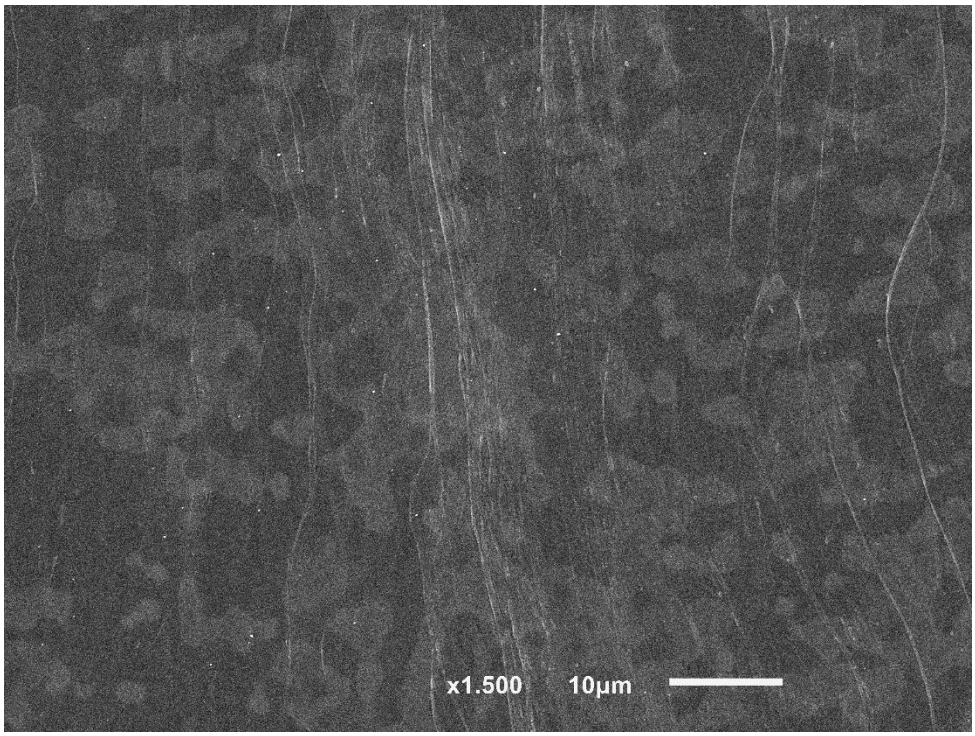

5. Sample 3, area B2;

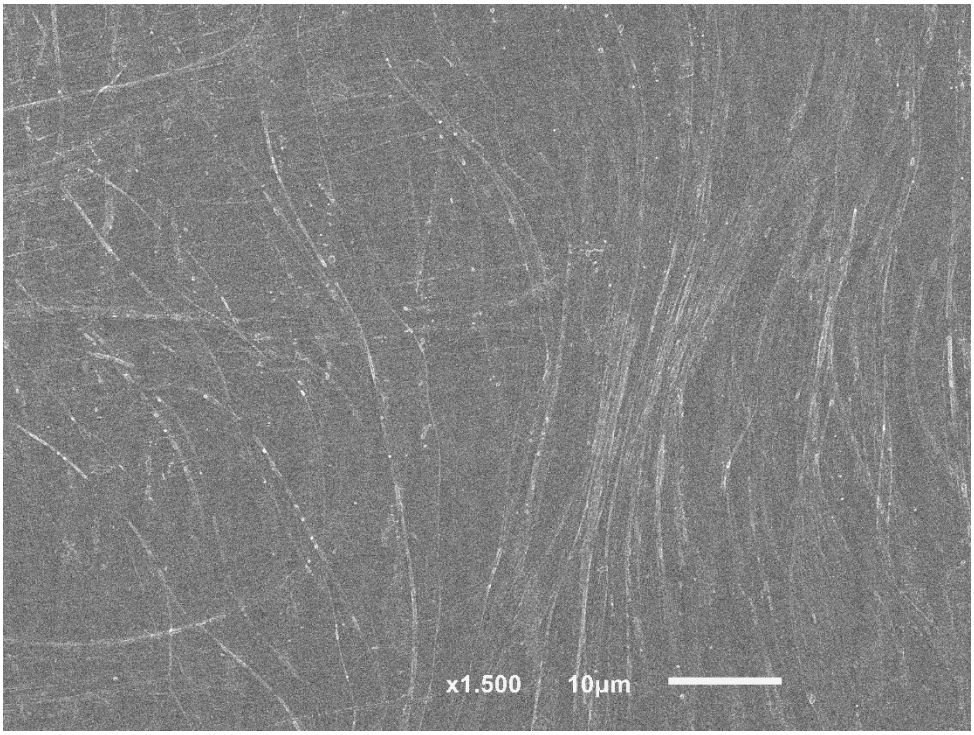

6. Sample 3, sector C;

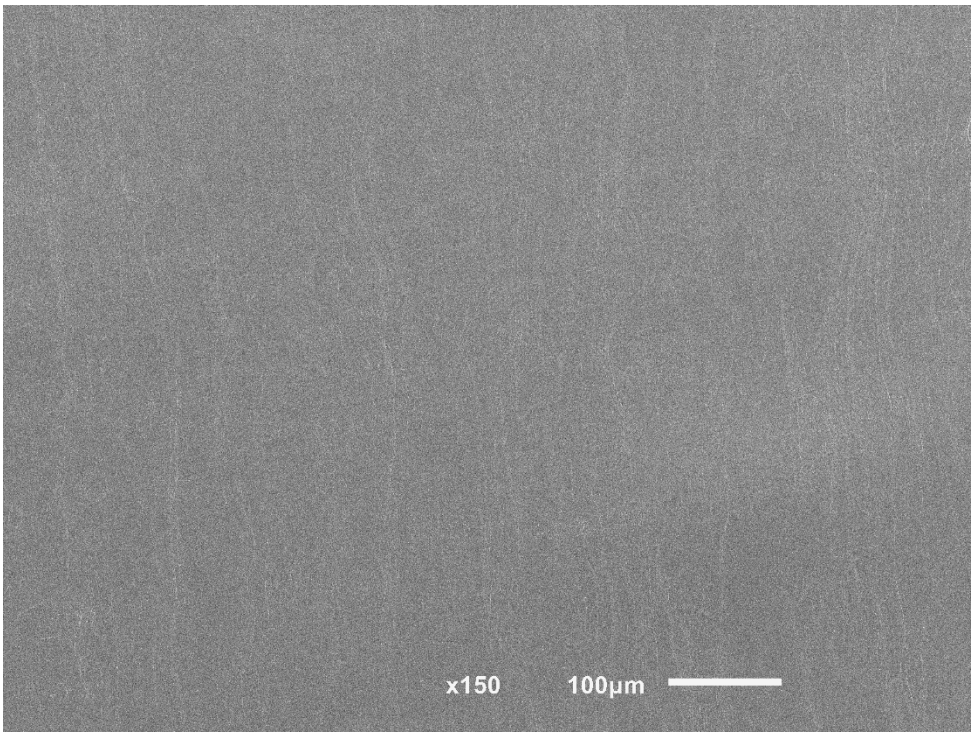

7. Sample 3, area C;

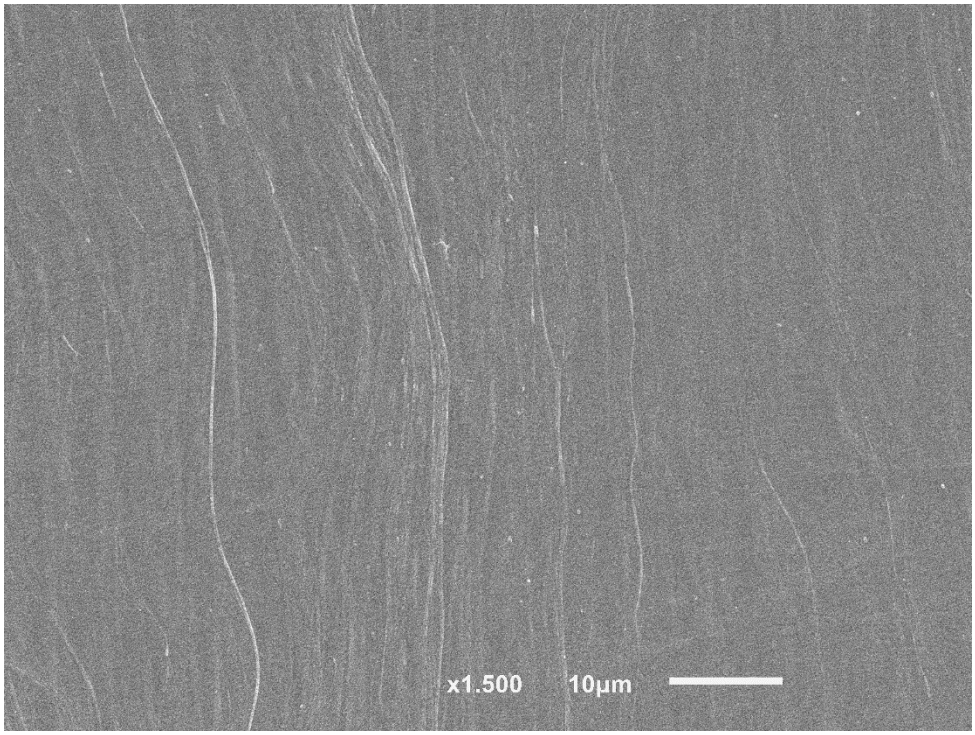

Sample 4:

1. Sample 4, sector A;

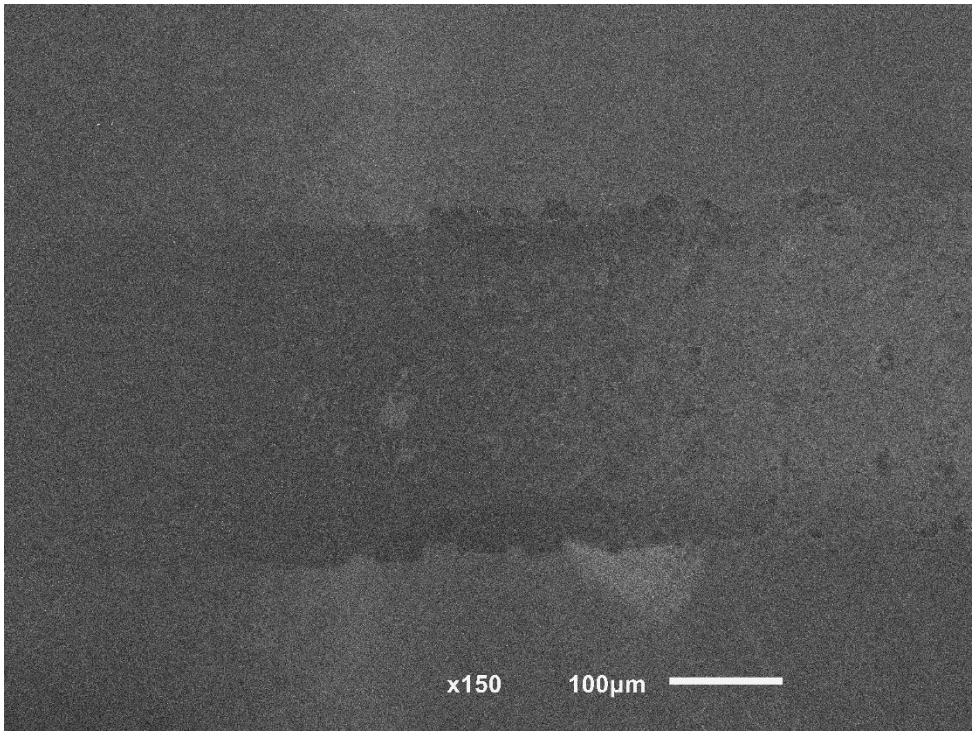

2. Sample 4, area B1;

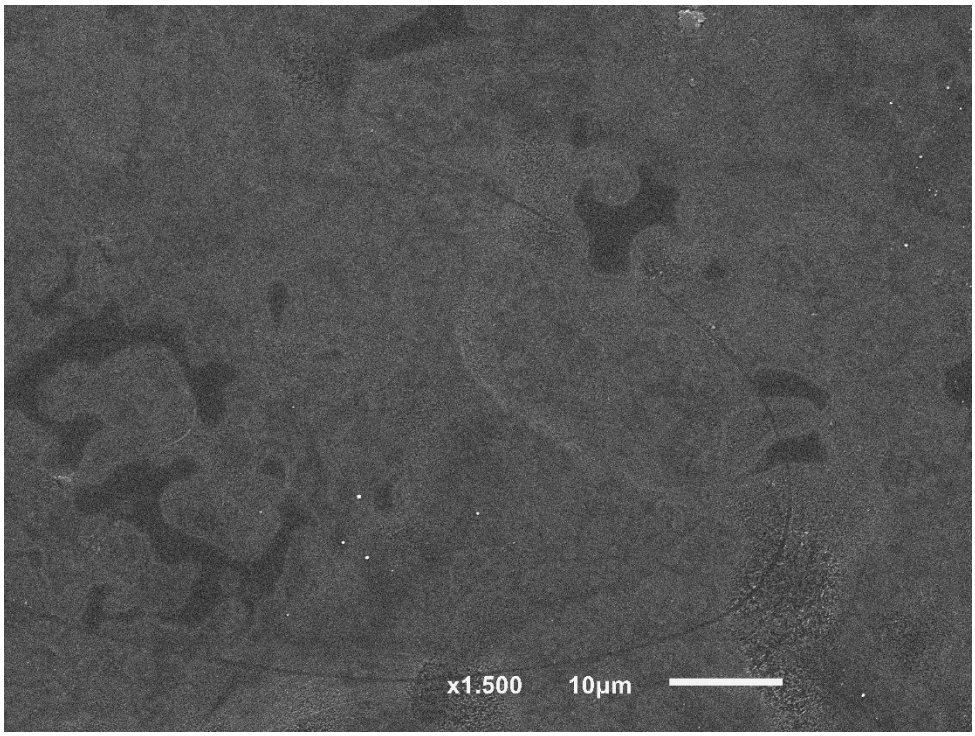

3. Sample 4, area B2;

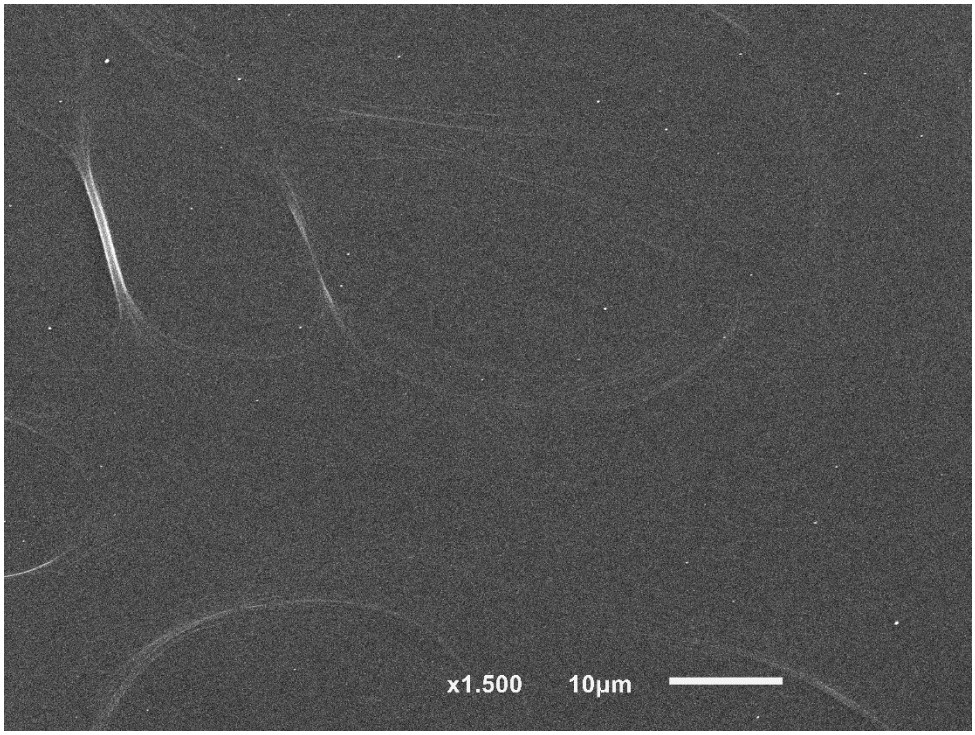

4. Sample 4, sector C;

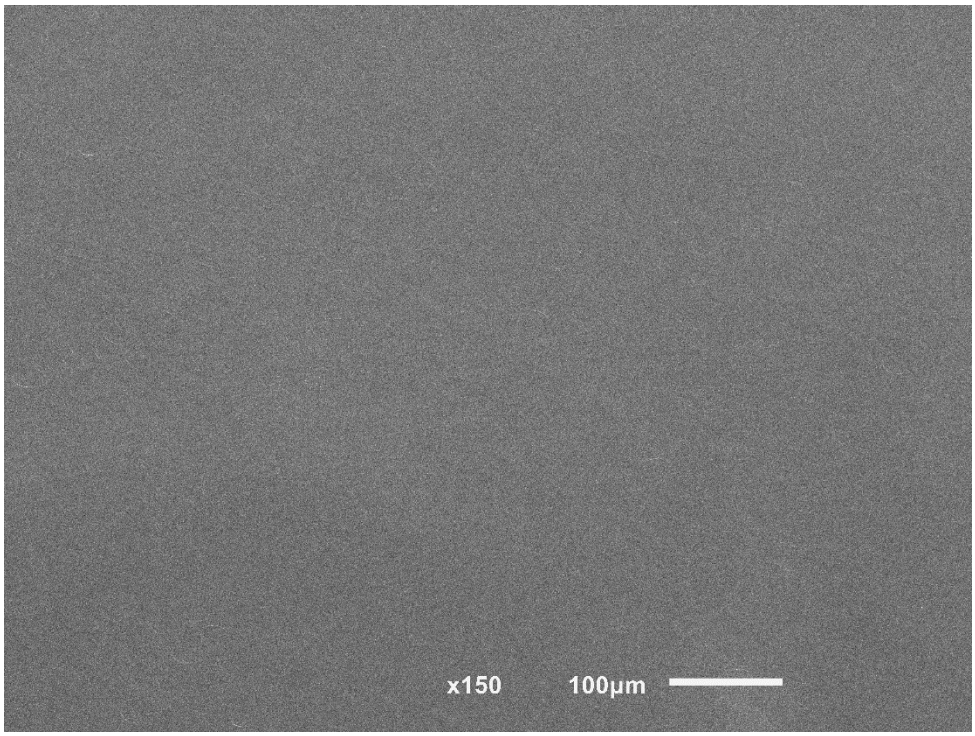

5. Sample 4, area C;

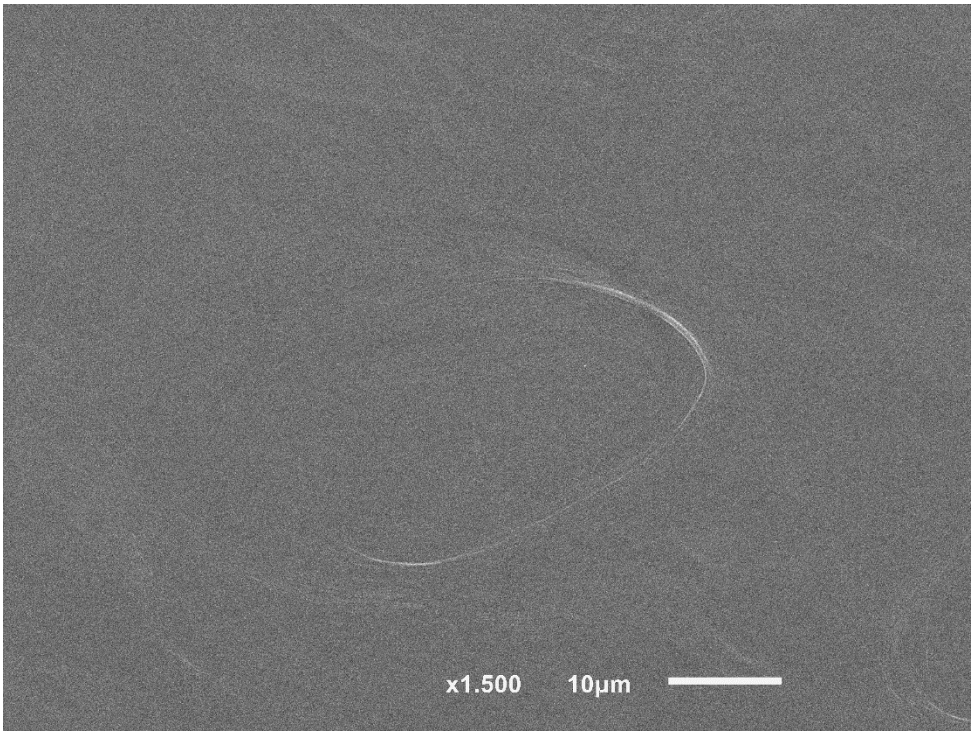

Sample 5:

1. Sample 5, sector A;

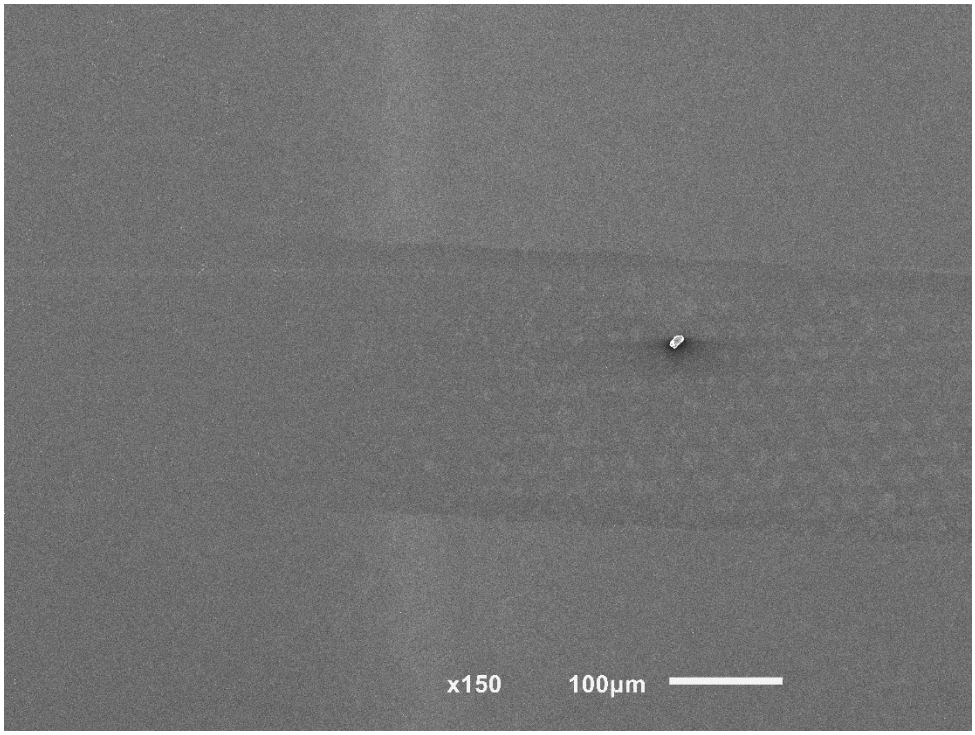

2. Sample 5, area A1;

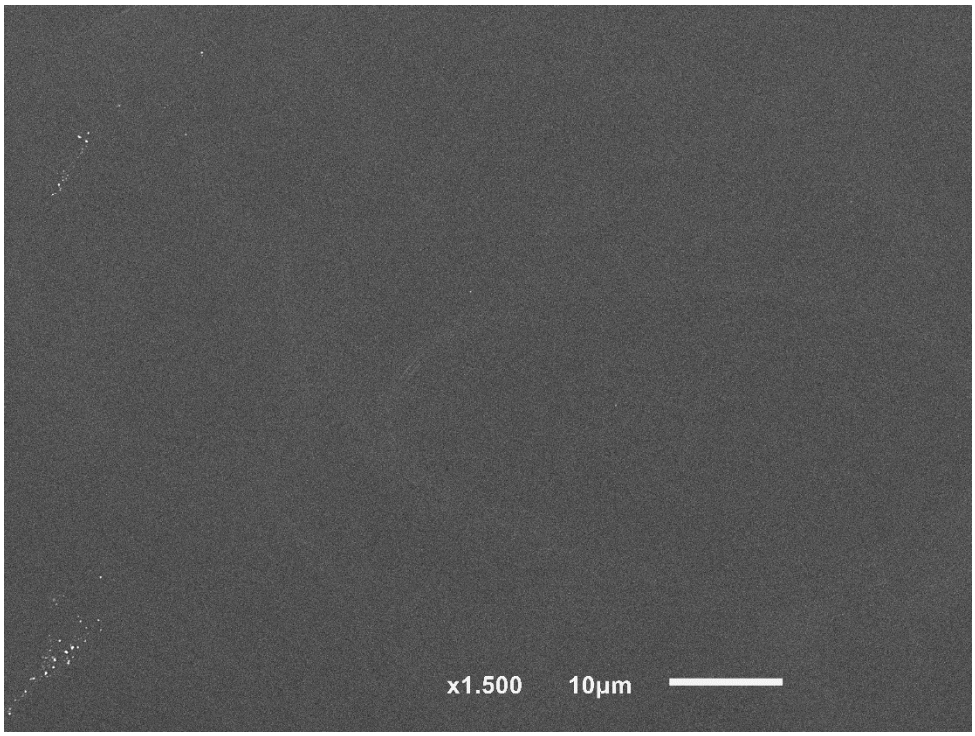

3. Sample 5, area A2;

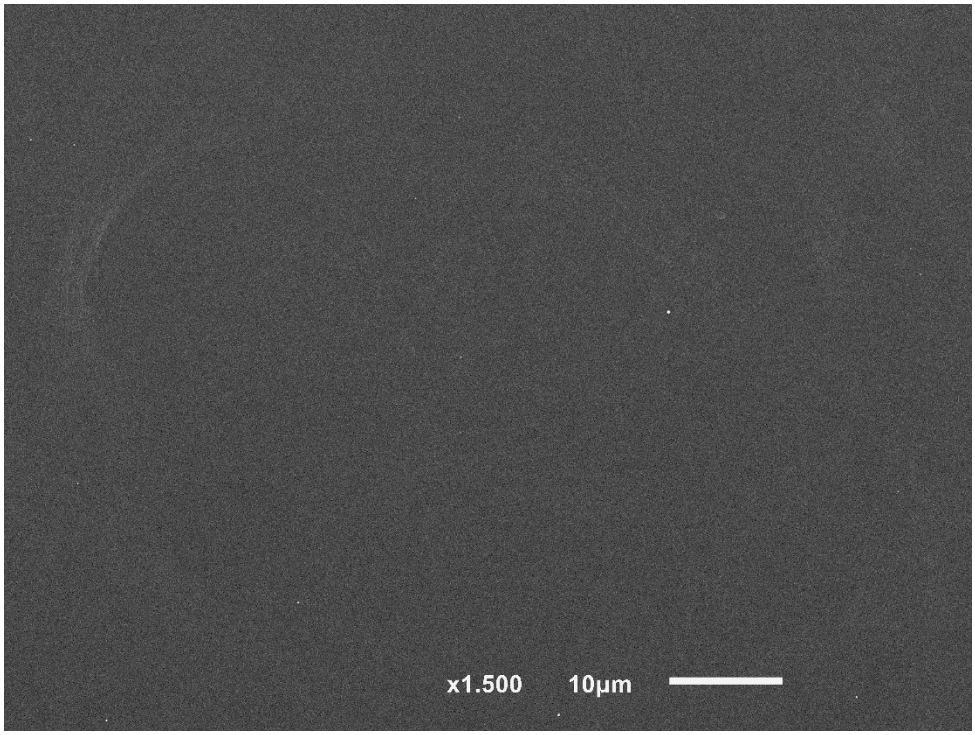

4. Sample 5, area B1;

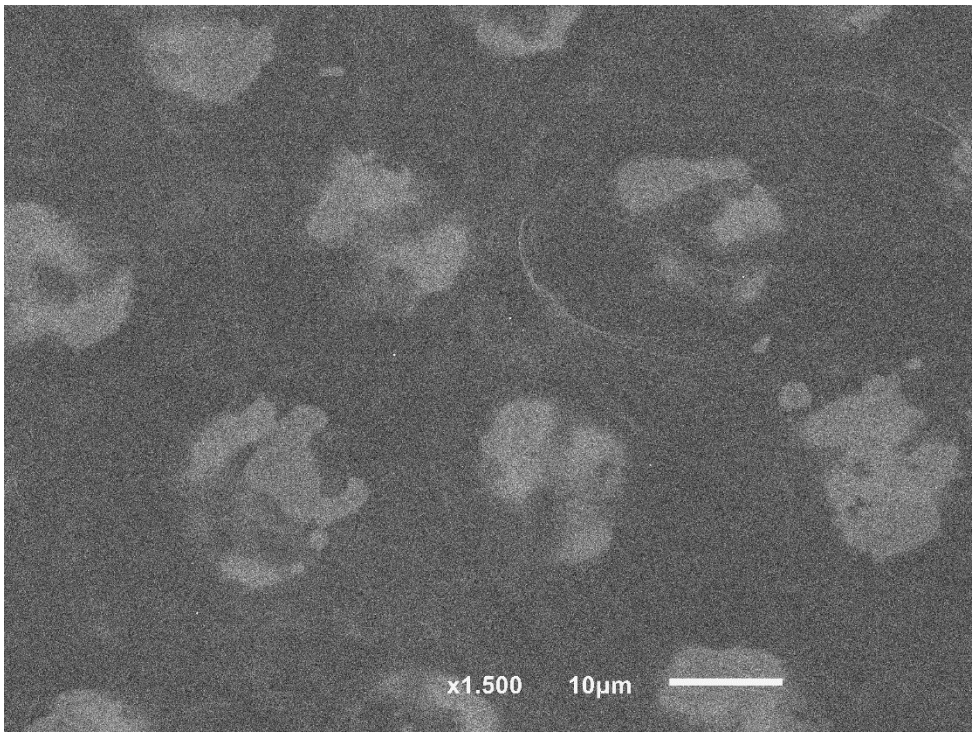

5. Sample 5, area B2;

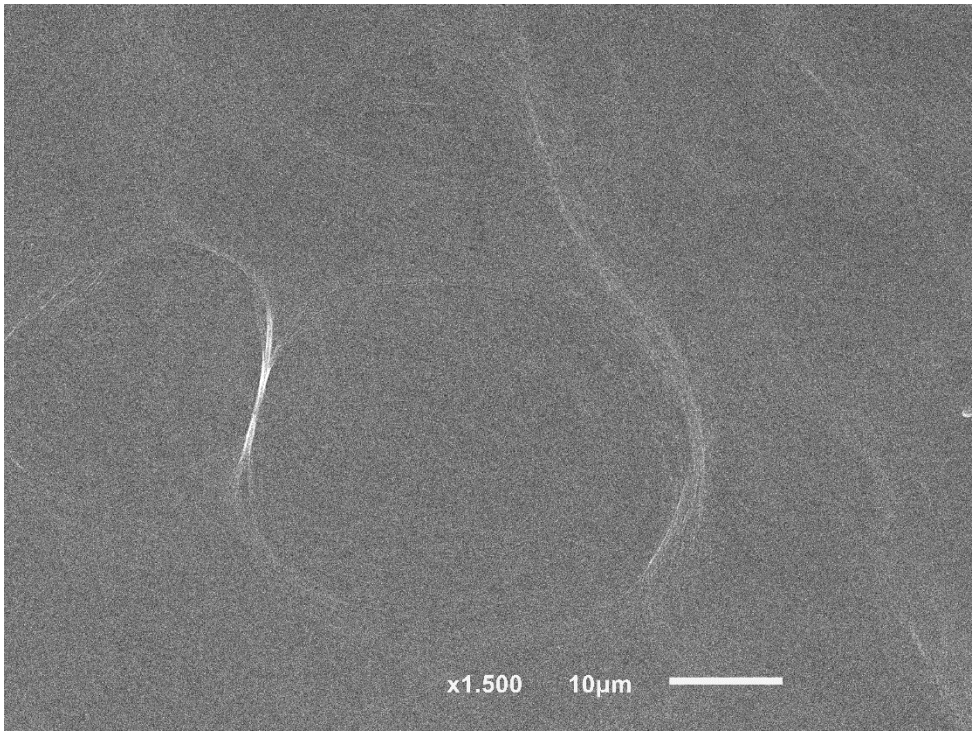

6. Sample 5, sector C;

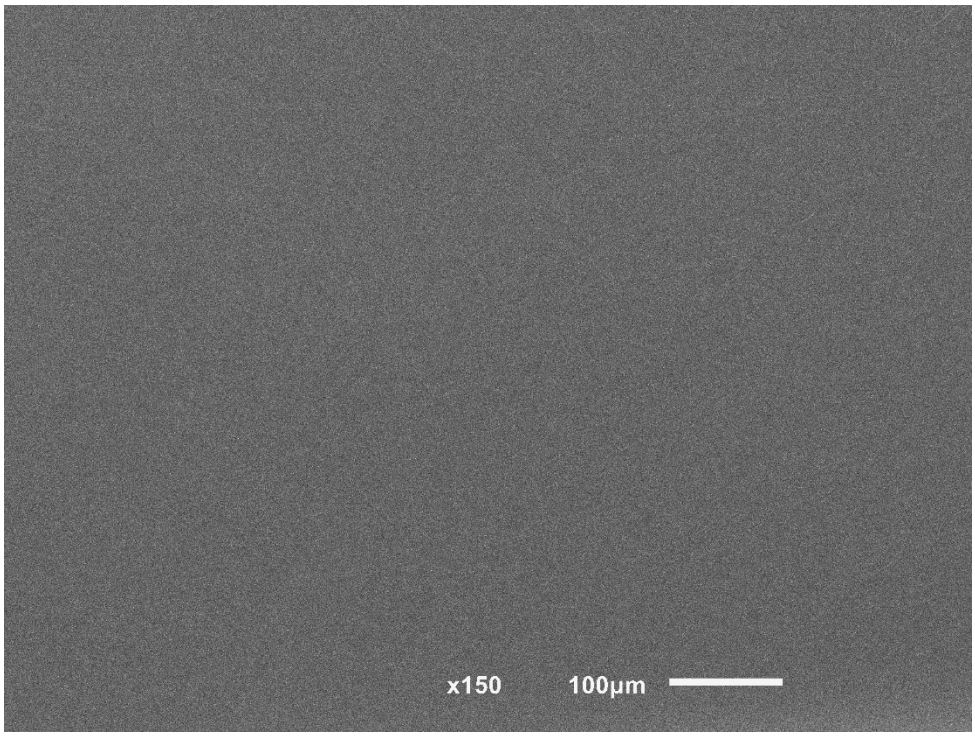

7. Sample 5, area C;

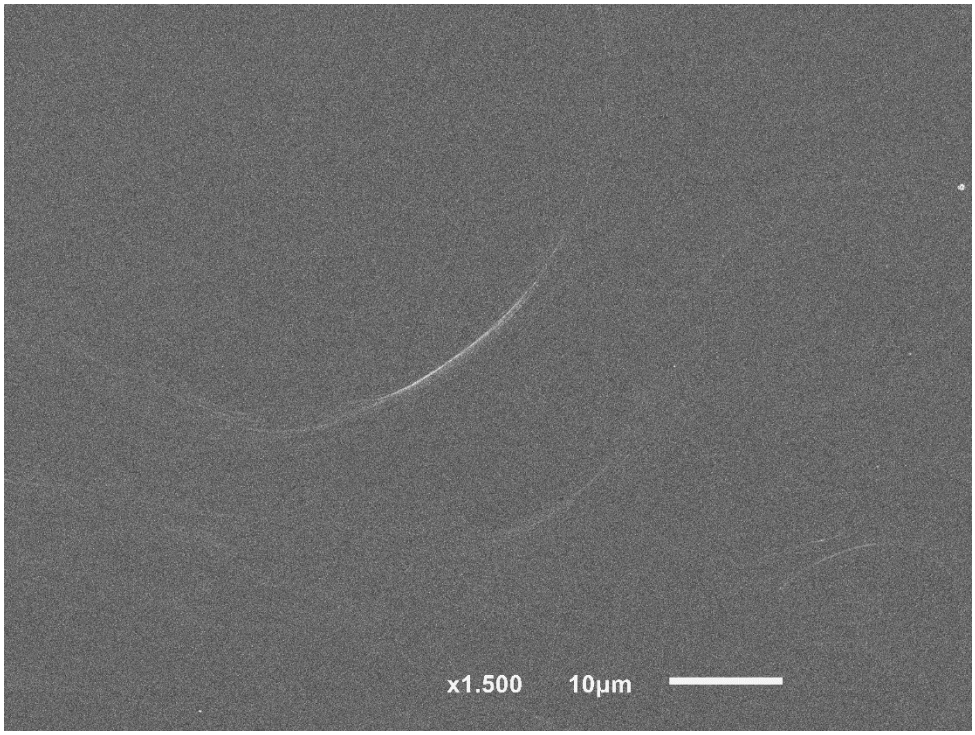

Annex IV – EDS

Sample 1:

1. Sample 1, area A1;

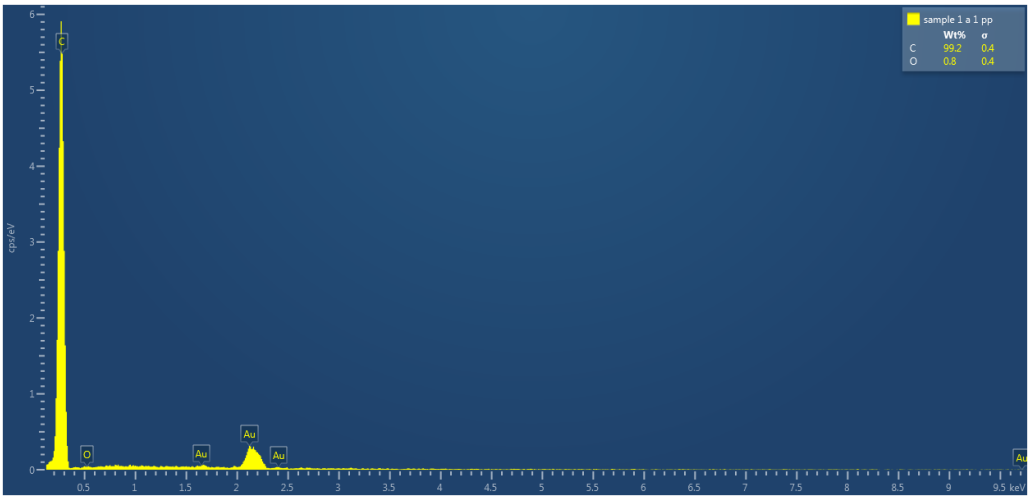

2. Sample 1, area A2;

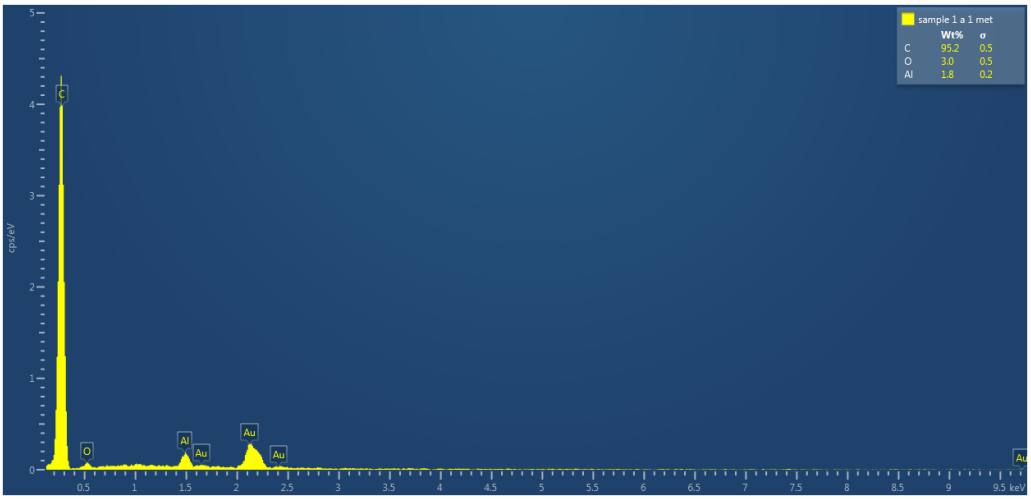

3. Sample 1, area B1;

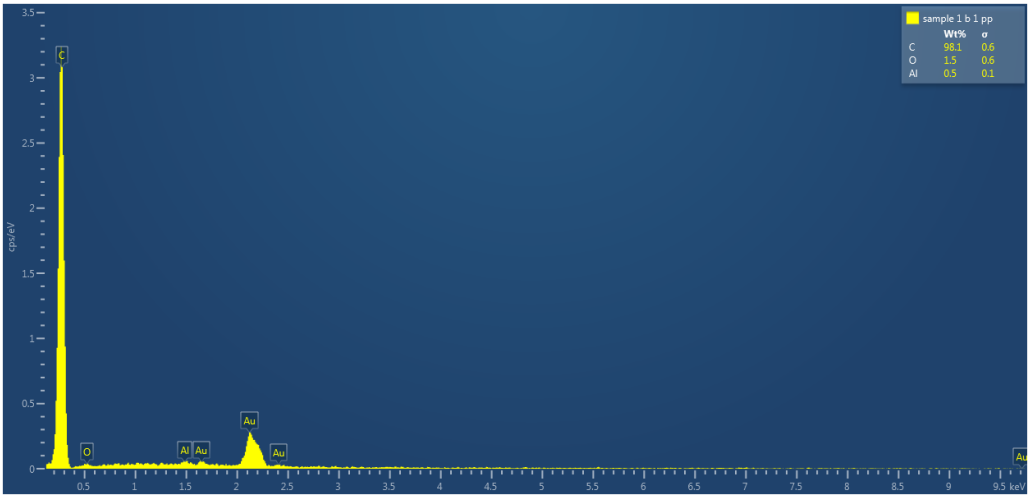

4. Sample 1, area B2;

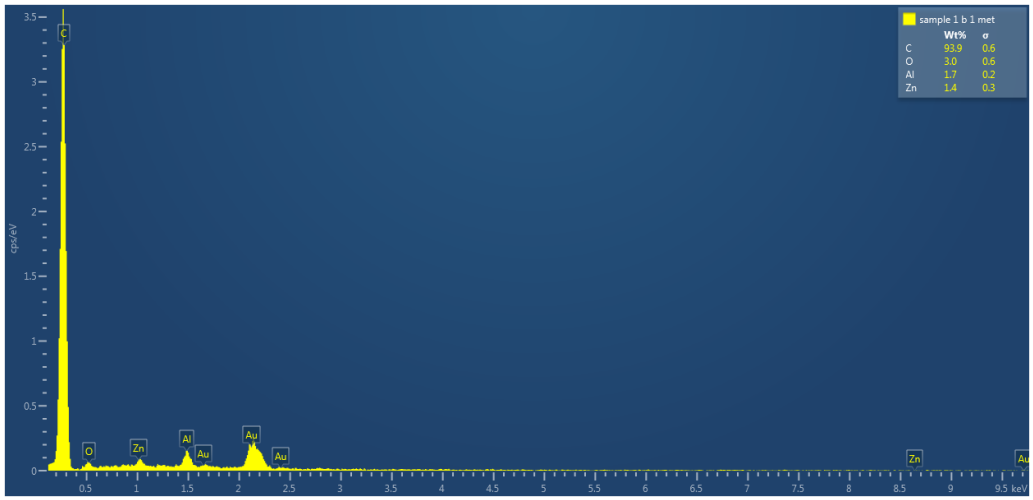

5. Sample 1, area C;

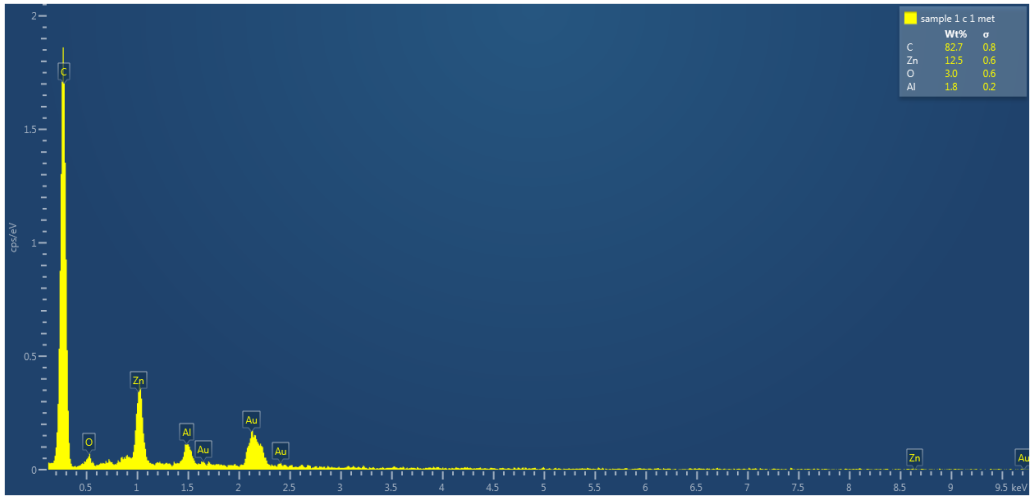

Sample 2:

1. Sample 2, area A1;

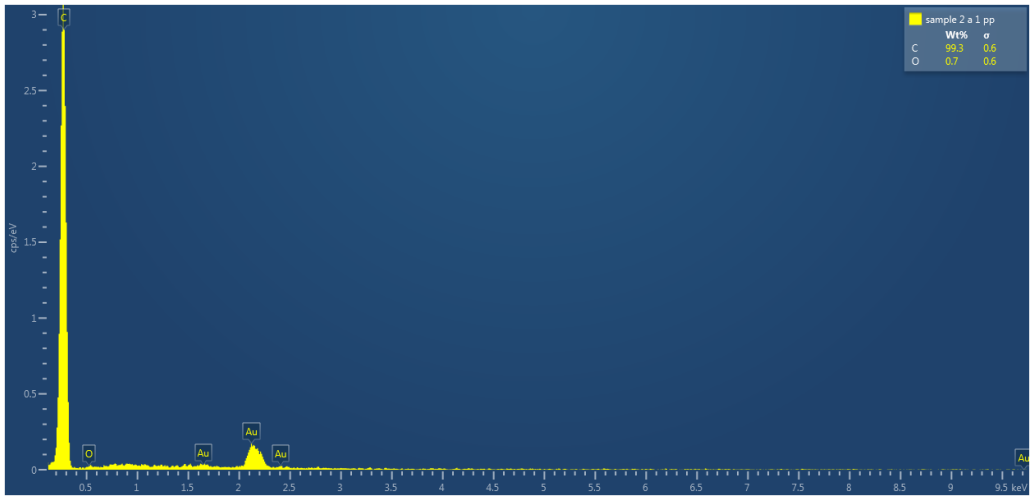

2. Sample 2, area A2;

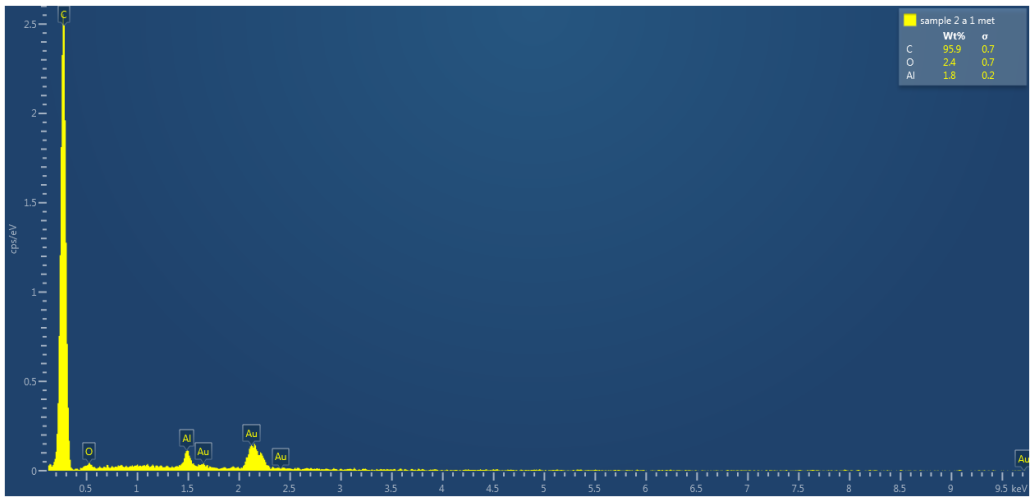

3. Sample 2, area B1;

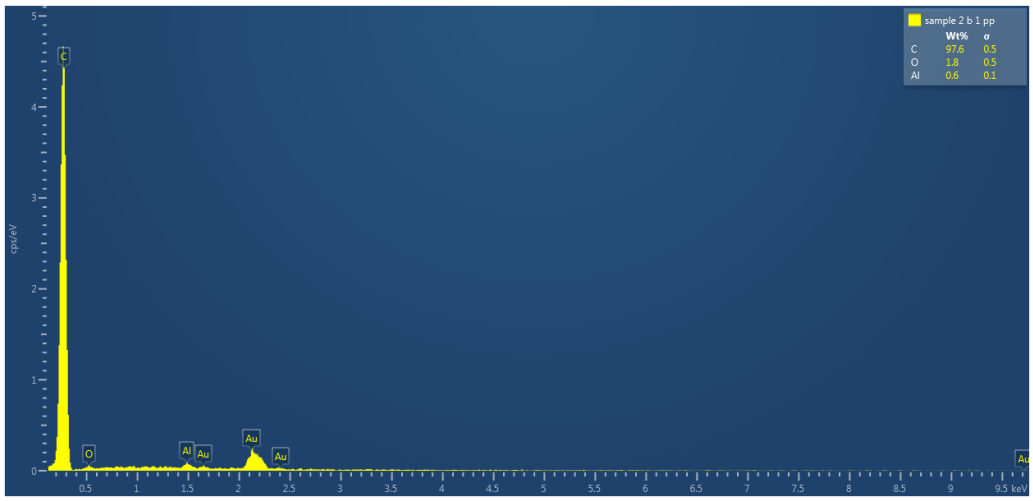

4. Sample 2, area B2;

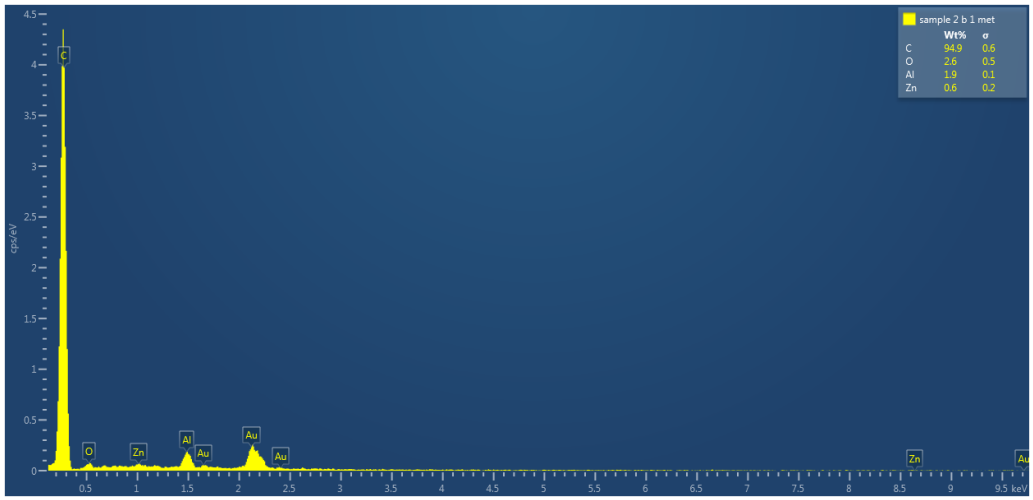

5. Sample 2, area C;

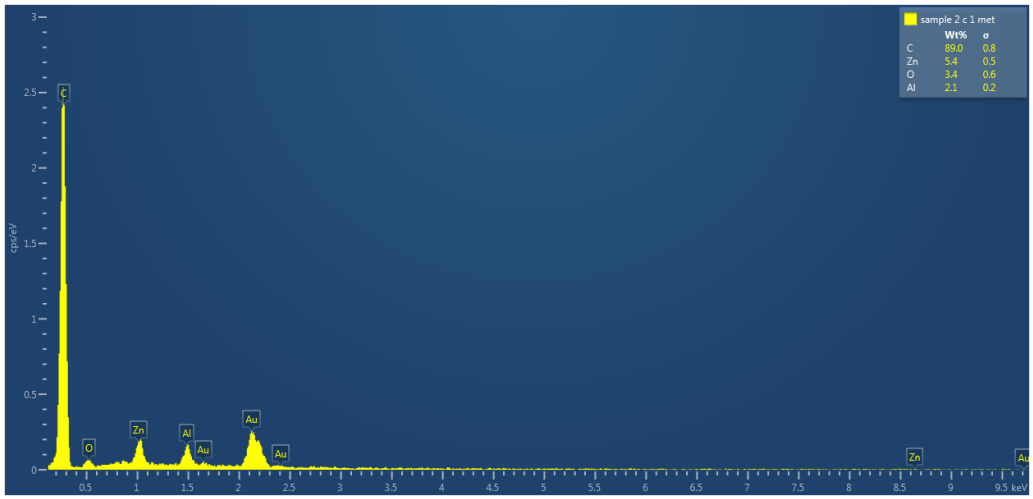

Sample 3:

1. Sample 3, area A1;

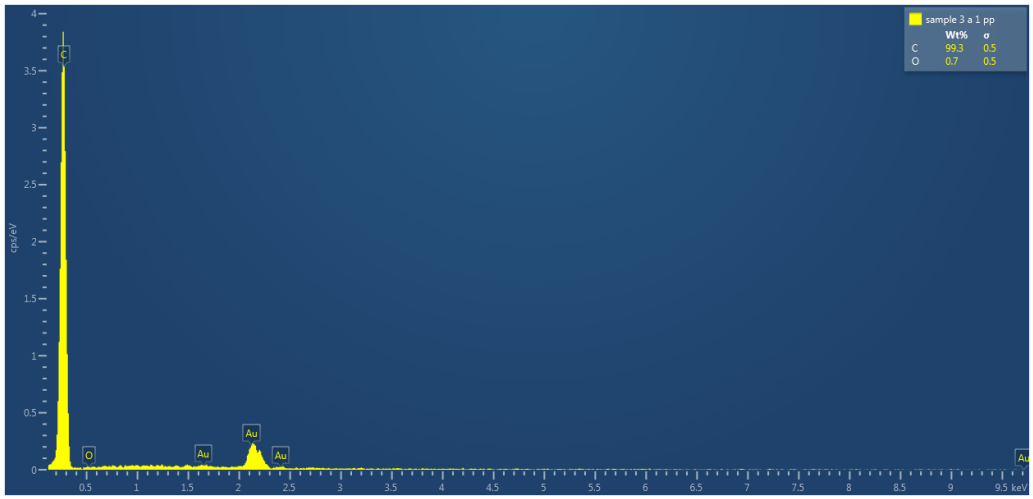

2. Sample 3, area A2;

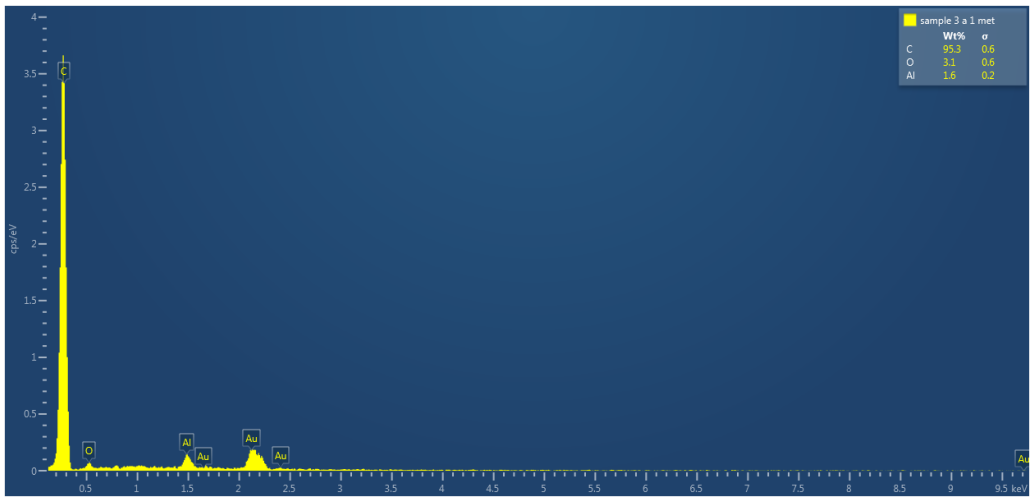

3. Sample 3, area B1;

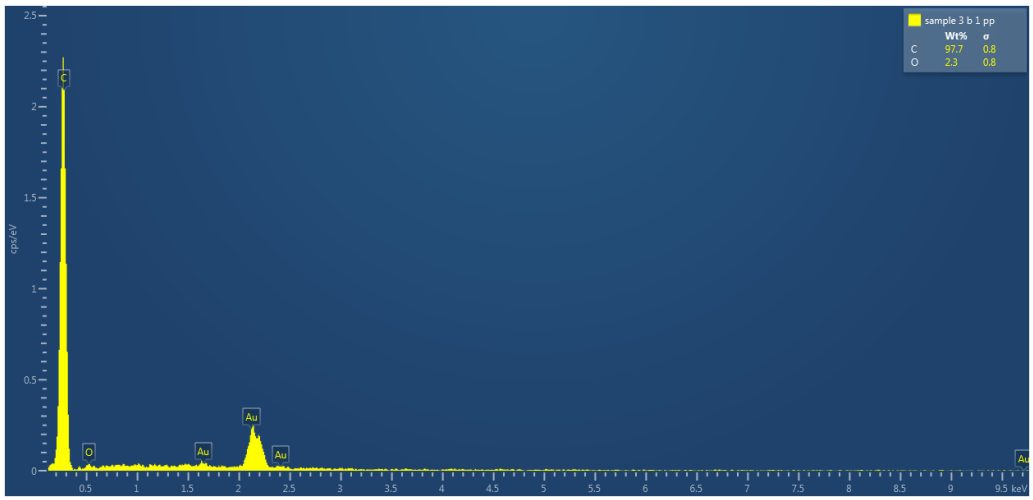

4. Sample 3, area B2;

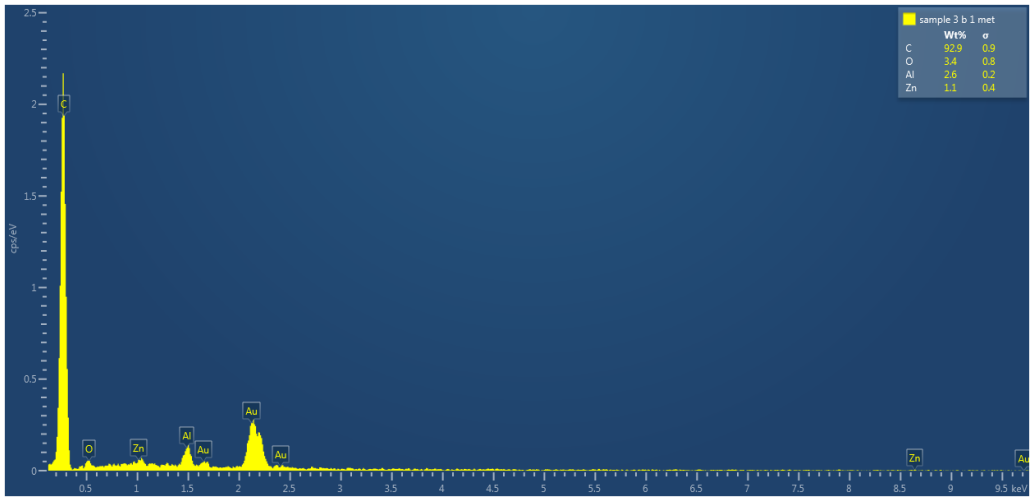

5. Sample 3, area C;

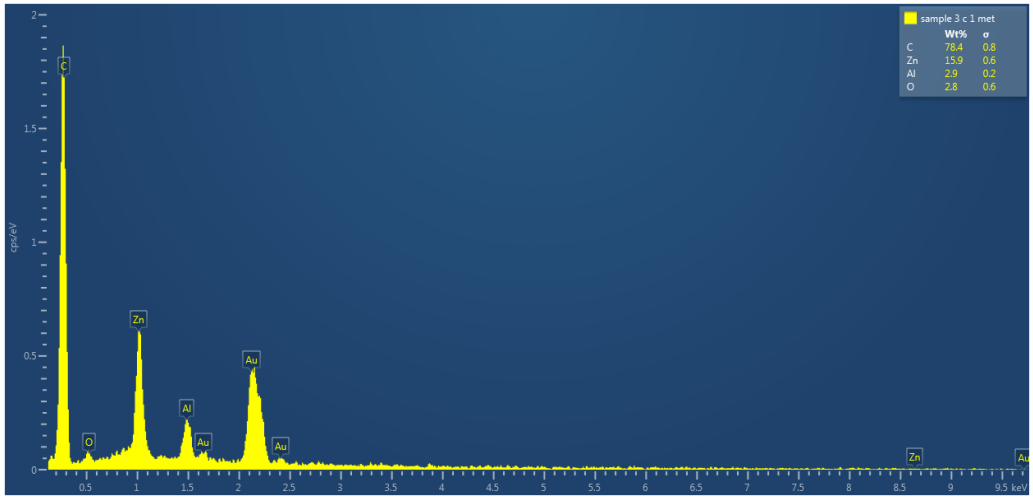

Sample 4:

1. Sample 4, area A1;

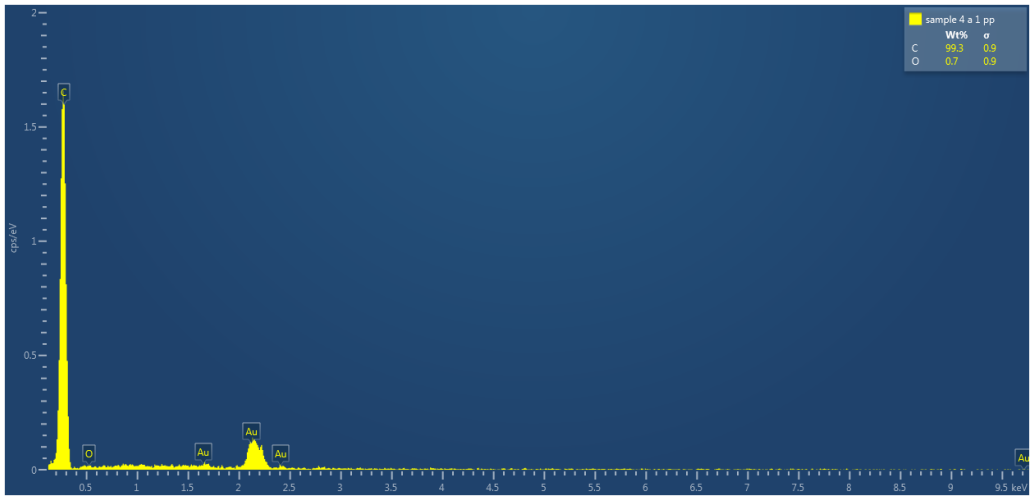

2. Sample 4, area A2;

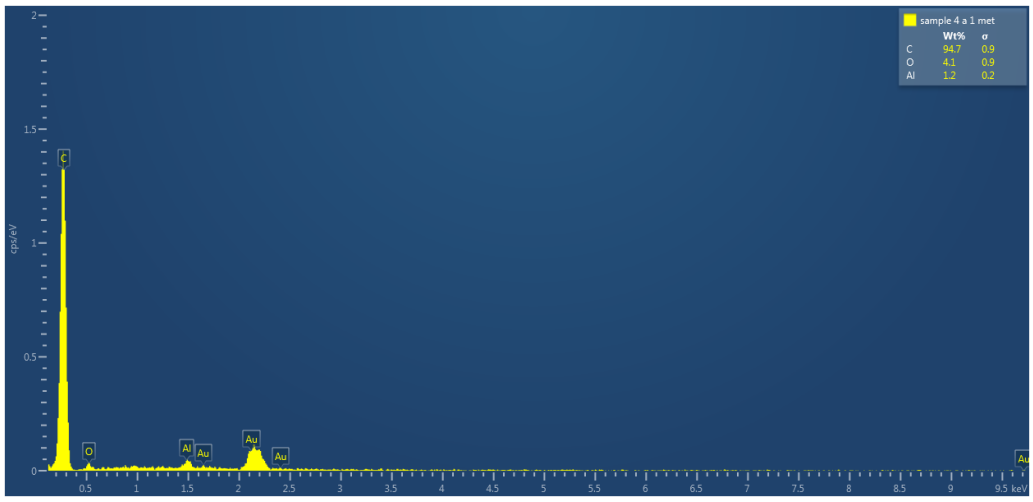

3. Sample 4, area B1;

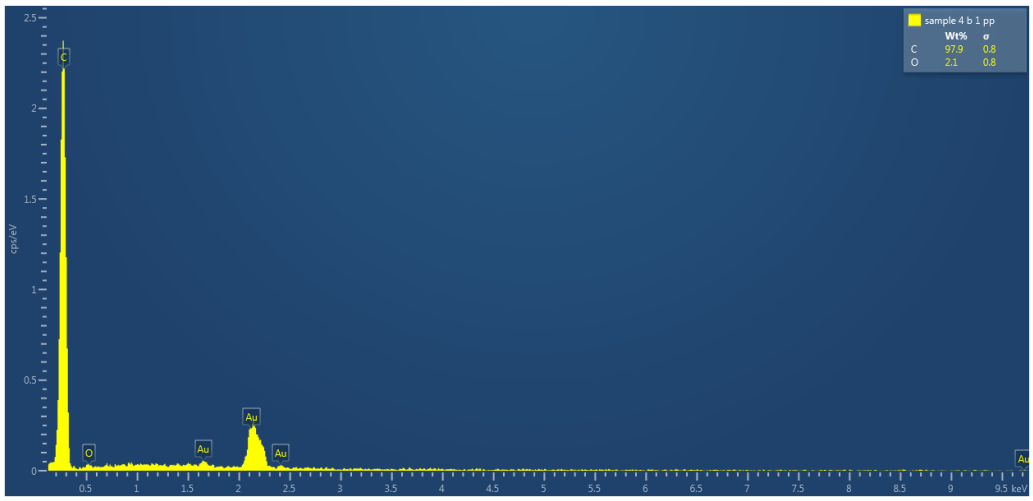

4. Sample 4, area B2;

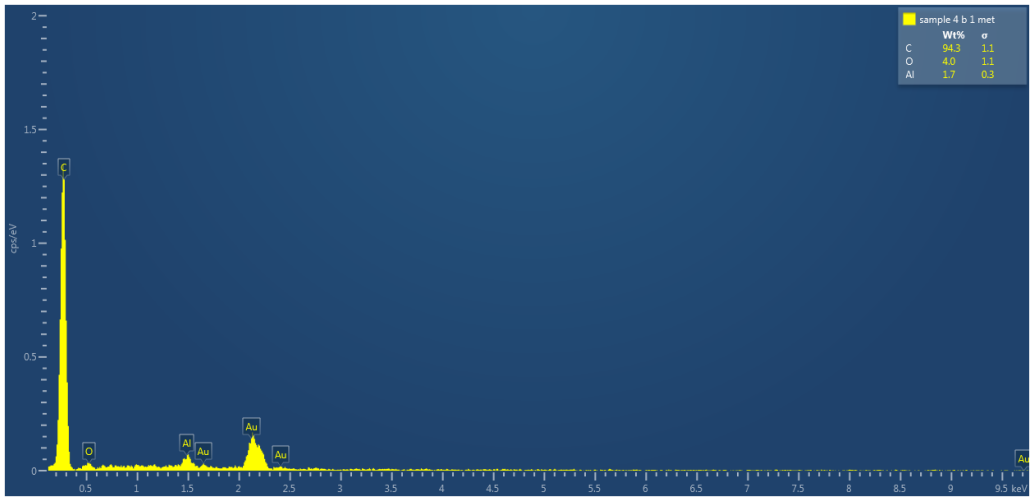

5. Sample 4, area C;

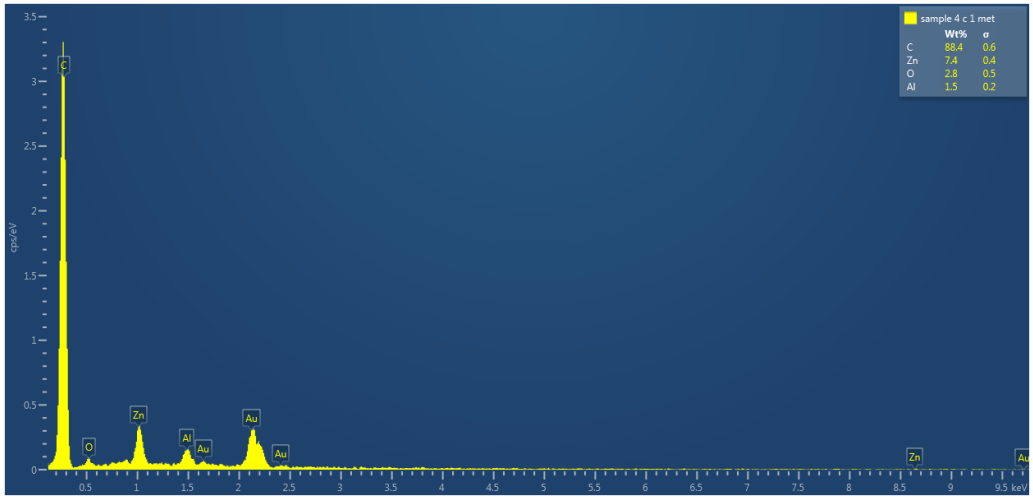

Sample 5:

1. Sample 5, area A1;

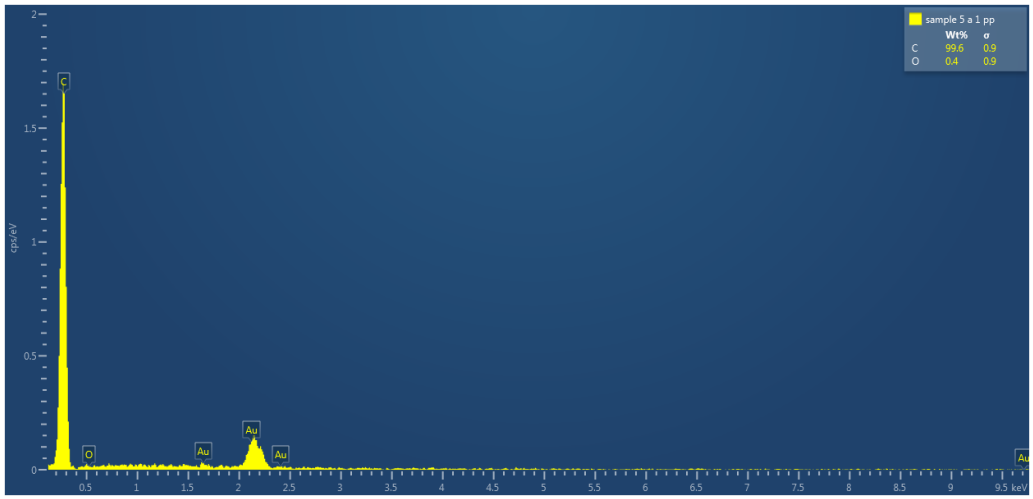

2. Sample 5, area A2;

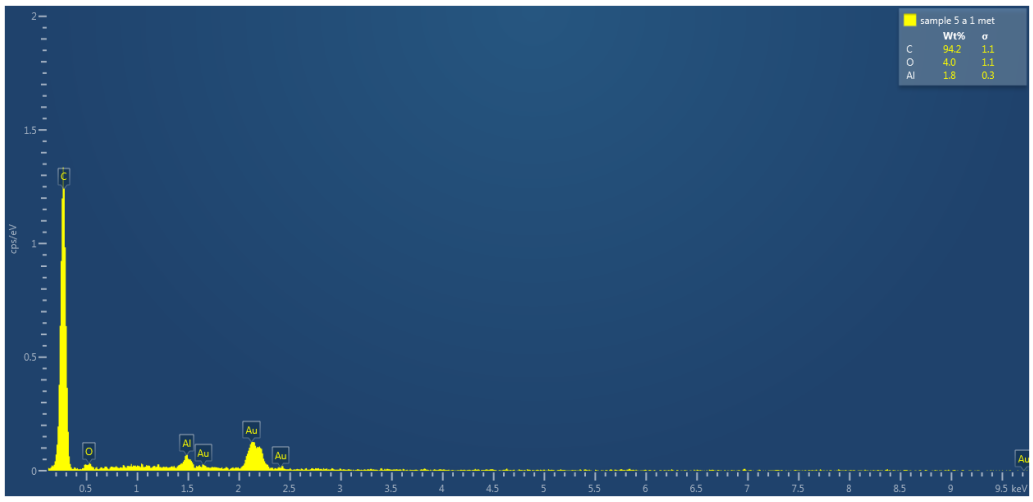

3. Sample 5, area B1;

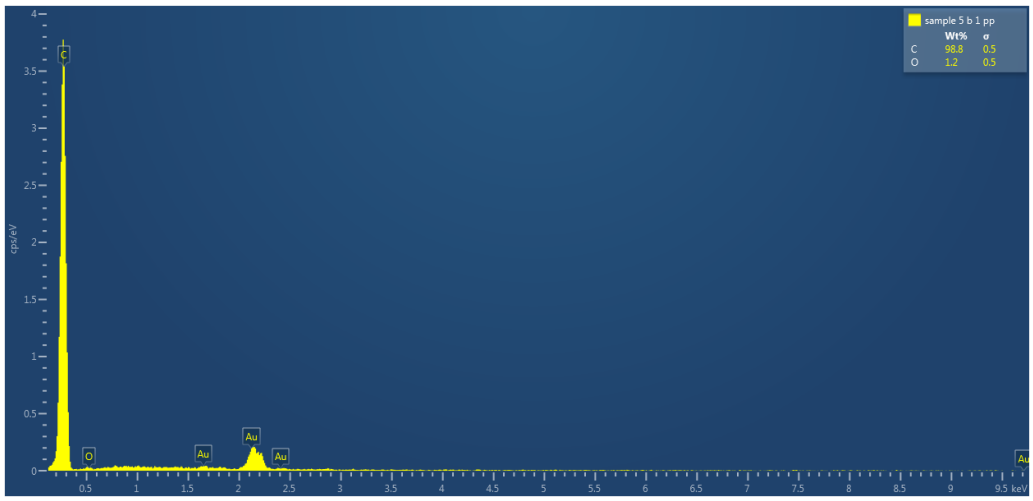

4. Sample 5, area B2;

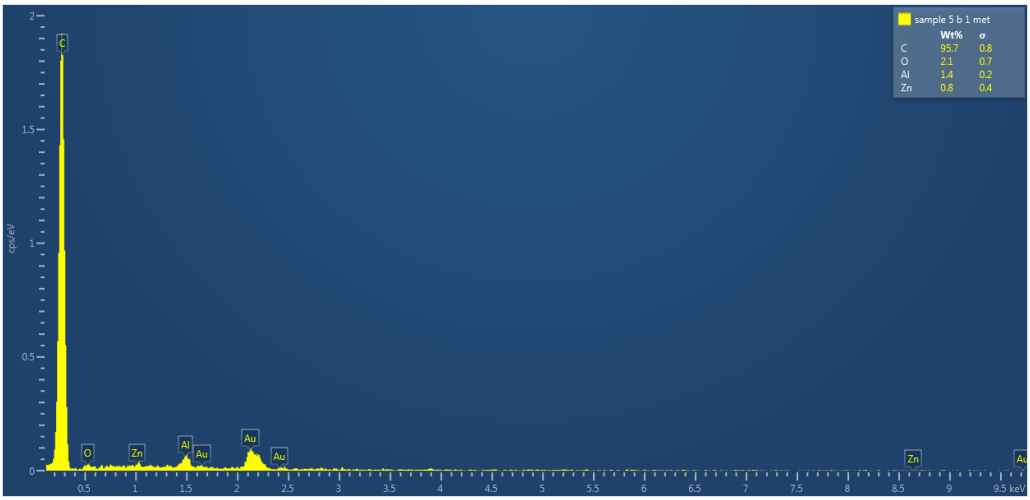

5. Sample 5, area C;

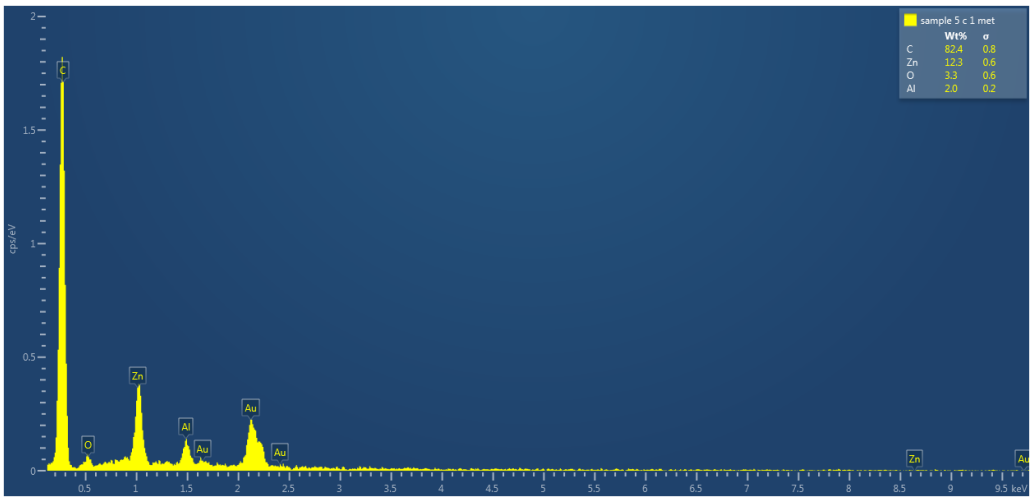

Annex V – Statistical tests methodology

After the elaboration of the mechanical tests and obtaining the mechanical parameters results for each sample, a statistical t-test was performed to evaluate if the differences observed between the different samples were statistically significant. Initially, to identify and remove possible outliers present on the different samples results for each parameter, a Dixon's test, according with **equation 10**, was applied for each group of results. If the obtained result value (Qexp) is higher than Q-critical (confidence level of 95%, number of observations (n)), then this value is considered an outlier and must be removed from data.

$$Qexp = Q10 = \frac{|outlier's\ value - nearest\ value|}{largest\ value - smallest\ value}$$ **Equation 10**

After identifying and removing the outliers detected through Dixon's test, a boxplot was developed, through Rstudio software, comparing the different samples mechanical properties regarding the factors in study. This boxplot also enabled the detection of additional outliers that weren't detected through Dixon's test and their removal from the results.

T-test was needed to assure that the differences observed were statistically significant. Before this evaluation, a F-test was applied to confirm if there are statistical differences between the sample's variances. This F-test was performed using the following **equation 11**, which corresponds to the ratio between the variance of two groups of results (a,b), of different samples, for the same mechanical parameter, and comparing the obtained F-value with a listed F-critical at a 95% confidence level, for a given degree of freedom. If F-value is lower than F-critical, then no significant differences are observed between the variances of each group of results and the applied T-test corresponds to the **equation 12**, which includes the mean value of group A (Xa), mean value of group B (Xb) and the global standard deviation (sg). If there are statistically significant differences between the variances of both groups of results, then the applied T-test corresponds to **equation 13**, which includes the variance of both groups of results $(s(a)^2$ and $s(b)^2)$.

$$F = \frac{s(a)^2}{s(b)^2} \qquad \textbf{Equation 11}$$

$$T = \frac{|Xa - Xb|}{sg\sqrt{\frac{1}{na} + \frac{1}{nb}}} \qquad \textbf{Equation 12}$$

$$T = \frac{|Xa - Xb|}{\sqrt{\frac{s(a)^2}{na} + \frac{s(b)^2}{nb}}} \qquad \textbf{Equation 13}$$

The obtained T-value was compared with a tabulated value (t-critical) regarding a specific degree of freedom and confidence level (95%). If T-value is higher than T-critical, than there are significant differences between the mean values of the analysed groups of results for a particular mechanical parameter.

All the T-tests and F-tests were calculated through Excel software using the integrated "data analysis toolPack".